Mapping the allosteric pathway leading from a mutation in the nicotinic acetylcholine receptor to a Congenital Myasthenic Syndrome

Jaimee Allison Domville

A thesis submitted to the Faculty of Graduate and Postdoctoral Studies in partial fulfillment of the requirements for the M.Sc. degree in Biochemistry

Department of Biochemistry, Microbiology, and Immunology

Faculty of Medicine

University of Ottawa

Abstract

The peripheral and highly lipid-exposed M4 α-helix, although distant from the agonist binding site, channel gate, and other important gating structures, is involved in modulating function of the nicotinic acetylcholine receptor. M4 "senses" changes in the surrounding lipid environment and may consequently affect receptor function by altering specific interactions between the M4 C-terminus and the Cys-loop. An example of this lipid sensing ability is demonstrated by a lipid-facing Cys418 to Trp substitution on αM4 (αM4 C418W) of the muscle-type receptor, which subtly alters protein-lipid interactions and potentiates channel function 16-fold, leading to a slow-channel congenital myasthenic syndrome. Through the use of mutational studies and mutant cycle analysis, I determine that, contrary to previous studies, M4–Cys-loop interactions are not critical to wild-type muscle-type receptor function, nor are they involved in C418W-induced potentiation. Instead, C418W potentiates channel activity by enhancing local M4-M1 interactions mediated by three polar side-chains, which are absolutely critical to potentiation. I show that altered M4-M1 interactions are ultimately translated to two important gating structures, which work in tandem to stabilize the open conformation of the receptor. These studies highlight how altered protein-lipid interactions can affect channel function and contribute to our understanding of the underlying gating mechanism of the muscle-type receptor.

Acknowledgements

First and foremost, I would like to thank my supervisor, Dr. John Baenziger. These past few years working under your supervision have been a real pleasure. You have taught me so much, not only about science, but also about life. My success at this level would not have been possible without your guidance. Sincerely, thank you for everything. Now, get back to work!

To the members of my thesis advisory committee, Dr. Natalie Goto and Dr. Jean-Marc Renaud, thank you for your insightful comments. You really made me evaluate my work from many different angles. Your help was invaluable.

To my lab members, thank you for all the moral support. To my first ever lab mates, Camille, Dan, and Jiayin, all three of you taught me everything I know today, I couldn't have done any of this without your help. To those I've worked closely with over the years, Claire, Dan (#2), Shobhi, Annie, Charlotte, and Michael, it's been a great pleasure working alongside you. To the newest members of the Baenziger lab, Jacob and Mack, you have quite the road ahead of you, I wish you the best of luck, and don't forget to enjoy the ride!

To my parents, I wouldn't be where I am today without you (both figuratively and literally!). From the always nutritious and delicious meals (thanks Dad!), to the never ending love and support. Thank you for always believing in me and taking an interest in my work.

To my sister, you have been a great source of support for me. I'm so proud of what you have accomplished in your life and I'm so excited to see what the future holds for the both of us in the world of real adults!

Finally, to my boyfriend, Carl. You have been my greatest source of support over these past two years. You were always there to lend an ear when I needed to rant about my bad days, and you listened patiently as I rambled on and on about my good days. Your love and patience has been invaluable and I will never forget it. Thank you for being my best friend.

Table of Contents

List of Abbreviations

3,4-DAP	3,4-diaminopyridine
5-HT_3	Serotonin receptor
ΔΔG	Gibbs free energy
ACh	Acetylcholine
AChE	Acetylcholinesterase
ALG2/ALG14	Alpha-1,3-mannosyl transferase 2/14
C418W-nAChR	C418W mutant by itself
CD	Cytoplasmic domain
ChAT	Choline acetyltransferase
CMS	Congenital Myasthenic Syndrome
ColQ	Collagenic tail Q
cRNA	Clonal ribonucleic acid
Dok-7	Docking protein 7
DPAGT1	Dolichyl-phosphate [UDP-N-acetylglucosamine] N-acetylglucosaminephosphotrasnferase 1
EC_{50}	Half maximal effective concentration
ECD	Extracellular domain
ELIC	*Erwinia* ligand-gated ion channel
ER	Endoplasmic reticulum
$GABA_{A/C}$	γ-aminobutyric acid receptor type A/C
GFPT1	Glutamine fructose-6-phosphate transaminase
GLIC	*Gloeobacter* ligand-gated ion channel
GluCl	Glutamate-activated chlorine channel
GlyR	Glycine receptor
LRP4	Lipoprotein-related protein 4
M1	Transmembrane α-helix 1
M2	Transmembrane α-helix 2
M3	Transmembrane α-helix 3
M4	Transmembrane α-helix 4

MuSK	Muscle-specific kinase
MWC	Monod-Wyman-Changeux
nAChR	Nicotinic acetylcholine receptor
PA	Phosphatidic acid
PAM	Positive allosteric modulator
PC	Phosphatidylcholine
PDB	Protein Data Bank
pLGIC	Pentameric ligand-gated ion channel
PNU	PNU-120596
Post-M4	The M4 C-terminus
Rapsyn	Receptor-associated protein of the synapse
TEVC	Two-electrode voltage clamp
TMD	Transmembrane domain
WT-nAChR	Wild-type human muscle-type nicotinic acetylcholine receptor

List of Figures

List of Tables

Chapter 1

General Introduction

1.1 Congenital myasthenic syndromes - inheritable diseases of the neuromuscular junction

Congenital myasthenic syndromes (CMSs) are a family of related genetic diseases characterized primarily by a progressive fatigable muscle weakness (myasthenia), which can lead to respiratory difficulties, reduced mobility, and progressive muscle wasting. The severity of CMS can vary greatly from one patient to the next, with severe cases typically presenting at infancy and mild cases often not presenting until well into adulthood. Currently, only a few pharmaceutical treatment options exist, and most have limited effectiveness.

The focus of the research in this thesis is on one CMS-causing mutation (αM4 C418W), which occurs on the lipid-facing surface of a protein receptor called the nicotinic acetylcholine receptor (nAChR). This mutation leads to enhanced agonist-induced nAChR activation. In this thesis, I use a novel mutant cycle analysis approach to shed light on the pathway by which the αM4 C418W mutation ultimately alters nAChR channel gating to enhance function. By understanding better the mechanism by which this CMS-causing mutation alters nAChR activity, my research provides a basis for the development of targeted allosteric modulators for the treatment of CMS. Given the impact of neuronal nAChRs on other disease phenotypes, such as Alzheimer's disease, Parkinson's disease, epilepsy, etc., the results of this thesis have broader implications for our understanding of human health and disease.

To place my research into context, I will briefly discuss communication at the neuromuscular junction, as well as those proteins involved in neuromuscular junction formation and maintenance. This will be followed by a review of our current knowledge of how CMS-causing mutations ultimately influence communication at the muscle synapse. Given the central importance of the nAChR in both synaptic communication and CMS, I devote considerable time

to reviewing nAChR structure and function. Finally, the αM4 C418W mutation is on the lipid-facing surface of the nAChR; thus, C418W-induced changes in nAChR activity likely result from altered lipid-nAChR interactions (Shen et al., 2006). Given the relevance of my work to nAChR lipid sensing, I will present a brief review of lipid-nAChR interactions.

1.2 Signalling and formation of the neuromuscular junction

Synaptic transmission at the mature neuromuscular junction is initiated when an action potential travels down the pre-synaptic neuron and triggers the release of acetylcholine (ACh) from the nerve terminal. ACh then diffuses quickly across the synaptic cleft to bind nAChRs on the post-synaptic membrane, resulting in an endplate potential, which, if sufficient, spreads across the surface of the muscle cell to initiate muscular contraction (Hughes et al., 2006). Binding to, and subsequent activation, of nAChRs occurs within microseconds, owing to its high channel opening rate constant (Chakrapani and Auerbach, 2005). This is also what allows for repeated channel opening events during each ACh occupancy (as reviewed by Sine and Engel, 2006). After activation, the channel closes, resulting in the rapid dissociation of ACh from the binding sites, where it is cleared from the synaptic cleft either by diffusion or degradation by the synaptic enzyme acetylcholinesterase (AChE), effectively terminating the synaptic response. CMS-causing mutations can affect synaptic transmission at any step of this process, from ACh formation and subsequent release, to the ultimate termination of the synaptic response.

Note that many proteins, in addition to the nAChR, are required for the development and proper functioning of the neuromuscular junction, and many of these proteins are relevant to CMS, including: agrin, lipoprotein-related protein 4 (LRP4), muscle-specific kinase (MuSK), docking protein 7 (Dok-7), and receptor-associated protein of the synapse (rapsyn). These proteins are involved in complex signalling pathways during development of the neuromuscular

junction. Specifically, fetal nAChRs are expressed in high levels intracellularly and concentrated within the central region of muscle cells by a process known as "pre-patterning". The accumulation of nAChRs at this location is stabilized by agrin and MuSK. Agrin forms a complex with LRP4, located on the post-synaptic membrane, which is then able to bind to, and activate, MuSK. Activated MuSK clusters with LRP4 as well as Dok-7 at the membrane where it can affect the actions of rapsyn. Rapsyn specifically promotes the differentiation of the motor endplate via enhanced expression of synapse specific genes and additionally clusters nAChRs at the motor endplate through a direct protein-protein interaction (Ohno et al., 2002; Ramarao and Cohen, 1998; Zuber and Unwin, 2013), representing the first step of synapse formation.

Although innervation is not required for muscle production, it is required for the formation of synapses; thus, clustering of fetal nAChRs at the post-synaptic membrane by rapsyn is the critical first step in synapse formation. During embryonic development, branching motor neurons release ACh in response to a pre-synaptic signal. If these ACh molecules encounter fetal nAChRs on the muscle cell membrane, they elicit post-synaptic potentials, which positively regulate the localization and stabilization of the developing synaptic contacts. During this stage of development, several motor neurons may contact one synaptic site on each muscle fibre to stabilize an active contact site. As compared to adult muscle-type nAChRs, fetal nAChRs have lower conductance and an increased open channel lifetime (Mishina et al., 1986). The prolonged open times of fetal nAChRs at the immature synapse are presumably required for efficient depolarization of the muscle cell, which could not be supported by adult muscle-type nAChRs. During post-natal development, the multiple innervations of muscle fibres are reduced until only one motor neuron contacts a single muscle fibre. Additionally, fetal nAChRs are replaced by adult nAChRs (Mishina et al., 1986), and the post-synaptic membrane adopts its optimal

endplate geometry, which includes the formation of junctional folds upon which adult muscle-type nAChRs concentrate (Sanes and Lichtman, 2001).

1.3 Etiology of CMS

CMSs have not always been recognized as unique clinical entities. In fact, due to their phenotypic similarities, CMSs were initially classified along with two autoimmune disorders, myasthenia gravis and Lambert-Eaton myasthenic syndromes. A genetic basis for CMS was initially discovered in the 1970s using whole exome sequencing. Since then, roughly 20 CMS-implicated disease genes have been identified, with each gene encoding a protein either expressed at the neuromuscular junction or involved in the folding/trafficking of these proteins (Engel et al., 2015). The majority of CMS-causing mutations occur in the nAChR, a protein that is central to neuromuscular junction development and function. Such mutations subtly alter agonist-induced nAChR activity and/or expression levels, with the latter sometimes affecting formation of the neuromuscular junction. CMS-causing mutations are now classified as influencing activity at the pre-synaptic neuron, within the synapse, or on the post-synaptic membrane of the neuromuscular junction, although a fourth "class" of CMS-causing mutations has also been identified. Specifically, recent studies have shown that CMS can also result from deficiencies in the glycosylation of proteins located at the neuromuscular junction. Deficient glycosylation enzymes, due to CMS-causing mutations, ultimately influence proteins involved pre-synaptically, synaptically, or post-synaptically (Figure 1.1).

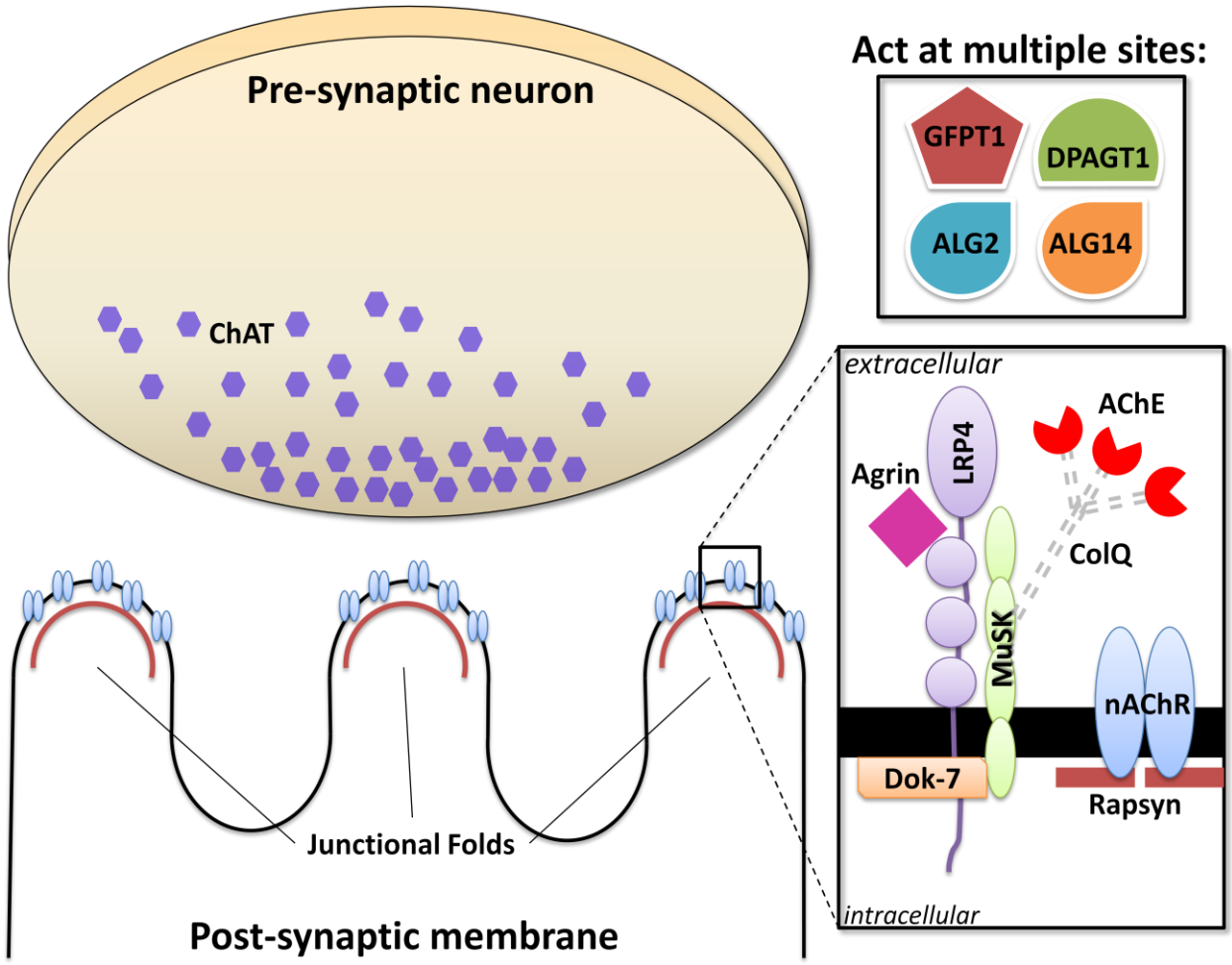

Figure 1.1 - Proteins at the neuromuscular junction implicated in CMS. A representative figure showing the pre-synaptic nerve terminal and post-synaptic membrane of the neuromuscular junction, where the specific synaptic location of proteins which have been implicated in a CMS are shown. The glycosylation enzymes, GPFT1, DPAGT1, ALG2, and ALG14, act to glycosylate all of the proteins shown in this figure, and can act at any synaptic location of the neuromuscular junction.

1.3.1 Pre-synaptic CMS

Pre-synaptic CMSs are primarily defined by a deficiency in the enzyme choline acetyltransferase (ChAT). In cholinergic neurons, this enzyme catalyzes the synthesis of ACh from acetyl-CoA and choline. ACh is the chemical messenger which relays the signal from the pre-synaptic neuron to the post-synaptic membrane; thus, ACh deficiency results in deficiency of the synaptic response. The severity of the disease phenotype can vary from mild to severe dependent upon the location of the ChAT mutation within the protein and its impact on enzymatic activity. Mutations which render ChAT completely unable to synthesize ACh are likely embryonic lethal, while some mutations may only reduce the efficiency of ACh production leading to milder phenotypes. The treatment for pre-synaptic CMSs involves the use of indirect-acting cholinergic agonists, such as pyridostigmine and 3,4-diaminopyridine (3,4-DAP). Pyridostigmine acts by inhibiting AChE, which breaks down ACh within the synaptic cleft at the neuromuscular junction; while, 3,4-DAP blocks potassium channel efflux, which increases the duration of the action potential, thereby increasing the number of ACh quanta released by the pre-synaptic neuron at each nerve impulse. Patients are often treated with a combination of both drugs to increase the overall efficacy and improve the synaptic response to ACh. Generally, patients with milder forms of CMS respond better to treatment than those with more severe forms; additionally, these treatments can become less effective in some patients with prolonged use (as reviewed by Engel, 2007).

1.3.2 Synaptic CMS

Synaptic CMSs are often caused by AChE deficiency linked to deficiency in a triple-stranded collagenic tail, ColQ. ColQ attaches to AChE, anchoring it to the synaptic basal lamina at the post-synaptic membrane. As mentioned previously, AChE breaks down ACh within the synaptic cleft at the neuromuscular junction. If ColQ is deficient on the post-synaptic

membrane, AChE diffuses away from the synapse. This results in prolonged synaptic responses as ACh is not being degraded within the synaptic cleft and can instead repeatedly bind and activate nAChRs on the post-synaptic membrane. Again, the severity of these types of CMSs can vary. Treatment of synaptic CMSs usually involves the use of long-lived, open-channel blockers of the nAChR, such as quinidine and fluoxetine, which serve to attenuate the synaptic response to ACh in a concentration dependent manner. Patients can experience improvement with such treatments over the course of many months; however, treatment with quinidine and fluoxetine comes with a list of serious side effects, often needing to be attenuated through the use of additional drugs, and cannot be tolerated by all patients (as reviewed by Engel, 2007).

1.3.3 Post-synaptic CMS

Post-synaptic CMSs are the most common form of CMS and involve mutations in many different proteins, most notably the nAChR. The mechanisms of disease and symptoms can vary wildly based upon which proteins are deficient and in what way this deficiency arises; thus, it is imperative to receive a molecular diagnosis before a course of treatment can be determined in such patients. Post-synaptic CMSs can be further subdivided into two categories: defects in the maintenance and development of the motor endplate, and defects in the muscle-type nAChR itself. As discussed in a previous section, agrin, LRP4, MuSK, Dok-7, and rapsyn are all essential for forming complex signalling networks that are essential to the development and maintenance of the endplate. Mutations in all five of these proteins have been implicated in post-synaptic CMSs; disruption in the activity of any of these proteins disrupts signalling pathways that are integral to developing and maintaining the motor endplate, leading to the disease phenotype. These forms of CMS are often treated using pyridostigmine and 3,4-DAP as described previously.

The second category of post-synaptic CMSs involves defects in the nAChR. Of all the CMS-causing mutations that have been discovered to-date, the vast majority of them are found in the four genes that encode the adult muscle-type nAChR subunits: α1-subunit (*CHRNA1*), β1-subunit (*CHRNB1*), δ-subunit (*CHRND*), and ε-subunit (*CHRNE*). These mutations affect either cell-surface expression of the nAChRs, resulting in primary nAChR deficiency, or nAChR channel activity at the post-synaptic membrane, resulting in either fast-channel or slow-channel syndromes. We will discuss the specific features of CMSs involving the nAChR in section 1.4. Although primary nAChR deficiencies cannot be satisfactorily treated at this time, fast-channel syndromes are currently treated using pyridostigmine and 3,4-DAP (as described previously), while slow-channel syndromes are treated using quinidine and fluoxetine (as described previously). Although current treatment methods may offer relief from and mask some CMS-related symptoms in patients with mild forms of CMS, they do not address the disease mechanisms at the nAChR protein level. Since CMS-causing mutations within the nAChR are the most common way in which the disease manifests itself, it would be beneficial to study the mechanisms of disease specific to the nAChR in greater detail with the ultimate aim of creating targeted allosteric modulators for the treatment of CMS.

1.3.4 Defects of glycosylation leading to CMS

Protein glycosylation is a process whereby sugar molecules are added to specific protein residues to increase protein solubility and stability, as well as to aid in proper protein folding, assembly, and intracellular trafficking. To-date, mutations in four enzymes involved in the glycosylation of neuromuscular junction proteins have been found to cause a CMS: glutamine fructose-6-phosphate transaminase (GFPT1) (Selcen et al., 2013; Senderek et al., 2011), dolichyl-phosphate [UDP-N-acetylglucosamine] N-acetylglucosaminephosphotransferase 1

(DPAGT1) (Belaya et al., 2012; Selcen et al., 2014), and alpha-1,3-mannosyl transferase 2 and 14 (ALG2 and ALG14) (Cossins et al., 2013). These enzymes are involved in the glycosylation of previously discussed proteins located at the neuromuscular junction. Deficient glycosylation can compromise protein activity at any location of the neuromuscular junction, leading to a range of disease phenotypes, and requiring a range of treatment options as discussed previously.

1.4 Subtypes of CMS involving the nAChR

The muscle-type nAChR is a part of the larger pentameric ligand-gated ion channel (pLGIC) superfamily, which includes the γ-aminobutyric acid ($GABA_{A/C}$), glycine (GlyR) and serotonin ($5\text{-}HT_3$) receptors. All members of this superfamily of ion channels mediate fast synaptic communication throughout the central and peripheral nervous systems by converting chemical signals into electrical impulses. $GABA_{A/C}$ and GlyR are anion selective, and thus relay inhibitory signals; whereas, nAChR and $5\text{-}HT_3$ are cation selective, and thus relay excitatory signals. Recently, two prokaryotic pLGICs, *Gloeobacter* ligand-gated ion channel (GLIC) and *Erwinia* ligand-gated ion channel (ELIC), were discovered (Tasneem et al., 2005) and have been used extensively in biophysical studies of pLGIC function owing to their ease of expression in bacterial systems. All pLGICs have the same general structure; they are composed of five subunits, either identical or homologous, which arrange pseudo-symmetrically about a central axis to form three distinct domains: an extracellular domain (ECD), where two ACh molecules bind in the muscle-type nAChR, a membrane-spanning transmembrane domain (TMD), where the ion channel and gate are located, and a relatively short cytoplasmic domain (CD). The ECD-TMD interface is thought to be important for coupling agonist binding in the ECD to channel gating in the TMD. Prokaryotic pLGICs lack the disulfide linkage in the eponymous Cys-loop

of all eukaryotic pLGICs, in addition to the CD, but otherwise retain the same general three-dimensional structure (Figure 1.2).

CMS-causing mutations have been identified in all regions of the nAChR protein (ECD, TMD, and CD) and affect folding, oligomerization, and/or trafficking of the nAChR to the cell surface, or activity of the fully assembled and trafficked receptor on the post-synaptic membrane. Altered nAChR expression and/or function are both able to modulate the synaptic response to ACh, whether negatively or positively. In the following sections I will discuss the three different types of CMS involving the nAChR (primary nAChR deficiency, fast-channel syndromes, and slow-channel syndromes) and identify mutations associated with each type.

1.4.1 Primary nAChR deficiency

CMSs causing primary nAChR deficiency are the result of recessive missense, nonsense, or splice site and promoter region mutations, which can be found in all nAChR subunit genes, resulting in either no expression, or very low expression, of the nAChR to the cell surface, severely attenuating the synaptic response (Engel et al., 2003b). Most of these types of mutations have been discovered in the ε-subunit; in fact, most CMS-causing mutations in general have been linked to the nAChR ε-subunit. This is likely because patients who would be homozygous for such mutations in the *CHRNA1*, *CHRNB1*, and/or *CHRND* genes would not survive as there is no suitable replacement for the α1-, β1-, or δ-subunit in the muscle for formation of a functional pentameric receptor. Indeed, patients who are heterozygous for such low expression mutants in the α1-, β1-, or δ-subunit have been shown to be severely impacted and do not generally survive infancy, likely because formation of the neuromuscular junction is severely impaired. In contrast, such mutations in the ε-subunit are better tolerated as they can be

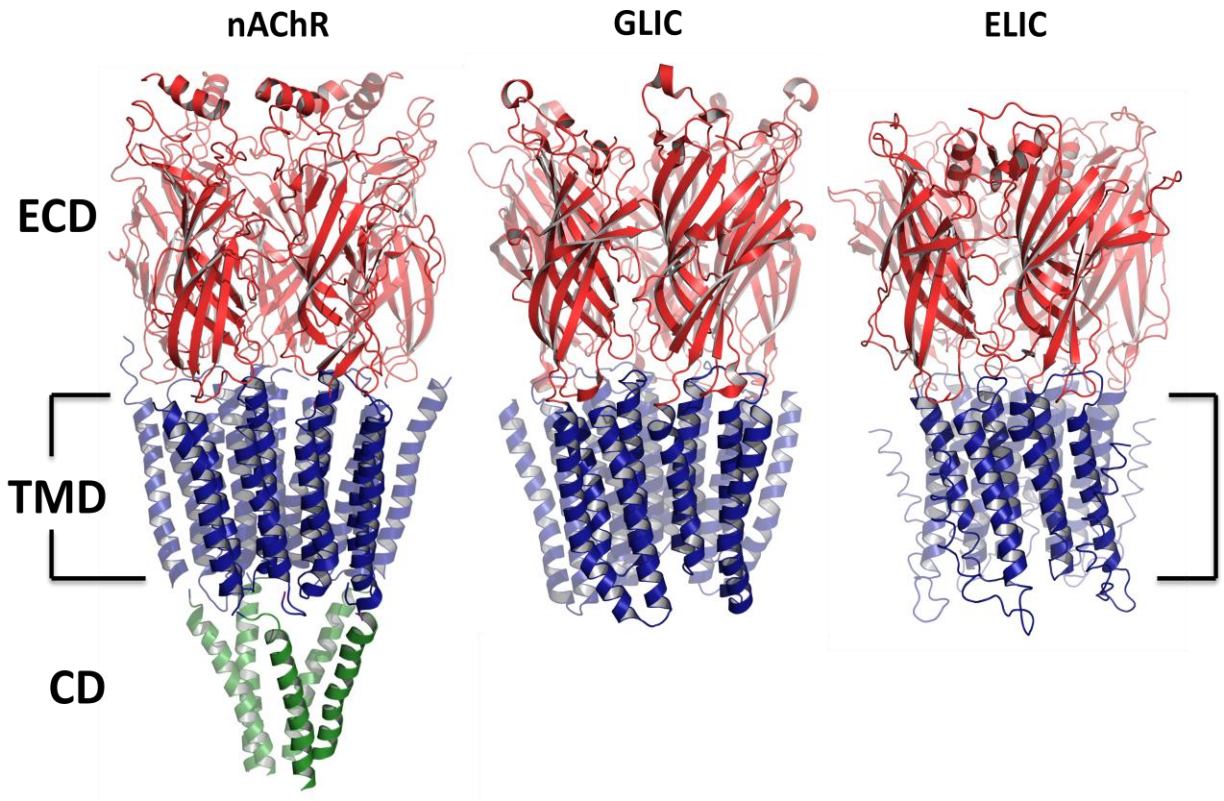

Figure 1.2 - General three-dimensional structure of pLGICs. Structures of the nAChR (PDB: 2BG9), GLIC (PDB: 4HFI), and ELIC (PDB: 2VL0). Each protein is composed of five subunits, homologous or identical, which arrange pseudo-symmetrically about a central axis to form three distinct domains: the extracellular domain (ECD; shown in red), the transmembrane domain (TMD; shown in blue), and, in the eukaryotic pLGIC, the cytoplasmic domain (CD; shown in green).

phenotypically rescued by the fetal γ-subunit allowing for the formation of a functional pentameric receptor leading, ultimately, to proper formation of the neuromuscular junction (Engel et al., 1996b; Milone et al., 1998; Ohno et al., 1997). However, this is not a perfect solution as the γ-subunit is not kinetically identical to the ε-subunit (Mishina et al., 1986), and it also can only rescue about 10% of the wild-type nAChR content at the mature endplate; thus, the synaptic response to ACh at the endplate is considerably reduced with such mutations, even in the ε-subunit, leading to the disease phenotype.

As of 2012, 146 mutations resulting in primary nAChR deficiency have been discovered (Beeson, 2012). Detailed mechanisms of nAChR trafficking and expression are outside the scope of this body of work; however, we will discuss two particular mutations causing nAChR deficiency on the lipid-exposed TMD M4 α-helix of the ε-subunit. The first mutation, 1369delG in *CHRNE*, results in a frameshift at position 457 of εM4, causing 27 missense amino acids followed by a nonsense codon at the C-terminus, while the second mutation results in truncation of εM4 at position 458 (Y458X) (Ealing et al., 2002). Both of these mutations abolish cell-surface expression of the nAChR resulting in a primary nAChR deficiency and revealing a role for the M4 C-terminus in nAChR expression, which is in addition to the role of M4 in function highlighted by the CMS-causing mutation that is the topic of this thesis (αM4 C418W).

1.4.2 Fast-channel syndromes

Fast-channel syndromes are caused by an autosomal recessive mutation in one nAChR subunit allele accompanied by a null, low expressing, or second fast-channel mutation in the second allele (Engel et al., 2003b). Such mutations cause abnormally brief channel opening events, which lead to abnormally rapid decay of the endplate current. In addition, the nAChR is less likely to open in response to physiological concentrations of ACh, which leads to a decrease

in the amplitude of both the synaptic currents and post-synaptic potentials. Interestingly, fast-channel mutations have been discovered in all domains of all muscle-type subunits except for the β1-subunit (Beeson, 2012). As with all other types of CMS, fast-channel syndromes can result in varied severities of the disease phenotype based upon location of the mutation within the nAChR protein and the specific mechanism of disease. The disease phenotype can manifest itself via various disease mechanisms, which include: reducing affinity of the nAChR for ACh (Ohno et al., 1996; Shen et al., 2012a), interfering with the coupling of agonist binding to channel gating (Shen et al., 2003; Shen et al., 2008; Shen et al., 2012b), reducing the stability of receptor gating transition states (Shen et al., 2005), or a combination of these factors (Shen et al., 2003; Shen et al., 2012b; Sine et al., 2002).

As of 2012, 15 fast-channel mutations have been discovered (Beeson, 2012; Figure 1.3). Many fast-channel mutations are found in and around the agonist binding site and reduce affinity for ACh by disturbing one, or many, direct nAChR-ACh interaction(s), indirectly altering the geometry of the ACh binding site, or a combination of both of these factors. A few examples of these types of mutations include: εD175N, which slows ACh association and speeds dissociation (Sine et al., 2002), εP121L and εW55R, which reduce nAChR affinity for ACh in the open state, with almost no effect on affinity in the closed state, profoundly diminishing gating efficiency (Ohno et al., 1996; Shen et al., 2012a), and αV132L, located on the Cys-loop of the ECD, which reduces binding affinity for ACh in addition to altering coupling efficiency (Shen et al., 2003). Other fast-channel mutations affect nAChR function primarily by altering coupling efficiency. For example, αV188M and δL42P, both located in the ECD, interfere with coupling of agonist binding to channel gating (Shen et al., 2008; Shen et al., 2012b), while αV285I, in the TMD, reduces gating efficiency presumably by altering ECD-TMD interface geometry through the

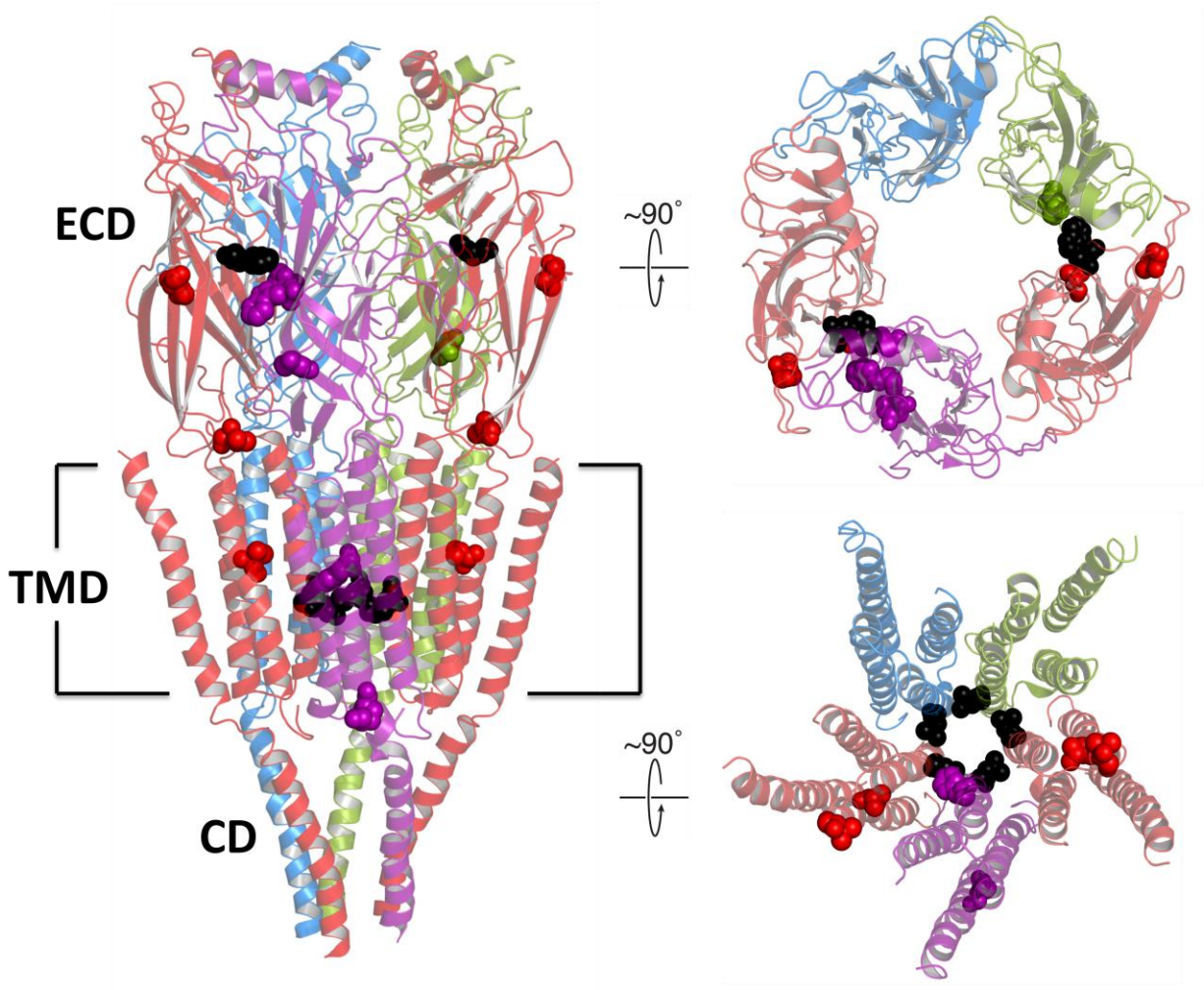

Figure 1.3 - Fast-channel mutations of the nAChR. The cryo-electron microscopy structure of the *Torpedo* nAChR (PDB: 2BG9). The side view of the nAChR (left) shows the three protein domains: ECD, TMD, and CD. The image at the top right is a top-down view of the ECD, and the image at the bottom right is a top-down view of the TMD. Each subunit is colour-coded as follows: α-subunits are shown in red, the β-subunit is shown in blue, the δ-subunit is shown in green, and the ε-subunit is shown in purple. Residues which form part of the agonist-binding site (αTrp149) and channel gate (αLeu251 and equivalent) are shown as black spheres. Residues that have been implicated in fast-channel syndromes are shown as spheres and colour-coded according to the subunit to which they belong. There are no fast-channel mutations in the β-subunit.

TMD interfacial loop, also known as the M2-M3 linker (Wang et al., 1999). Some mutations are pathogenic by a combination of altered ACh affinity and altered coupling efficiency (Shen et al., 2003; Shen et al., 2012b; Sine et al., 2002). Finally, some fast-channel mutations result in attenuated nAChR responses by less common mechanisms, such as: reducing the stability of the diliganded receptor (εN436del in the CD) (Shen et al., 2005), or altering gating kinetics favouring an increased proportion of brief channel openings (εA411P in the CD) (Milone et al., 1998; Wang et al., 2000). In addition, a particularly atypical fast-channel mutation discovered in the TMD channel-lining helix of the ε-subunit, resulting in the deletion of residue F266, does not affect expression or function of the receptor, but rather affects the conductance (Webster et al., 2012). This deletion results in reduced ion flow across the membrane, ultimately affecting depolarization, lending it many similarities with other fast-channel mutations. As of yet, it is the only fast-channel mutation resulting from altered conductance that has been identified in a clinical setting.

As a general rule, fast-channel mutations in the ECD diminish ACh affinity, those in the TMD impair the efficiency of coupling agonist binding to channel gating, and those in the CD of the ε-subunit destabilize channel kinetics (as reviewed by Engel et al., 2003a). Symptoms are generally mild when the main effects of these mutations are on gating efficiency (Wang et al., 1999), they are moderately severe, specifically, when channel kinetics are destabilized to affect gating efficiency (Milone et al., 1998; Wang et al., 2000), and are severe when either affinity for ACh or a combination of affinity and gating efficiency are disturbed (Brownlow et al., 2001; Ohno et al., 1996).

1.4.3 Slow-channel syndromes

Slow-channel syndromes are physiologically opposite from fast-channel syndromes; instead of producing abnormally brief channel openings, they produce abnormally long channel opening events. These long channel openings lead to prolonged synaptic currents and potentials at the post-synaptic membrane. Slow-channel syndromes are most often the result of autosomal dominant mutations in any of the four muscle-type nAChR subunits (Engel et al., 2003b). Further, the disease phenotype can vary from mild to severe, depending upon the location of the mutation within the protein. Such mutations are primarily found in and around the ACh binding site where they directly affect agonist binding, or in and around the channel gate where they directly affect channel gating. Generally, these mutations act by increasing the channel opening rate, decreasing the channel closing rate, and/or increasing affinity for ACh (Engel et al., 1996a; Ohno et al., 1995; Sine et al., 1995). These properties stabilize the open state of the nAChR and destabilize the closed state, leading to a prolonged synaptic response.

The clinical consequences produced by slow-channel mutations are not as intuitively interpreted as those produced by primary nAChR deficiency and fast-channel syndromes where disease results from a disruption of the synaptic response, causing a loss-of-function. In such cases, the pre-synaptic signal is not efficiently translated into muscular contraction, leading to weakness and motor difficulties (among other symptoms). However, slow-channel mutations produce nAChRs with an increased response to physiological levels of ACh, resulting in a gain-of-function. Thus, what leads to the disease phenotype in such slow-channel syndromes? In fact, these prolonged, and sometimes spontaneous, opening events caused by slow-channel mutations lead to: a depolarization block of the post-synaptic muscle cell resulting from the slow decay of synaptic potential (Engel et al., 1982), a repetitive compound muscle action potential

resulting from the potential at the post-synaptic cell outlasting the absolute refractory period of the muscle fibre (Milone et al., 1997), excessive accumulation of calcium, leading to cationic overload (Engel et al., 1996a), and finally, myopathy of the post-synaptic cell, which is characterized primarily by degeneration of the junctional folds and mainly attributed to the excess accumulation of calcium (Gomez et al., 1997). This last symptom in particular is of clinical significance, as the nAChRs cluster on these junctional folds in order to relay the pre-synaptic signals. Slow-channel syndromes are progressive and, if the disease phenotype is severe enough, can lead to muscle cell death, severely impairing patients.

As of 2012, 25 slow-channel mutations have been discovered (Beeson, 2012; Figure 1.4). A large proportion of slow-channel mutations are found on the TMD channel-lining helices, including: αT254I, αV249F, βV266M, βL262M, δS268F, εL269F, εV265A, and εT264P (as reviewed by Engel et al., 2003a). Mutations at this location generally show prolonged openings and some exhibit an abnormally high rate of spontaneous openings, presumably due to the destabilization of the closed channel pore (Croxen et al., 1997; Gomez et al., 1996; Milone et al., 1997; Ohno et al., 1995). One slow-channel mutation has even been reported to activate in the presence of serum concentrations of choline (Zhou et al., 1999). Other slow-channel mutations located within the ECD (εL78P and αV156M), or at the ECD-TMD interface (αS269I and εL221F) show prolonged openings, presumably due to increased gating efficiency (Croxen et al., 1997; Croxen et al., 2002). Additionally, two mutations, one near the ACh binding site, αG153S (Sine et al., 1995), and the other located in the TMD, αN217K (Wang et al., 1997), prolong openings by significantly decreasing the rate of agonist dissociation, leading to repeated opening events during a single ACh occupancy. Generally, the clinical consequences of mutations in the ECD are less severe than those in the TMD (as reviewed by Engel et al., 2003a); owing to the

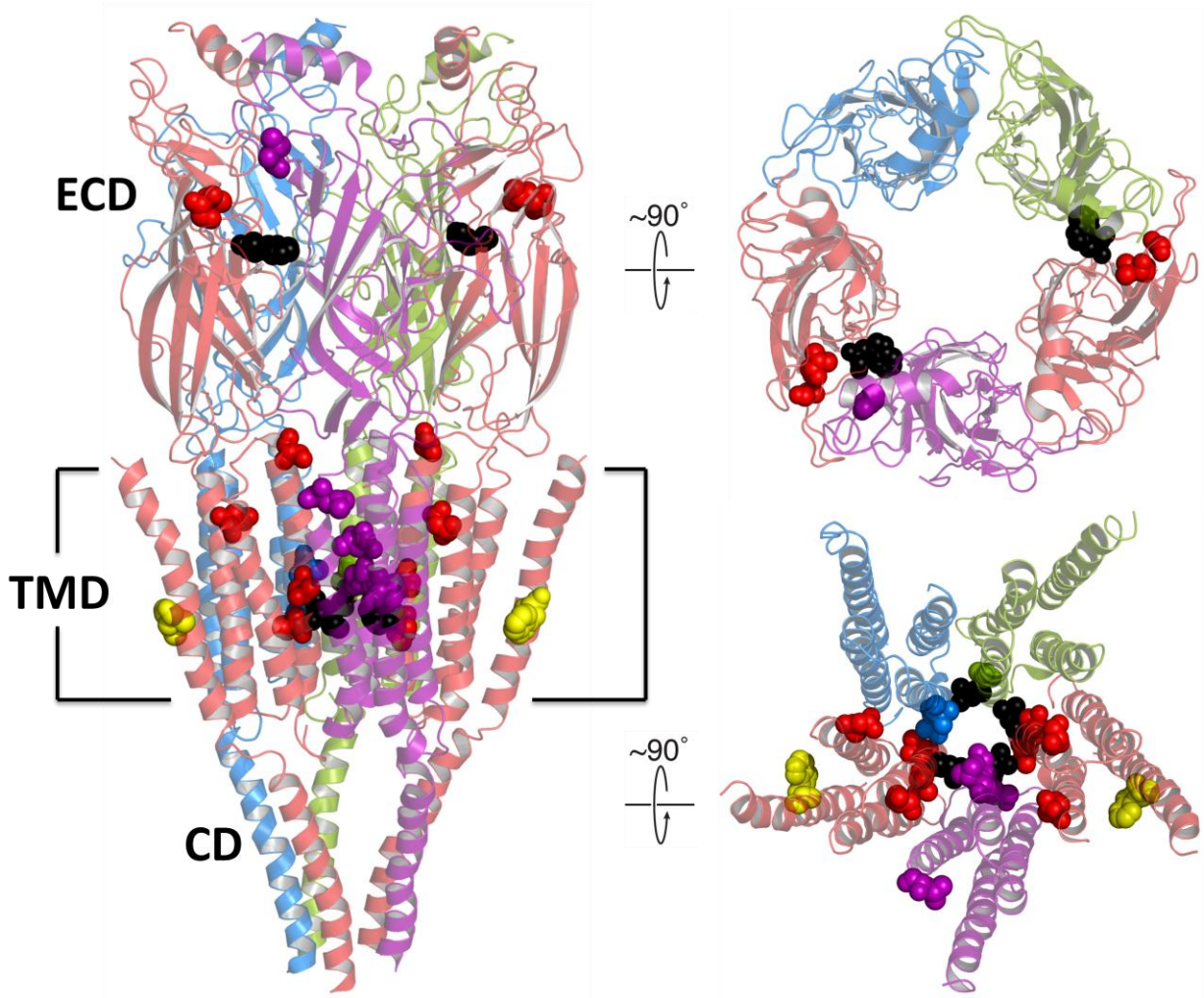

Figure 1.4 - Slow-channel mutations of the nAChR. The cryo-electron microscopy structure of the *Torpedo* nAChR (PDB: 2BG9). The side view of the nAChR (left) shows the three protein domains: ECD, TMD, CD. The image at the top right is a top-down view of the ECD, and the image at the bottom right is a top-down view of the TMD. Each subunit is colour-coded as follows: α-subunits are shown in red, the β-subunit is shown in blue, the δ-subunit is shown in green, and the ε-subunit is shown in purple. Residues which form part of the agonist-binding site (αTrp149) and channel gate (αLeu251 and equivalent) are shown as black spheres. Residues that have been implicated in slow-channel syndromes are shown as spheres and colour-coded according to the subunit to which they belong. The αM4 C418W mutation is shown as yellow spheres.

possibility that TMD mutations, located within or near the channel, can render the channel so leaky that it opens in the absence of agonist, causing severe phenotypes (Engel et al., 1996a; Milone et al., 1997).

All slow-channel mutations are similar in that they are located within the ECD where they generally increase affinity for ACh, at the ECD-TMD interface where they generally increase gating efficiency, or are located within or near the channel, where they stabilize the open channel pore or destabilize the closed channel pore. However, a peculiar slow-channel mutation, discovered in 2006, was identified at the lipid face of the highly lipid-exposed αM4 TMD α-helix, at the approximate centre of the bilayer (Shen et al., 2006; Figure 1.5). A Cys residue at position 418 is substituted by a Trp, leading to a ~20-fold gain-of-function. αM4 C418W promotes functional states of the nAChR with high affinity for agonist, such as the open state, but it has no effect on the association or dissociation of ACh in the resting nAChR. Shen *et al* (2006) found that the increased response seen with αM4 C418W was not correlated to increased cell-surface expression, but instead concluded that the pronounced slow-channel properties of the C418W-mutant receptor were due to enhanced gating efficiency, likely caused by altered interactions between M4 and the lipids. How exactly a mutation at the lipid-face of αM4 is able to increase gating efficiency from the periphery of the protein, where it interacts directly with none of the critical gating structures (ACh binding site, ECD-TMD interface, channel gate) will be the topic of my research. Before we can elucidate this mechanism, I must first delve deeper in the structural specifics of the nAChR as well its gating mechanism and conformational changes. Secondly, to understand how a subtle change at the protein-lipid interface could affect the gating mechanism and enhance gating efficiency, I will next explore

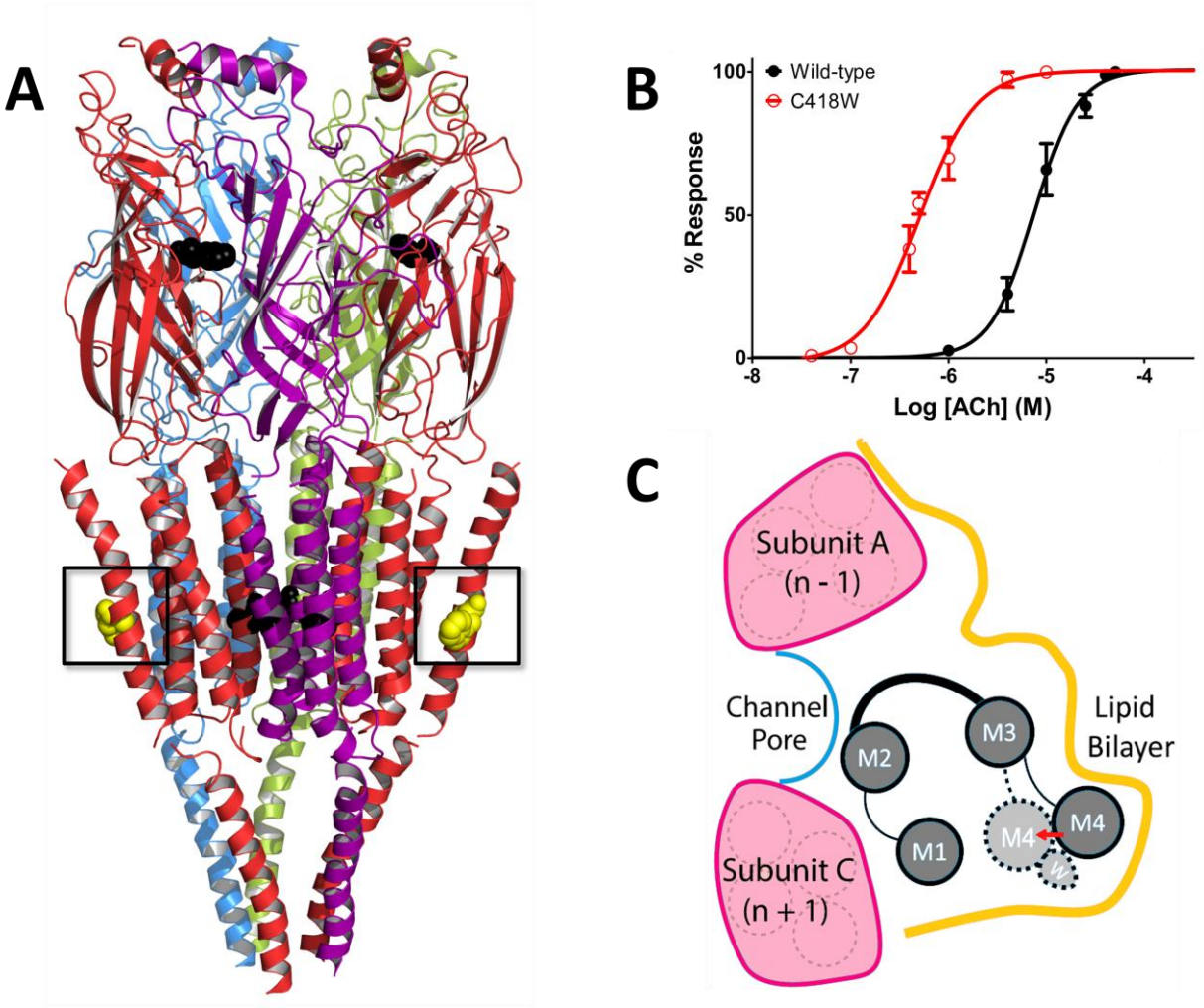

Figure 1.5 - αM4 C418W alters nAChR-lipid interactions and potentiates channel function. (A) The cryo-electron microscopy structure of the *Torpedo* nAChR (PDB: 2BG9). The side view of the nAChR where each subunit is colour-coded as follows: α-subunits are shown in red, the β-subunit is shown in blue, the δ-subunit is shown in green, and the ε-subunit is shown in purple. Residues which form part of the agonist-binding site (αTrp149) and channel gate (αLeu251 and equivalent) are shown as black spheres. The αM4 C418W mutation is shown as yellow spheres. (B) Averaged dose response curves for the wild-type and C418W mutant showing that C418W potentiates channel function (C) Schematic, adapted from Carswell et al., 2015b, proposes mechanism whereby altered interactions between Trp418 and the lipids enhance interactions between M4 and M1/M3.

nAChR lipid sensitivity and the role of M4 as a lipid sensor and allosteric modulator of nAChR function.

1.5 The nicotinic acetylcholine receptor

nAChRs are expressed in both neuronal and non-neural cells, such as muscle, immune cells, lymphocytes, lung epithelium, etc. In vertebrates, there exist a total of 17 different subunit genes: 10 α-subunits (α1-α10), four β-subunits (β1-β4), and one of each δ-, ε-, and γ-subunit. Although the 17 subunits could theoretically form a vast multitude of homopentameric and heteropentameric receptor combinations, not all subunits are compatible. The α1-, β1-, δ-, and ε/γ-subunits form a heteropentameric nAChR in muscle cells where the fetal γ-subunit is replaced by the ε-subunit in adult muscle cells. The α7 and α8 subunits can form homopentamers by themselves or heteropentamers in combination; similarly, α9 and α10 subunits can also form homopentamers by themselves or heteropentamers in combination. The remaining α2-α6 and β2-β4 subunits form a range of complex heteropentamers, involving two or three α-subunits, and are expressed mostly in neurons (as reviewed by Le Novère et al., 2002). Heteropentameric nAChRs generally have two or three ACh binding sites, whereas, homopentameric nAChRs have five; however, binding of ACh to all five orthosteric sites is not required for full activation of homopentameric receptors. Finally, not all subunits contribute equally, if at all, to the ACh binding sites. The α1- α4- and α6-subunits all contribute to the principal portion of the ACh binding site, while β2-, β4-, δ-, γ-, and ε-subunits all contribute to the complementary portion, and the α5-, β1- and β3-subunits do not contribute at all.

Although all nAChR subunits are homologous, they are not structurally or functionally equivalent; thus, nAChRs composed of different subunits have variable electrical properties (i.e. conductance, ion selectivity, and rectification), pharmacological properties (i.e. affinities for

agonists, competitive antagonists, and allosteric effectors), and different kinetics of activation and desensitization (as reviewed by Le Novère et al., 2002). In particular, the kinetics of activation and desensitization are crucial in shaping the physiological response to ACh (Jones and Westbrook, 1996), and different nAChR subtypes have indeed been shown to exhibit varied desensitization kinetics. For example, α2β2 nAChRs do not desensitize, even in response to very high ACh concentrations, while α7 nAChRs desensitize very quickly (Chavez-Noriega et al., 1997). Not all nAChR subunits are expressed in all cell types; thus, one could conclude that subunits expressed uniquely in specialized tissues are critical to the synaptic response at these locations. However, this is not a steadfast rule, as subunit redundancies throughout the brain and muscle have been revealed (Duclert and Changeux, 1995; Le Novère et al., 2002; Xu et al., 1999). Nonetheless, subunits expressed in specialized tissues, such as the muscle, assemble unique pentamers, which shape and fine-tune the synaptic response according to specialized requirements that cannot be accommodated by other nAChR subtypes.

1.5.1 The muscle-type nAChR - structural specifics

The muscle-type nAChR is the prototypic member of the pLGIC superfamily and was initially discovered at the beginning of the 20th century (Langley, 1905). The muscle-type nAChR was first purified in the 1970s from the electric fish, *Torpedo* (Changeux et al., 1970) and was observed for the first time at low resolution three years later by electron microscopy (Cartaud et al., 1973). Since then, technology has significantly advanced, allowing for the production of our current structural model of the muscle-type nAChR solved by cryo-electron microscopy at a resolution of 4 Å (Unwin, 2005). This structure shows that the muscle-type nAChR is a heteropentamer composed of four different subunits with a stoichiometry of 2:1:1:1 for α1:β1:δ:γ/ε, where the γ-subunit is replaced by ε in the adult nAChR. Note, for the purpose

of this thesis, I will refer to the α1 and β1 subunits as α and β for the sake of simplicity. As mentioned previously, these subunits arrange pseudo-symmetrically about a central axis to form the three distinct domains: ECD, TMD, and CD.

1.5.1.1 The extracellular domain (ECD)

The ECD is composed of roughly 200 amino acid residues, forming first a short N-terminal α-helix followed by 10 β-strands, which assemble into a twisted β-sandwich structure (Figure 1.6). The inner β-sheet of the β-sandwich is composed of six β-strands: β1, β2, β3, β5, β6, and β8; while the outer sheet is composed of the remaining four β-strands: β4, β7, β9, and β10. The ECD of the muscle-type nAChR has two orthosteric ACh binding sites, the first is located at the subunit interface between α-δ and the second between α-ε/γ. Each binding site has a unique binding affinity for ACh, where the α-δ orthosteric site binds ACh with a high affinity, approximately 5-fold higher as compared to the α-ε site (Sine, 2002). High affinity at the first site may act as a priming mechanism for nAChR activity; whereas, low affinity at the second site might allow rapid termination of the post-synaptic response (Jackson, 1989). The α-subunit composes the principal face of each binding site, contributing three loops: Loops A, B, and C. Conversely, the δ- and ε/γ-subunits compose the complementary face of the binding sites, each also contributing three loops: Loop D, E, and F. All six of these loops are composed of key aromatic, polar, and charged residues, which form critical stabilizing interactions with the ammonium group of ACh in the binding pocket (Brejc et al., 2001; Changeux and Edelstein, 2001; Changeux and Taly, 2008; Hansen et al., 2005; Sine, 2002). Further, α-subunits possess two highly conserved Cys residues within this orthosteric site, a feature that distinguishes α from non-α subunits, which form a disulphide bridge that is also involved in ACh binding and

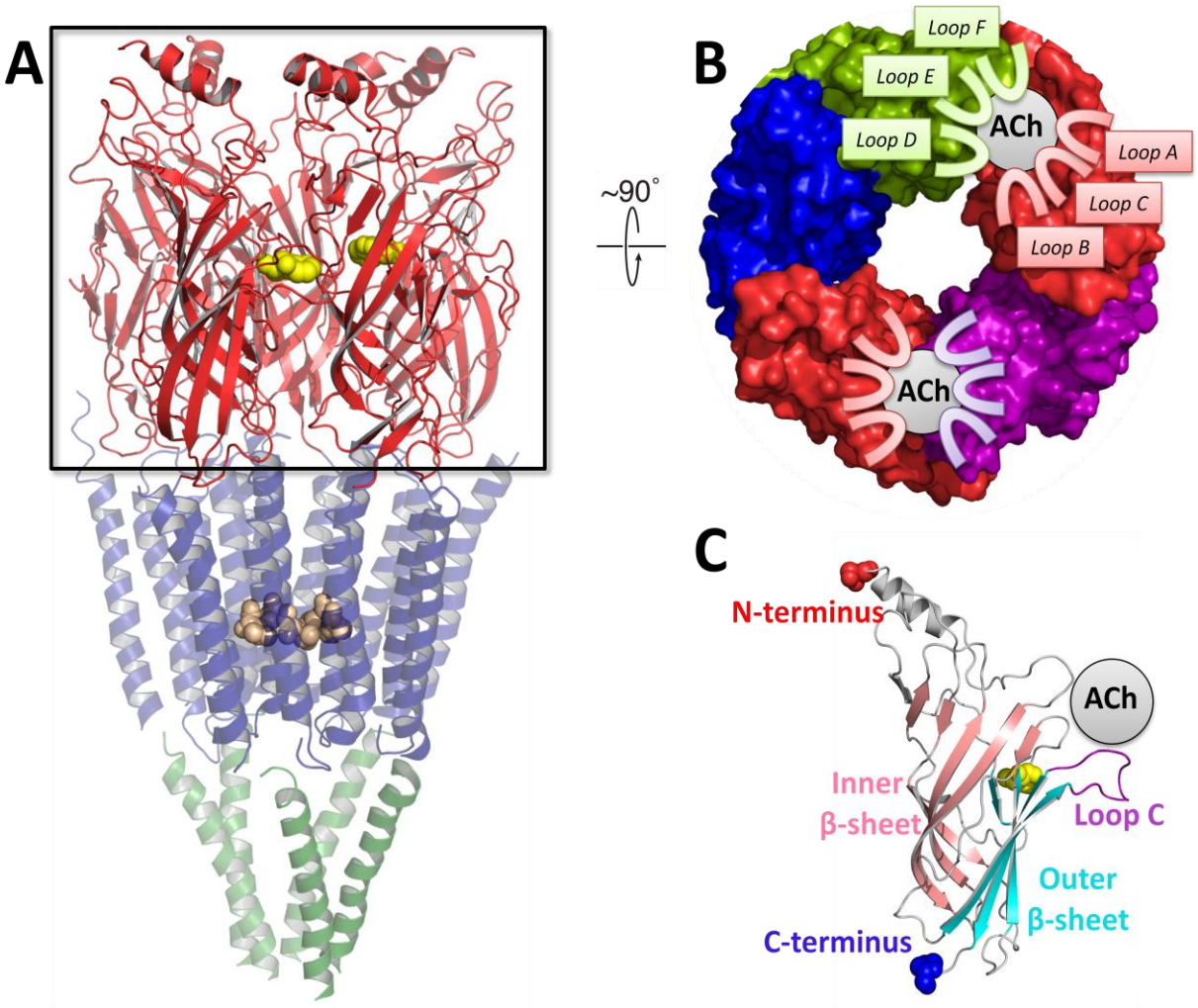

Figure 1.6 - The extracellular domain of the nAChR. The cryo-electron microscopy structure of the *Torpedo* nAChR (PDB: 2BG9). (A) The side view of the nAChR where the ECD is shown in red, the TMD is shown in blue, and the CD is shown in green. Residues which form part of the agonist-binding site (αTrp149) and channel gate (αLeu251 and equivalent) are shown as yellow and tan spheres, respectively. (B) Figure showing a surface representation of the top-down view of the ECD, where the α-subunits are shown in red, the β-subunit is shown in blue, the δ-subunit is shown in green, and the ε-subunit is shown in purple. The two ACh binding sites between subunits are shown and demonstrate that the α-subunit contributes three loops (Loop A-C) to the principal face of the binding site, while the δ/ε-subunits contribute three loops (Loops D-F) to the complementary face. (C) Tertiary fold of a single nAChR subunit where the important structures are colour-coded as indicated in the image.

recognition. Binding of ACh is thought to trigger the movement of Loop C inward, capturing ACh within the binding site, and initiating the gating transition (Celie et al., 2004; Hansen et al., 2005). Interestingly, although the β-subunit does not form an orthosteric binding site, it could potentially form a pseudo-orthosteric binding site where allosteric modulators have been shown to affect pLGIC function (Boileau et al., 1999).

1.5.1.2 The transmembrane domain (TMD)

The TMD is composed of roughly 150 amino acid residues, where each subunit contributes four transmembrane α-helices: M1-M4 (Figure 1.7). The M2 α-helices form the ion channel pore, M1 and M3 assemble around the M2 helices to shield the channel pore from the hydrophobic lipid environment, and M4 is located at the periphery of each subunit where it forms the majority of the protein-lipid interface. The nAChR channel is cation-selective, but not very restrictive in terms of ion size, allowing passage of most cations (sodium, potassium, calcium, etc.). This cation selectivity is conferred by three rings of polar or negatively charged residues formed by the M2 helices: one on the intracellular portion of the channel, formed by αGlu241 (and equivalent), and two at the extracellular portion of the channel, formed by αGlu262 (and equivalent) and αSer266 (and equivalent), respectively (as reviewed by daCosta and Baenziger, 2013). The narrowest pore constriction in the apparent resting-state, with an estimated diameter of 6 Å (Huang et al., 1978), is located around the midpoint of each M2 α-helix and is deemed as the "hydrophobic gate" of the ion channel. This gate is formed by two rings of conserved hydrophobic residues: αLeu251 (and equivalent) and αVal255 (and equivalent). Although sodium and potassium ions are only approximately 2.5 Å in diameter, the presence of a surrounding hydration shell increases this diameter substantially to about 8 Å. Thus, it would be too energetically unfavourable for these ions to lose their hydration shell in

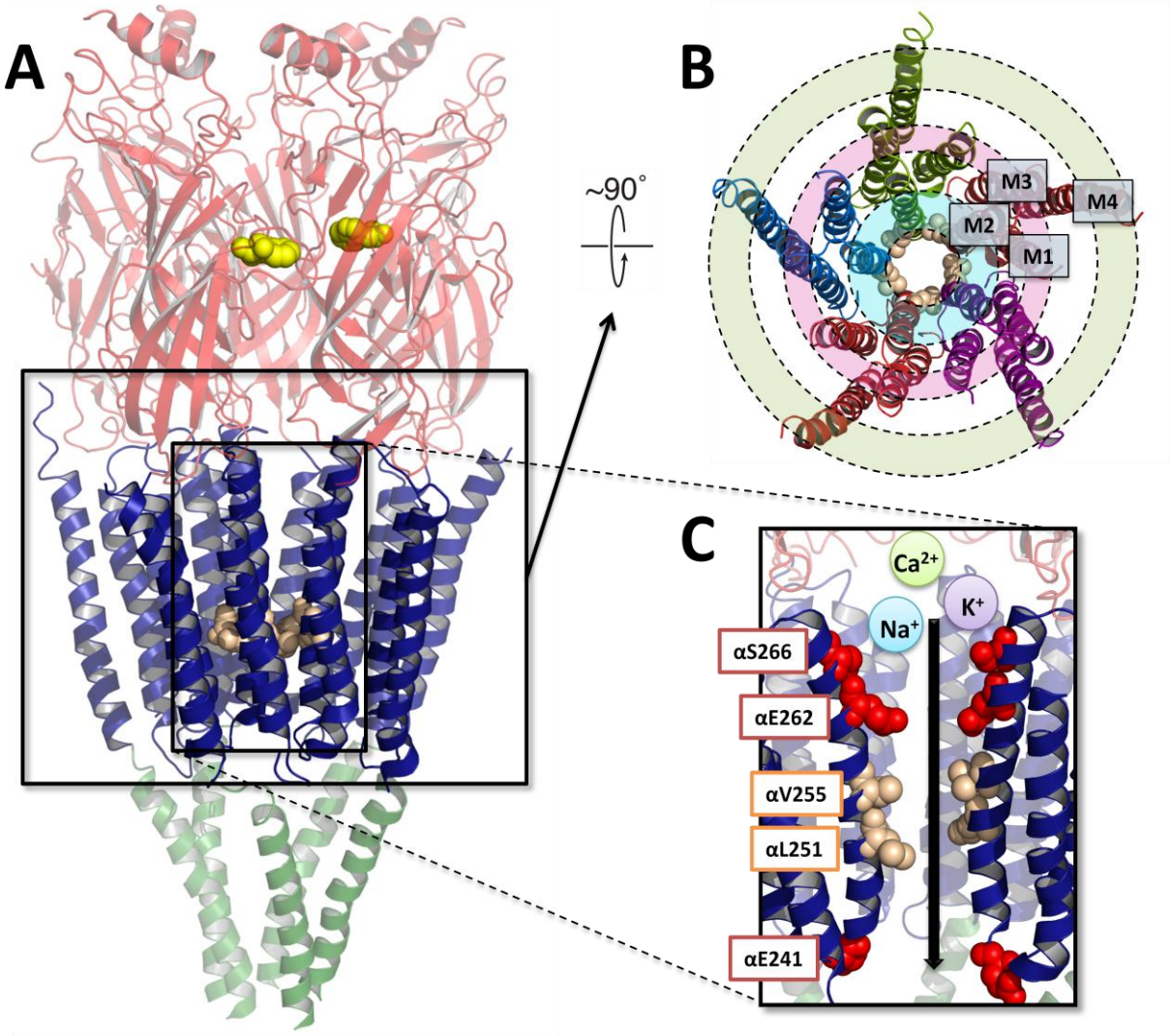

Figure 1.7 - The transmembrane domain of the nAChR. The cryo-electron microscopy structure of the *Torpedo* nAChR (PDB: 2BG9). (A) The side view of the nAChR where the ECD is shown in red, the TMD is shown in blue, and the CD is shown in green. Residues which form part of the agonist-binding site (αTrp149) and channel gate (αLeu251 and equivalent) are shown as yellow and tan spheres, respectively. (B) Figure showing a top-down view of the TMD, where the α-subunits are shown in red, the β-subunit is shown in blue, the δ-subunit is shown in green, and the ε-subunit is shown in purple. Each subunit contributes four α-helices to the TMD, which are labelled M1-M4 and form three concentric circles of α-helices. (C) Cross-section of the TMD showing the channel pore. Residues involved in forming the cation selectivity filter and hydrophobic gate are shown as red and tan spheres, respectively.

order to pass through the "hydrophobic gate" formed by αLeu251 and αVal255 in the resting-state (Beckstein and Sandom, 2006; Ivanov et al., 2007; Miyazawa et al., 2003). Interestingly, although complex movements of the M2 helices during gating may only increase the pore diameter by about 1 Å (Unwin and Fujiyoshi, 2012), these movements also unmask polar residues, rendering the pore more hydrophilic, and making it more energetically favourable for the passage of cations. Additionally, in accordance with the "hydrophobic gate" hypothesis, mutations which render the pore more hydrophilic at the level of the channel gate do in fact render the channel more permeable to ions (Labarca et al., 1995).

1.5.1.3 The ECD-TMD interface

The interface between the ECD and TMD forms an important network of interacting loops, which communicate structural changes from the ECD, due to ACh binding, to the ion pore in the TMD, resulting ultimately in opening of the channel gate (Figure 1.8). Molecular complementarity between the ECD and TMD is critical for effectively translating agonist binding into channel gating (Bouzat et al., 2004), for the formation of fast gating kinetics (Grutter et al., 2005), and accords each pLGIC its unique gating characteristics, such as open channel lifetime and rate of desensitization (Bouzat et al., 2008; as reviewed by Bouzat, 2012). The ECD and TMD are covalently linked through the extracellular β10-strand and the transmembrane M1 α-helix; this linkage at the ECD-TMD interface is deemed pre-M1. Further, the ECD contributes three loops to this interface: the β1-β2 loop, the β6-β7 loop (also known as the Cys-loop in eukaryotic pLGICs), and the β8-β9 loop; while the TMD contributes one loop, known as the M2-M3 linker. The C-terminus of M4 (post-M4) has also been proposed to contribute to this ECD-TMD interface (daCosta and Baenziger, 2009). In the *Torpedo* nAChR structure, the β1-β2 and Cys-loop appear to form a "vice-grip" structure around the M2-M3

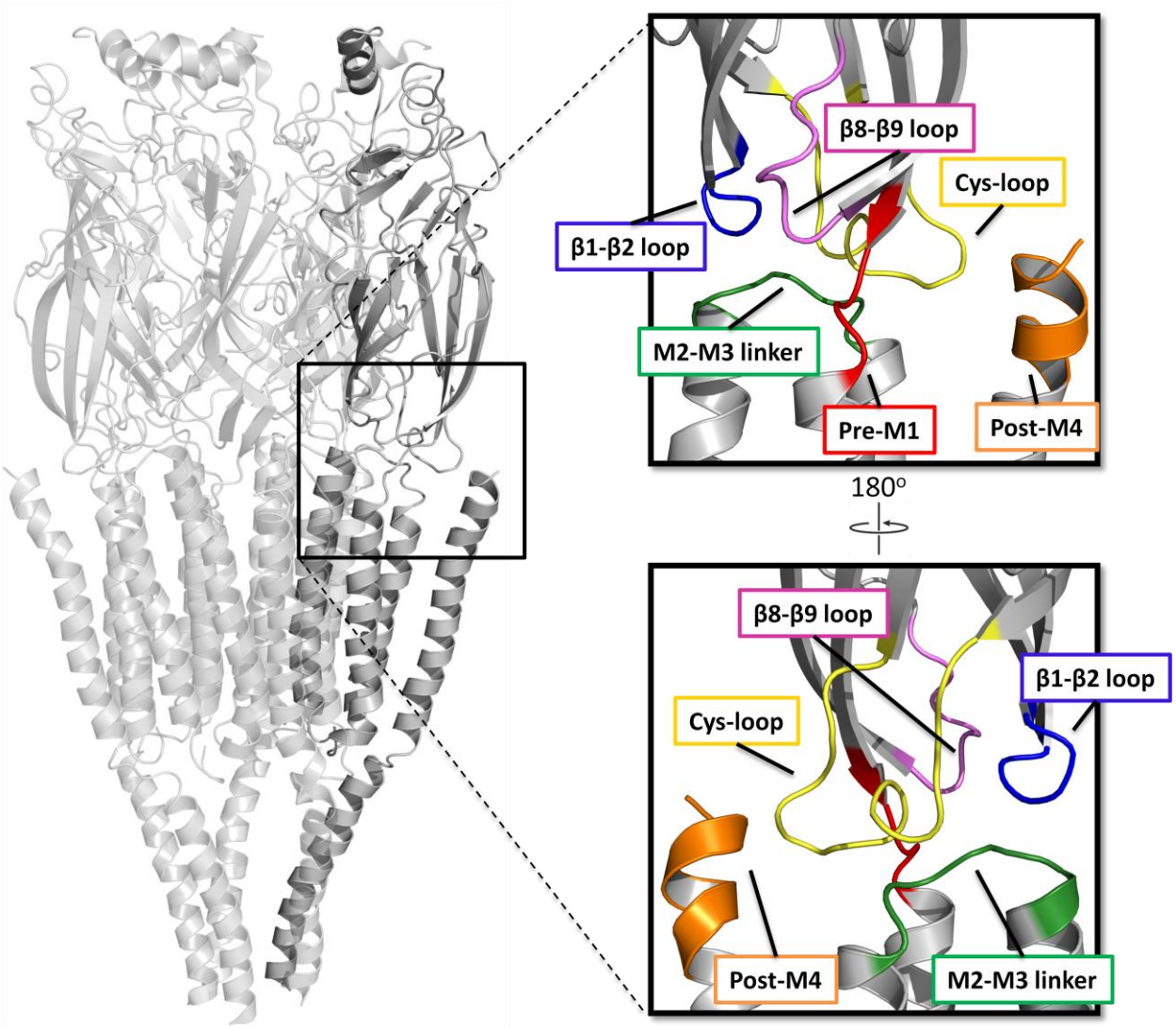

Figure 1.8 - The interface between the extracellular and transmembrane domains. The cryo-electron microscopy structure of the *Torpedo* nAChR (PDB: 2BG9). Each important structure at the interface between the ECD and TMD has been colour-coded as follows: pre-M1 is shown in red, the M2-M3 linker is shown in green, the β1-β2 loop is shown in blue, the β8-β9 loop is shown in pink, the Cys-loop is shown in yellow, and post-M4 is shown in orange.

linker, suggesting potentially critical interactions at this location, which would energetically link the ECD to the TMD (Unwin, 2005). Additionally, all structures at the ECD-TMD interface have been shown to be involved in nAChR channel gating: pre-M1 (Purohit and Auerbach, 2007), the β1- β2 loop (Lee and Sine, 2005; Lee et al., 2008), the Cys-loop (Jha et al., 2007; Lee et al., 2009), the β8-β9 loop (Hibbs et al., 2006; Law et al., 2005; Lyford et al., 2003), and the M2-M3 linker (Campos-Caro et al., 1996; Castillo et al., 2006; Grosman et al., 2000b, Jha et al., 2007); although, the roles of the β8-β9 loop and post-M4 in the overall gating mechanism are less understood (as reviewed by Sine and Engel, 2006). Furthermore, in addition to participation in gating, the Cys-loop has also been implicated in nAChR assembly (Fu and Sine, 1996; Green and Wanamaker, 1997). We will discuss in further detail the gating mechanism involving loops at this interface in section 1.5.2.

1.5.1.4 The cytoplasmic domain (CD)

The length of the CD is variable between each muscle-type nAChR subunit. The structure of the CD is not well-resolved in the 4 Å *Torpedo* nAChR structure (Unwin, 2005); however, we do observe the presence of an amphipathic α-helix immediately preceding M4. Although the role of the CD is not abundantly clear within the pLGIC superfamily, it has been shown to be involved in attachment to the cytoskeleton, it contains phosphorylation sites which may be important for desensitization, and, uniquely, the CD of the nAChR ε-subunit contains residues involved in gating kinetics and fidelity (Milone et al., 1998; Wang et al., 2000). Further, in the 5-HT_3 receptor, the CD is involved in conductance of ions (Kelley et al., 2003).

1.5.2 The nAChR gating mechanism

As mentioned previously, muscle-type nAChRs bind two molecules of ACh in the ECD, which leads to opening of a cation-selective channel within the TMD. The orthosteric binding

site is located approximately 50 Å away from the channel gate, leading to the central question: how does agonist binding couple to channel gating? Many studies suggest that the ECD-TMD interface acts as a coupling region and is able to translate quaternary changes from the ECD into quaternary changes of the TMD through the conformational modification of five key interfacial structures: pre-M1, the β1-β2 loop, the Cys-loop, the β8-β9 loop, and the M2-M3 linker. We will next explore interactions between these interfacial loops and their importance to the overall gating mechanism.

Gating is initiated by binding of the agonist, ACh, within two aromatic-rich binding pockets in the ECD. This binding event causes Loop C to change from an "uncapped" to "capped" conformation, which traps ACh within the orthosteric binding site (Gao et al., 2005, 2006; Hansen et al., 2005; Law et al., 2005). Loop C is connected directly to pre-M1 via the β10 strand; thus, movement of pre-M1 may represent the first conformational change at the ECD-TMD interface, specifically in the α-subunit. However, other β-strands are also directly connected to loops that form the binding site, so it is possible that, in response to ACh binding, the entire ECD of the α-subunit moves in concert, thus changing the conformation of many or all ECD interfacial loops at the same time.

Upon analysis of the *Torpedo* nAChR structure and subsequent experimental studies, Lee and Sine (2005) identified an electrostatic salt bridge interaction between the conserved, positively-charged Arg209 on pre-M1 and the negatively-charged Glu45 on the β1-β2 loop. This interaction energetically links pre-M1 with the β1-β2 loop and was determined to be critical to channel gating. In addition, the Unwin (2005) nAChR structure shows that the β1-β2 loop and the Cys-loop form a "vice-grip" around the M2-M3 linker, highly suggestive of possible interactions between these three structures. Interactions at this location could be critical to the

channel gating mechanism, could ultimately link the ECD to the TMD, and could possibly be affected by the pre-M1 interaction with the β1-β2 loop. Indeed, Miyazawa *et al* (2003) had already proposed a "pin-in-socket" interaction functionally linking the β1-β2 loop with the M2-M3 linker via the aliphatic residue, Val46 (the pin), on the β1-β2 loop, and the respective aliphatic and polar residues, Pro272 and Ser269, on the M2-M3 linker (forming the socket). Later studies confirmed that these three residues were indeed energetically coupled and essential for rapid and efficient channel gating (Chakrapani et al., 2004; Jha et al., 2007; Lee and Sine, 2005); thus, this "pin-in-socket" interaction, along with the electrostatic linkage between pre-M1 and the β1-β2 loop were deemed as the "principal pathway" in muscle-type nAChR channel gating (Lee and Sine, 2005). This gating mechanism was revised a few years later with the addition of a second "pin-in-socket" interaction involving Pro272 of the M2-M3 linker (the pin) with Val46 of the β1-β2 loop and Val132 of the Cys-loop (forming the socket), implicating the Cys-loop and highlighting its functional role in gating (Lee et al., 2008; Figure 1.9).

Later, additional Cys-loop residues (Phe135 and Phe137) were identified as forming a coupled tetrad with residues of both pre-M1 (Leu210) and the M2-M3 linker (Leu273) (Lee et al., 2009; Figure 1.9). These interactions, dubbed the "Cys-loop pathway", were found to be critical to channel gating and, interestingly, not energetically coupled to any components of the "principal pathway", suggesting that the two pathways are separate but equally important to the overall gating mechanism (Lee et al., 2009). Further, the β1-β2 loop and the Cys-loop were shown to change conformation at the same time during gating, suggesting that the two pathways may act in concert (Jha et al., 2007).

Features of the gating mechanism proposed in the muscle-type nAChR α-subunit are not all consistently observed amongst receptors within the pLGIC superfamily, which may suggest

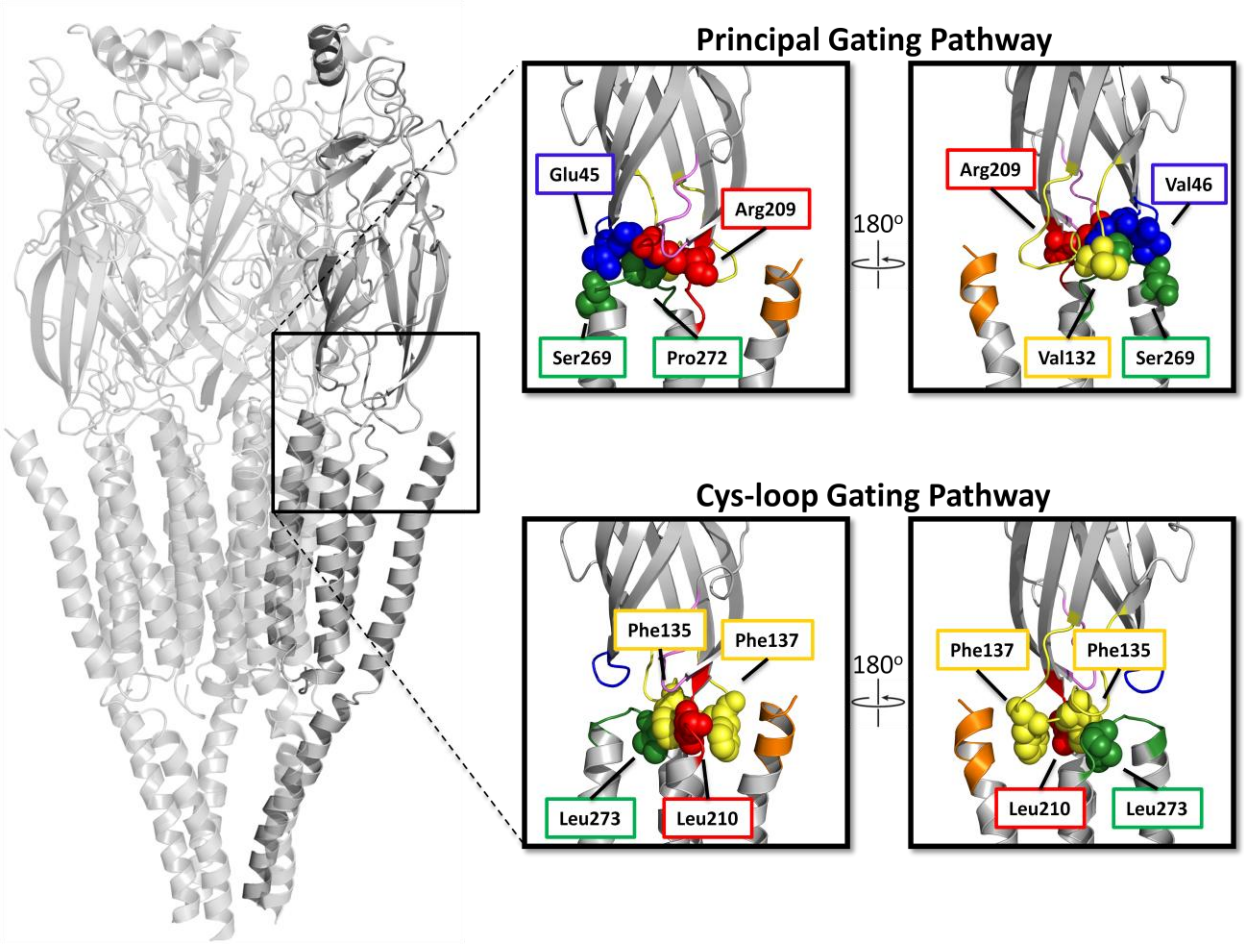

Figure 1.9 - Residues involved in the principal and Cys-loop gating pathways. The cryo-electron microscopy structure of the *Torpedo* nAChR (PDB: 2BG9). Each important structure at the interface between the ECD and TMD has been colour-coded as follows: pre-M1 is show in red, the M2-M3 linker is shown in green, the β1-β2 loop is shown in blue, the β8-β9 loop is shown in pink, the Cys-loop is shown in yellow, and post-M4 is shown in orange. Residues involved in each pathway are shown as spheres and colour-coded according to which ECD-TMD interfacial structure they belong.

that members of different subfamilies have slightly different gating mechanisms. For example, although the proposed electrostatic linkage in the nAChR, Arg209-Glu45, is conserved in $GABA_{A/C}$ receptors (Wang et al., 2007), it does not appear to exist in the 5-HT_3 receptor (Price et al., 2007). Further, while "pin-in-socket" interactions link the β1-β2 loop, Cys-loop, and M2-M3 linker in the nAChR, charged interactions instead serve to link these same loops in the anionic $GABA_A$ receptor and are critical to its gating mechanism (Kash et al., 2004). Comparatively, *cis-trans* isomerization of the conserved Pro residue on the M2-M3 linker has been proposed as critical to the gating mechanism in the 5-HT_3 receptor, while this hypothesis has been rejected many times over in the nAChR (Jha et al., 2007; Lee et al., 2008; Lummis et al., 2005). Amongst other evidence, the isomerization timescale is too slow to be compatible with fast gating in the nAChR; whereas, *cis-trans* isomerization of this Pro in the 5-HT_3 does seem to be compatible with its slow activation, although there is no absolute consensus on this point (Paulsen et al., 2009).

Considering all of the experimental evidence, various stabilizing interactions between pre-M1, the β1-β2 loop, the Cys-loop, and the M2-M3 linker act jointly to couple agonist binding to channel gating. Additional interactions including the β8-β9 loop and post-M4 may be involved in modulating this process, although their roles, as of yet, remain unclear. Therefore, the overall mechanism suggests that agonist binding causes concerted movement of the ECD interfacial loops, which results in displacement of the M2-M3 linker. Movement of the M2-M3 linker couples directly to movement of the channel-lining M2 α-helices (Yuan et al., 2016); thus, the displacement of the M2-M3 linker by movement of the ECD interfacial loops leads directly to dilation of the channel pore, allowing flow of cations. These proposed movements of the M2-M3 linker are conserved in GLIC, GlyR, and a glutamate-activated chlorine channel (GluCl),

where the M2-M3 linker is shown to interact with the bottom of the ECD and, during gating, undergo a large outward translation (as reviewed by Nemecz et al., 2016). Upon deactivation, the ion channel closes, relaxing the conformation of the M2-M3 linker back to its resting state, subsequently causing the ECD to relax, and resulting in the release of ACh from the orthosteric binding site to terminate the response.

1.5.3 nAChR structural conformations

As mentioned previously, muscle-type nAChRs bind ACh, which is released from the pre-synaptic neuron, leading to a channel opening event, which, if the signal is sufficient, may depolarize the post-synaptic membrane leading to muscular contraction. To effectively communicate the pre-synaptic signal and modulate the post-synaptic response, nAChRs interconvert between four structurally and functionally unique states: resting/closed, activated/open, desensitized, and the most recently characterized uncoupled state (daCosta and Baenziger, 2009; Figure 1.10). In the resting state, the ion channel is closed and affinity for ACh is relatively low (K_d = 800 nM; Boyd and Cohen, 1980); whereas, in the activated state, affinity for ACh increases, stabilizing the open channel conformation, and allowing flow of cations down their electrochemical gradient into the muscle cell. The desensitized state occurs in the presence of high ACh concentrations and/or prolonged agonist exposure (Katz and Thesleff, 1957; Papke et al., 2011) and is characterized by high affinity ACh-binding (K_d = 3-5 nM; Boyd and Cohen, 1980), and a channel that is not permeable to ions. Additionally, there exist two desensitized states: a fast desensitized state where interconversion between open and desensitized states occurs within hundreds of milliseconds, and a slow desensitized state from which recovery can take seconds (Sakmann et al., 1980). Finally, the newly discovered uncoupled state is characterized by a resting state-like affinity for ACh where agonist binding does not elicit

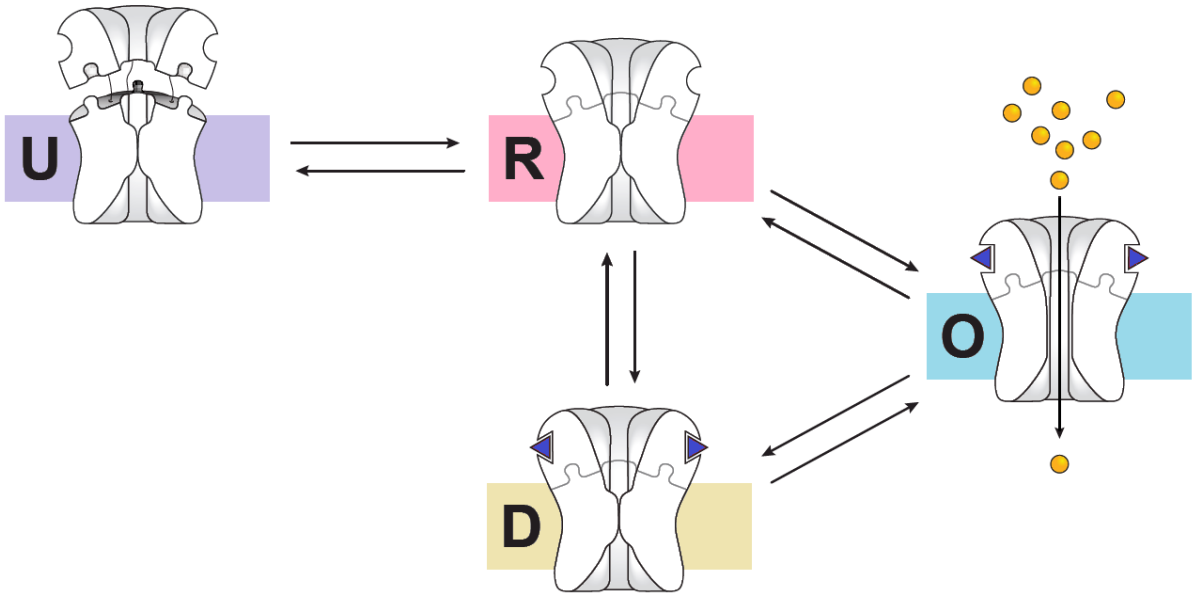

Figure 1.10 - nAChR structural conformations. nAChRs exist mainly in the resting state (R) where agonist is not bound and the channel is closed. Binding of agonist induces a conformational transition from the resting state to the open state (O) where the channel is open. Prolonged exposure to agonist induces transition to the desensitized state (D) where agonist is bound but the channel is closed. The newly discovered uncoupled conformation (U) is a lipid-dependent conformation where agonist binding does not lead to opening of the channel gate. Figure adapted from daCosta and Baenziger, 2009.

transition to the open or desensitized states of the ion channel. We will discuss this lipid-dependent state of the nAChR more in-depth in section 1.6.

The mechanism by which pLGICs interconvert between conformational states has been an important topic of research for many decades. The Monod-Wyman-Changeux (MWC) model of activation postulates that, even in the absence of agonist, allosteric pLGICs exist in a reversible equilibrium between at least two global conformational states; namely, at the most basic level, a resting/closed state and an activated/open state (Changeux and Edelstein, 2005; Monod et al., 1965). Additionally, the presence of agonist results in a conformational selection based upon each conformation's affinity for agonist (Changeux and Edelstein, 2005; Cui and Karplus, 2008). Indeed, owing to increased affinity for ACh in the open state, the muscle-type nAChR gating equilibrium constant has been estimated to increase about 10 million-fold when two molecules of ACh are bound. In refining the MWC model and accounting for desensitization, several additional slowly accessible, high-affinity, non-permeable pLGIC states were introduced (rev (Changeux and Edelstein, 2005), Lape et al., 2008/2012).

One of MWC's initial postulates is that pLGICs undergo symmetric gating transitions; however, the muscle-type nAChR does not follow this rule, instead, undergoing asymmetric gating transitions (as reviewed by Nemecz et al., 2016). This is most likely because the muscle-type nAChR is a heteropentamer, composed of α and non-α subunits. One study revealed that, upon agonist binding, the ECD of each α-subunit undergoes a conformational shift from α-like to non-α-like, which triggers channel gating (Unwin et al., 2002). Additionally, movement of channel-lining residues in just the α-subunit of muscle-type nAChRs may be sufficient to initiate opening of the channel gate (Miyazawa et al., 2003). Symmetric or not, the gating mechanism in pLGICs involves a conformational wave, which starts at the agonist-binding site in the ECD and

propagates to the TMD to open the channel gate (Calimet et al., 2013; Grosman et al., 2000a; Purohit et al., 2007; Sauguet et al., 2014). Kinetic studies suggest that this conformational wave follows a two-step gating mechanism (Purohit et al., 2013), where the first step may involve a quaternary inward twisting motion of the ECD, followed in the second step by an opposing outward, quaternary untwisting motion of the TMD to open the channel gate (Bocquet et al., 2009; Cheng et al., 2006; Liu et al., 2008). The individual differences observed within and between pLGIC subfamilies, with respect to the gating mechanism and channel kinetics, are likely due to the slight structural differences between homologous subunits.

1.6 Lipid sensitivity of the nAChR

Initial attempts to purify and reconstitute *Torpedo* nAChR activity in model membranes revealed its exquisite lipid sensitivity (Criado et al., 1984; Epstein and Racker, 1978; Fong and McNamee, 1986; Heidmann et al., 1980). Lipids were found to influence the function of the nAChR by stabilizing pre-existing resting/closed, activated/open, desensitized, and uncoupled conformations through allosteric mechanisms (daCosta et al., 2009). Lipids can allosterically alter the following functional properties: channel gating, kinetics of opening and closing, kinetics of desensitization, and the supramolecular distribution and translational dynamics of the protein at the cell surface (Almarza et al., 2014; as reviewed by Barrantes, 2004). It is of importance to understand the lipid sensitivities of nAChRs because their lipid environments change not only during trafficking, but also during aging and in the progression of neurodegenerative diseases.

daCosta *et al* (2009) found that nAChRs reconstituted in phosphatidylcholine (PC) membranes in the absence of "activating" lipids, namely anionic lipids such as phosphatidic acid (PA) and neutral lipids such as cholesterol, were stabilized in a non-activatable, uncoupled conformation. This is not surprising when we consider the lipid composition of the native

Torpedo membrane, where anionic lipids and cholesterols in combination make up 40-45 mol% of the membrane lipid composition (Gonzalez-Ros et al., 1982; Schiebler and Hucho, 1978). The uncoupled conformation does not gate open in response to agonist binding, and shows greater peptide backbone hydrogen exchange. This enhanced hydrogen exchange was proposed to be due to increased solvent accessibility between the ECD and TMD, indicating physical separation of the two domains (daCosta and Baenziger, 2009). In support of this point, a similar mechanism of lipid activation involving the coupling of binding and gating domains was demonstrated in the PIP2-activated potassium channel (Hansen et al., 2011). It is important to note that although a role for the uncoupled state in nAChR function *in vivo* has not yet been tested, *in vitro* studies suggest the presence of uncoupled nAChRs in biological systems. Specifically, electrically silent pools of neuronal nAChRs expressed in heterologous systems have been identified (Jin and Steinbach, 2010). Also, a shift in nAChRs from agonist-unresponsive to agonist-activatable conformations occurs with chronic nicotine exposure (Govind et al., 2012; Vallejo et al., 2005).

The mechanism by which lipids promote activatable versus non-activatable conformational states of the nAChR is of particular interest. In general, lipids can influence protein function by binding directly to conformationally sensitive protein binding sites, altering bulk membrane physical properties, which indirectly couple with different conformational states, or a combination of both (Lee, 2004). Additionally, simulation studies suggest that cholesterol may bind within the nAChR TMD to facilitate interactions between the TMD and ECD (Brannigan et al., 2008). However, a definite mechanism of how lipids affect nAChR function has not been elucidated. As the most lipid-exposed region of the nAChR, the M4 α-helices have been proposed as the main vehicle for sensing the surrounding lipid environment and translating

these features into altered nAChR function. Indeed, it has been well documented that mutation of lipid-facing residues on M4 influence the gating of the nAChR (Bouzat et al., 1998; Lasalde et al., 1996; Lee et al., 1994; Li et al., 1992; Mitra et al., 2004; Shen et al., 2006; Tamamizu et al., 1999/2000), although the underlying mechanism(s) remain(s) unclear, particularly given that M4 is peripheral to the key residues directly involved in coupling the agonist binding sites to the channel gate (Lee and Sine, 2005; Lee et al., 2008; Lee et al., 2009).

1.6.1 The M4 lipid sensor model

In the nAChR, molecular dynamics simulations have shown that M4 undergoes movements during gating, likely leading to changes in contacts with both M1/M3 and surrounding lipids (Xu et al., 2005). This movement may mask/unmask specific lipid binding sites, preferentially stabilizing different conformations and/or promoting/inhibiting transitions between these states. In support of this point, the entirety of M4 has been shown to interact with cholesterol at putative cholesterol-nAChR binding sites (Hamouda et al., 2006). It is conceivable that slight modifications of the M4 structure at the protein-lipid interface, such as the αM4 C418W mutation, could alter lipid binding sites, leading to stabilization of different nAChR conformations or transition states. Indeed, in the *Torpedo* nAChR, the lipid-facing C418W mutation was shown to alter the effects of cholesterol on the magnitude of agonist-evoked macroscopic currents, demonstrating that a single lipid-exposed position of the nAChR can modulate lipid interactions (Santiago et al., 2001).

The M4 lipid sensor model proposes that, in optimal lipid environments, interactions are promoted between M4 and the adjacent transmembrane α-helices, M1 and M3, which in turn stabilize critical interactions between the M4 C-terminus and the Cys-loop (daCosta and Baenziger, 2009; Figure 1.11). In non-optimal lipid membranes, those lacking anionic lipids

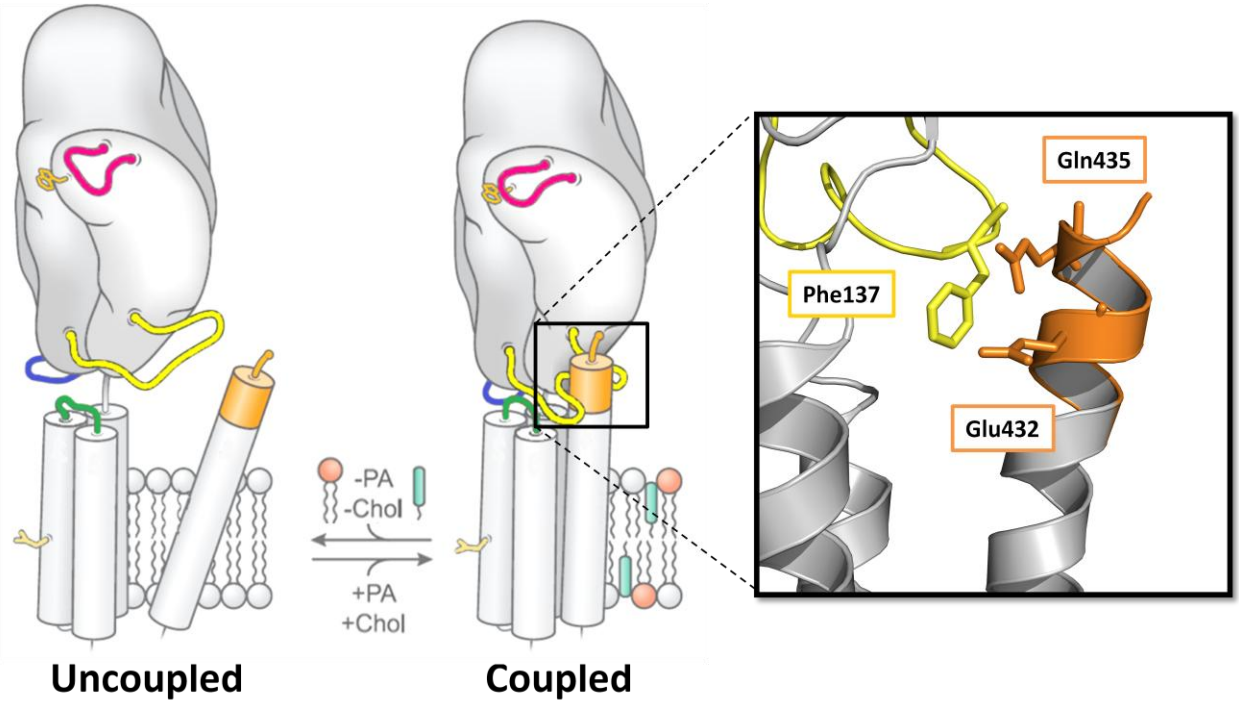

Figure 1.11 - The M4 lipid sensor model. Schematic showing the M4 lipid sensor model, illustrated as a single subunit, where M4 acts as the lipid sensitive moiety of the nAChR. Loop C is shown in pink, the β1-β2 loop is shown in blue, the Cys-loop is shown in yellow, the M2-M3 linker is shown in green, and post-M4 is shown in orange. In favourable lipid environments, post-M4 stabilizes functional nAChRs by interacting with the Cys-loop. Specifically, Glu432 and Gln435 of post-M4 interact with Phe137 of the Cys-loop. Figure adapted from daCosta and Baenziger, 2009.

and/or cholesterol, M4-M1/M3 interactions are not stabilized, leading to loss of M4–Cys-loop interactions, ultimately leading to a physical separation between the ECD and the TMD and, thus, an uncoupling of binding and gating (daCosta and Baenziger, 2009; Methot et al., 1995). A large body of evidence exists to support the importance of M4 C-terminal interactions with respect to pLGIC channel activity and expression (Ealing et al., 2002; Paradiso et al., 2001; Pons et al., 2004; Taly et al., 2005; Tobimatsu et al., 1987). It also seems that the intrinsic strength of M4-M1/M3 interactions, mediated primarily by aromatic interactions at this interface (Haeger et al., 2010), govern the lipid sensitivity of pLGICs. Those pLGICs with an abundance of optimized aromatic interactions between M4 and M1/M3, such as GLIC, remain relatively insensitive to surrounding lipid changes (Labriola et al., 2013); while, those without these stabilizing interactions, such as ELIC and the nAChR, are sensitive to lipid changes and may be more likely to become uncoupled. In line with this hypothesis, increasing the strength of M4-M1/M3 interactions, decreases lipid sensitivity and increases gating efficiency in ELIC (Carswell et al., 2015a/b). In fact, the intrinsic strength of M4-M1/M3 interactions was even shown to govern the degree of potentiation by C418W-analogous mutations in GLIC and ELIC, suggesting that αM4 C418W enhances channel function by promoting more extensive M4-M1/M3 interactions, which could, in turn, promote a critical interaction between M4 and the Cys-loop (Carswell et al., 2015b).

Recent studies suggest that pLGIC TMDs may fall into one of two archetypal categories: the first category including pLGICs whose TMD M4-M1/M3 interface possesses an abundance of aromatic contacts, essential to function and expression, and the second category including pLGICs whose TMD M4-M1/M3 interface lacks these aromatic contacts, likely to allow for greater conformational flexibility of the TMD (Therien and Baenziger, 2017; Figure 1.12).

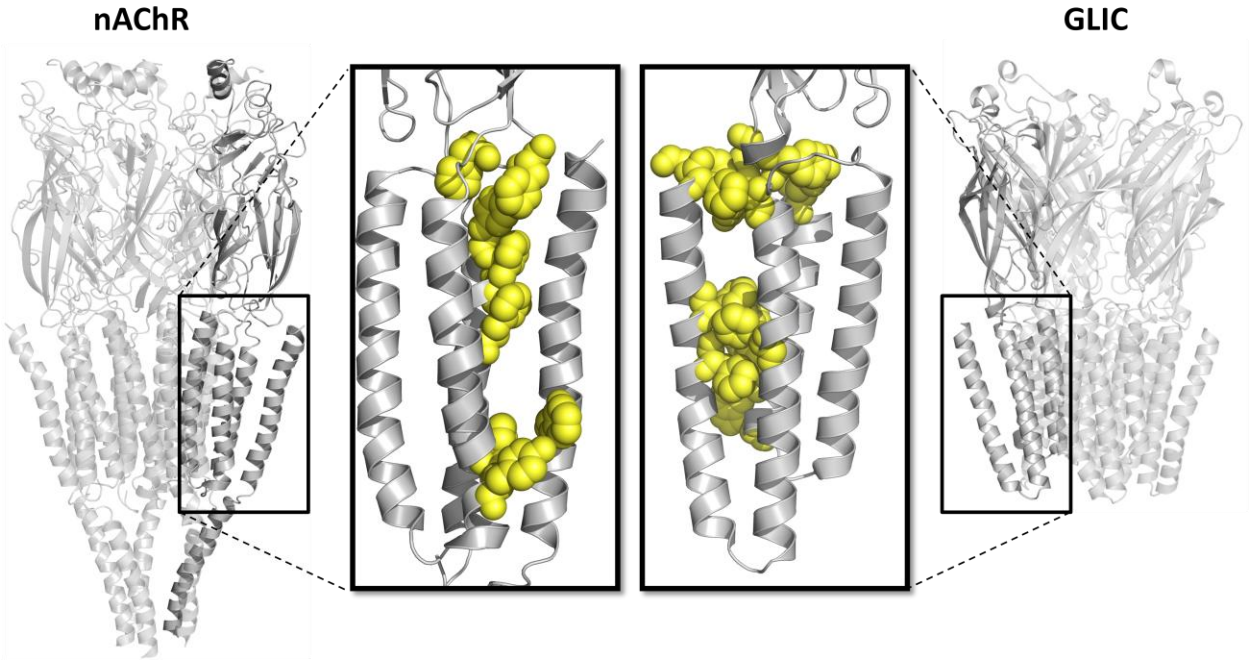

Figure 1.12 - Aromatic interactions between M4 and M1/M3 in two different pLGIC archetypes. The cryo-electron microscopy structure of the *Torpedo* nAChR (PDB: 2BG9) and the crystal structure of GLIC (PDB: 4HFI). Aromatic residues at the M4-M1/M3 interface are shown as yellow spheres. GLIC contains a multitude of optimized aromatic interactions at the M4-M1/M3 interface, while the nAChR contains fewer aromatic residues, with almost no interactions at this location.

GLIC, $GABA_{A/C}$, and GlyR make up the first archetypal pLGIC category; whereas, the ELIC, 5-HT_3, and the nAChR make up the second archetypal pLGIC category. These differences in M4-M1/M3 interfacial structure may highlight variable roles for M4 in each pLGIC archetype. In support of this hypothesis, a study focusing on how the structure of M4 affects pLGIC function in both GLIC and ELIC revealed a critical role for interactions between the M4 C-terminus and adjacent M3 N-terminus as well as the β6-β7 loop in GLIC; however, such interactions do not exist in ELIC (Hénault et al., 2015). As the nAChR falls into the second pLGIC archetypal category, I will need to consider that M4, and consequently αM4 C418W, may affect function in the muscle-type nAChR via a previously unexplored mechanism.

1.7 Thesis Objectives

The overarching goal of my research is to elucidate the mechanism by which the lipid-facing αM4 C418W mutation potentiates activity of the muscle-type nAChR to produce a slow-channel CMS. In order to accomplish this, I generated a multitude of mutants using site-directed mutagenesis, which were then analyzed using two-electrode voltage clamp electrophysiology (TEVC). I then used mutant cycle analysis to analyze the energetics of interactions between residues in both the presence and absence of the C418W mutation, as discussed in Chapter 2.

My research in pursuit of this goal is divided into two chapters. In Chapter 3, I test extensively the M4 lipid-sensor model and its role in C418W-induced potentiation. I demonstrate that, contrary to the M4 lipid sensor model, interactions between M4 and the Cys-loop are not critical to muscle-type nAChR function, nor are they involved in C418W-induced potentiation. Instead, αM4 C418W induces potentiation by altering interactions local to Trp418, which are mediated by a cluster of polar residues at the interface between M4 and M1. In Chapter 4, I explore further how the effects of these altered interactions between M4 and M1

ultimately propagate to the important structures involved in gating to potentiate nAChR function. I identify a number of interactions within the TMD that may work in tandem to stabilize the open state and thus potentiate nAChR function, although further interactions remain to be elucidated. These studies highlight how altered protein-lipid interactions can affect nAChR function and also contribute to our understanding of the nAChR gating mechanism.

Chapter 2

Experimental Procedures

2.1 cRNA constructs for oocyte expression

Wild-type human α1, β1, δ, and ε nAChR-pRBG4 clones were kindly provided by Steven Sine. The nAChR subunit DNA was transferred from pRBG4 into the pcDNA3 vector as an EcoRI fragment. The α1, β1, δ, and ε nAChR-pcDNA3 was linearized with XhoI and capped cRNA was produced by *in vitro* transcription using the mMESSAGE mMACHINE® T7 kit (Ambion). The concentration of cRNA was determined at Abs260 and the integrity of the RNA was determined by agarose gel electrophoresis. All mutants were created using QuikChange™ Site-Directed Mutagenesis kits (Agilent) and verified by sequencing using the forward T7 and reverse Sp6 promoters.

2.2 Electrophysiology

Stage V-VI oocytes were isolated as described previously (Laitko et al., 2006). Oocytes were injected in stoichiometric ratios: 5 ng of mutated α1-subunit cRNA along with 2.5 ng of each wild-type β1-, δ-, and ε-subunit cRNA. Oocytes were allowed to incubate for at least two days at 16˚C in $ND96^{+}$ buffer (5 mM HEPES, 96 mM NaCl, 2 mM KCl, 1 mM $MgCl_2$, 1 mM $CaCl_2$, and 2 mM pyruvate). Injected oocytes were then placed in the RC-1Z oocyte chamber (Harvard Apparatus; Hamden, CT) containing HEPES buffer (96 mM NaCl, 2mM KCl, 1.8 mM $BaCl_2$, 1 mM $MgCl_2$, 10 mM HEPES, pH 7.3). Whole cell currents were recorded using a TEVC apparatus (OC-725C oocyte clamp; Holliston, MA). The whole cell currents were recorded while flowing the HEPES buffer through the oocyte chamber at a rate of 5-10 mL/min.

Whole cell currents were recorded from injected oocytes immersed in HEPES buffer with 1 μM of added atropine to prevent activation of endogenous calcium-activated chloride channels via muscarinic acetylcholine receptors. Currents through the membrane in response to increasing acetylcholine concentrations were generally measured with the transmembrane

voltage clamped at -60 mV for the mutants which did not contain the potentiating αM4 C418W mutation, and -30 mV for the mutants which did contain the potentiating αM4 C418W mutation. The concentrations of acetylcholine used for mutants which did not contain the potentiating αM4 C418W mutation ranged from 1 μM to 100 μM. This concentration range was altered as required for specific mutants but remained generally consistent. The concentrations of acetylcholine used for any mutants containing the potentiating αM4 C418W mutation ranged from 0.04 μM to 40 μM and were also altered as required for specific mutants.

Dose responses for each mutant were acquired from at least two different batches of oocytes and were repeated at least 8 times wherever possible. Each individual dose-response experiment was normalized (I/I_{max}) and fitted with a variable slope sigmoidal dose-response using GraphPad Prism**.** The individual half maximal effective concentrations (EC_{50}) for ACh and the Hill coefficients from each experiment were averaged to give the values ± standard deviation. Note that EC_{50} values depend on both the nAChR affinity for ACh and the gating equilibrium constant, which governs transitions from the closed to open states of the receptor. However, given that none of the mutations I have performed are near the orthosteric ACh-binding sites, located at the subunit interfaces in the ECD, the changes in function observed likely reflect changes to the gating equilibrium constant only. Thus, a gain-of-function would represent enhanced coupling between the agonist binding site and the channel gate, while a loss-of-function would represent the opposite.

2.3 Homology Model

The homology model of the human muscle-type α-subunit was constructed using Swiss-Model (Schwede et al., 2003), with the *Torpedo* nAChR α-subunit as the template (Unwin, 2005; PDB code: 2BG9). The human and *Torpedo* α-subunits have 80% sequence homology.

2.4 Mutant Cycle Analysis

Mutant cycle analysis allows one to determine the extent to which two or more protein residues are energetically coupled (Carter et al., 1984; Daeffler et al, 2012; Horovitz and Fersht, 1990; Lee and Sine, 2005). My mutant cycles were performed using the averaged EC_{50} values for ACh as follows:

$$\Omega = \frac{\left(EC_{50}\left(mut_{1,2}\right)\right) * \left(EC_{50}(WT)\right)}{\left(EC_{50}(mut_1)\right) * \left(EC_{50}(mut_2)\right)}$$

where *WT* is the control, mut_1 is the first mutant of interest, mut_2 is the second mutant of interest, and $mut_{1,2}$ is the double mutant. Note that *WT* is not always the wild-type nAChR, depending on the context in which I am performing the analysis. I considered two residues to be energetically coupled when Ω differs from 1 by a factor of at least 2 (i.e. $\Omega \geq 2$ or $\Omega \leq 1/2$) (Daeffler et al, 2012).

To calculate the free energy contribution of coupling (ΔΔG) to the stabilization of the open state, I used the following formula:

$$\Delta\Delta G = RTln(\Omega)$$

where *R* is the gas constant (8.314 J/mol*K) and *T* is the temperature constant (298 K). As noted above, the mutations I perform are distant from the ACh binding sites, thus changes in EC_{50} values likely reflect changes to the gating equilibrium constant only. The ΔΔG values were thus interpreted in terms of the energy contributed by the interaction of interest to the nAChR gating reaction (i.e. to the stabilization of the open state). Since I only consider two residues to be energetically coupled when Ω differs from 1 by a factor of at least 2, a ΔΔG of at least 1.72

kJ/mol, or less than -1.72 kJ/mol indicates that two residues are significantly coupled and contribute that much energy to gating.

My mutant cycles were performed such that I calculated the free energy resulting from the removal of an interaction between two residues. For example, to test an interaction between two polar groups: Ser226 and Thr229, my *WT* would be the wild-type nAChR, where both polar groups are present, each single mutant represents the removal of one polar group (i.e. mut_1 = S226A and mut_2 = T229A), and the double mutant represents the removal of both polar groups (i.e. $mut_{1,2}$ = S226A+T229A). In a second scenario where I calculated an interaction between the C418W mutant and adjacent polar group (i.e. Ser226), the components of the equation would be as follows: *WT* = Ser226+Trp418, where the Trp and polar Ser group are both present, mut_1 = S226A+Trp418, where the polar group has been removed, mut_2 = wild-type nAChR (Ser226+W418C), where the Trp has been removed, and $mut_{1,2}$ = S226A+W418C where both the polar group and Trp have been removed. In both examples, a negative free energy ($\Delta\Delta G \leq -1.72$ kJ/mol) signifies that the interaction in question is beneficial to nAChR gating, while a positive free energy ($\Delta\Delta G \geq 1.72$ kJ/mol) signifies that the interaction in question is detrimental to nAChR gating. More specifically, when I am calculating energetic coupling between one or more residues and C418W itself, a negative free energy in this context signifies that the residue(s) is/are important to potentiation, while a positive free energy signifies the opposite.

2.5 [^{125}I]-α-bungarotoxin binding assay

Oocytes were injected with 50 ng of mutated α1-subunit cRNA and 25 ng of each wild-type β1-, δ-, and ε-subunit cRNA to preserve 2:1:1:1 stoichiometry. Oocytes were then incubated at 16^{o}C in ND96^{+} buffer (5 mM HEPES, 96 mM NaCl, 2 mM KCl, 1 mM $MgCl_2$, 1 mM $CaCl_2$, and 2 mM pyruvate). Binding experiments were performed on the surface of intact

oocytes 3 and 4 days after injection. Up to 8 oocytes were placed in 600 μL of reaction solution, which contained 2.5 nM of [^{125}I]-α-bungarotoxin and 1 mg/mL of BSA in MOR2 buffer (82 mM NaCl, 2.5 mM KCl, 5 mM $MgCl_2$, 1 mM NaH_2PO_4, 5 mM HEPES, and 0.2 mM $CaCl_2$, pH 7.4). Samples were incubated for 2 hours at room temperature with gentle shaking at 15 minute intervals. The reaction was terminated by washing the oocytes four times with MOR2 buffer. Binding was quantified by γ counting and non-specific binding was determined by incubating mock injected oocytes with the same binding reaction under identical conditions.

Chapter 3

αM4 C418W enhances local M4-M1 interactions to potentiate muscle-type nAChR function

3.1 Introduction

Although the central goal of my research is to understand how the CMS-causing αM4 C418W mutation alters nAChR function, a more general mechanistic question is how the structure of the outermost α-helix, M4, influences nAChR gating, particularly given that M4 is peripheral to key residues directly involved in coupling the agonist binding sites to the channel gate (Lee and Sine, 2005; Lee et al., 2008; Lee et al., 2009). One model proposes that M4 influences channel function via its interactions with the adjacent helices, M1 and M3, with enhanced M4-M1/M3 interactions promoting a critical interaction between the M4 C-terminus and the Cys-loop of the ECD (Carswell et al 2015b; daCosta and Baenziger, 2009).

In this chapter, I use point mutations, C-terminal deletions, and mutant cycle analysis to assess the role of the M4 C-terminus in both channel function and C418W-induced potentiation. Contrary to my working hypothesis, my data show unequivocally that M4–Cys-loop interactions are not essential to nAChR function and do not facilitate C418W-induced potentiation. Instead, αM4 C418W potentiates function via direct interactions between Trp418 and two residues on M1, Ser226 and Thr229. I identify key local polar interactions at the M4-M1 interface that facilitate the enhancement in channel function that occurs when Cys418 is mutated to Trp, thus leading to a CMS.

3.2 Results

3.2.1 The M4 C-terminus is not critical to nAChR channel function or C418W-induced potentiation

The CMS-causing Trp residue substituted at position 418 on αM4 is positioned to extend into the lipid bilayer where it likely perturbs the packing of the adjacent lipid fatty acyl chains. Based on previous data highlighting an important role for the M4 C-terminus in channel

function, I hypothesized that unfavorable steric interactions between C418W and lipids cause M4 to reorient relative to M1/M3 to promote more effective interactions between the C-terminus of M4 and the Cys-loop to enhance channel gating (Carswell et al., 2015b; daCosta and Baenziger, 2009). To test this hypothesis, a homology model of the human muscle-type α-subunit was created based upon the *Torpedo* nAChR 4 Å cryo-electron microscopic structure (Unwin, 2005; PDB code: 2BG9; see Chapter 2). Both the homology model and the *Torpedo* nAChR structure suggest that direct interactions are formed between the polar residues, Glu432 and Gln435 on M4 and the aromatic residue, Phe137, on the Cys-loop (Unwin, 2005). I also noted that a water molecule could bridge interactions between the polar Asn434 on M4 and negatively-charged Asp138 on the Cys-loop (Figure 3.1).

To test the functional importance of these putative interactions, I generated single, double, and triple Ala mutations and then measured the effects of the mutations on channel function using the TEVC apparatus (Table 3.1). Wild-type human muscle-type nAChR (WT-nAChR) expresses robustly in frog oocytes, yielding a sigmoidal dose response with an EC_{50} for ACh of 7.61 ± 1.25 μM (see appendix; Figure 6.1). Ala substitution of the three potential Cys-loop interacting residues on M4, E432A, N434A, and Q435A, each had no effect on the dose response, while Ala mutation of the potential M4-interacting residue on the Cys-loop, F137A, actually led to a slight leftward shift in the dose response, indicating a gain-of-function phenotype. Further, D138A did not express, consistent with the important role proposed for charged residues at the interface between the ECD and TMD (Xiu et al., 2005). Even the double mutants E432A+Q435A and N434A+Q435A, as well as the triple mutant, F137A+E432A+Q435A, had minimal effects on the EC_{50} value as compared to WT-nAChR (Figure 3.1). The fact that the various Ala substitutions had little effect on channel function

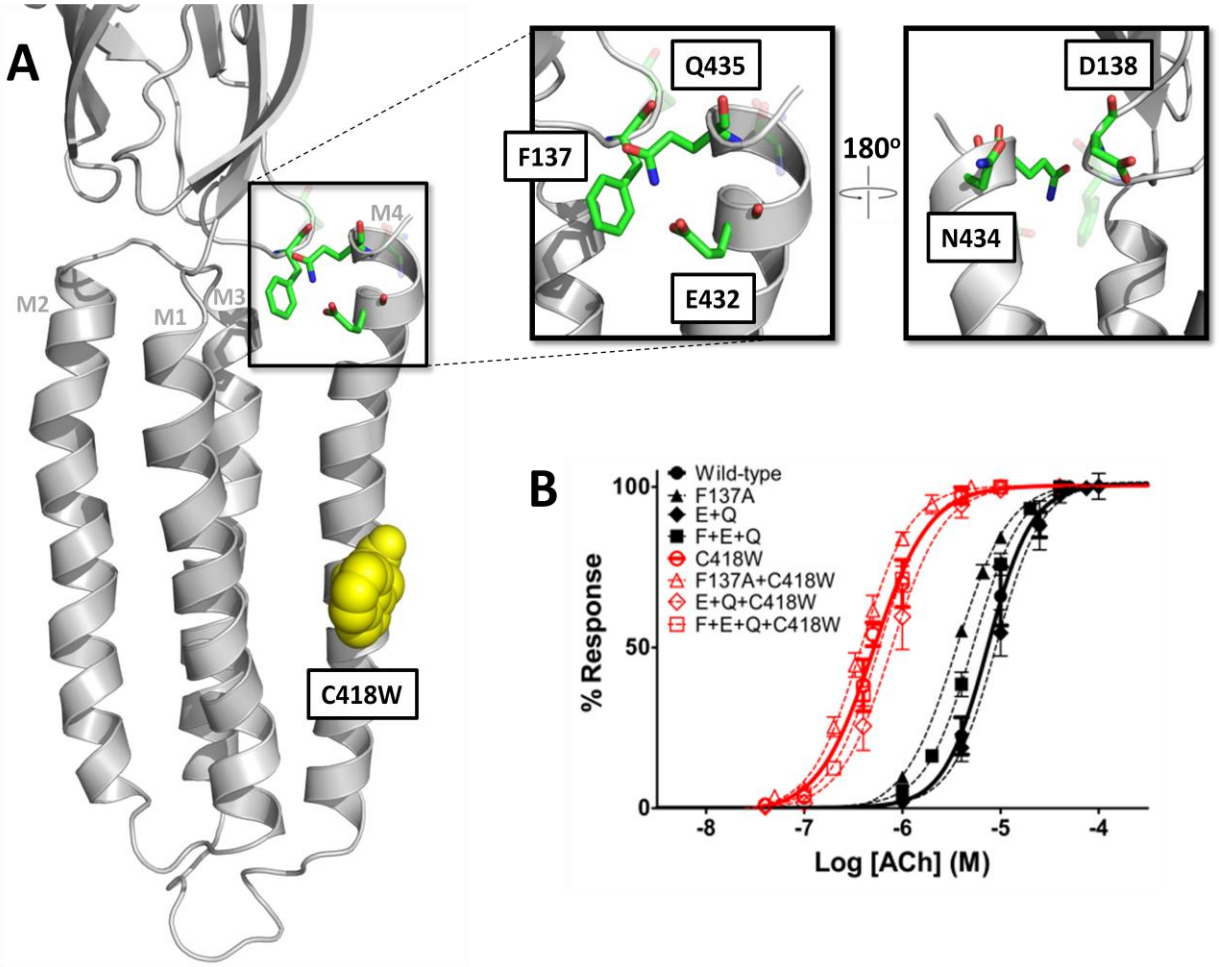

Figure 3.1 - Role of putative M4–Cys-loop interactions in nAChR function and C418W-induced potentiation. (A) The human muscle-type α-subunit homology model based on the cryo-electron microscopy structure of the *Torpedo* nAChR (PDB: 2BG9). The C418W mutant is shown as yellow spheres. The residues of interest involved in putative M4–Cys-loop interactions are shown as sticks where carbon atoms are green, nitrogen atoms are blue, and oxygen atoms are red. (B) Normalized dose response curves for select Ala mutations on the WT-nAChR and C418W-nAChR backgrounds showing that the substitutions have very little effect on nAChR function and C418W-induced potentiation. Error bars represent standard deviation, $n \geq 8$.

Table 3.1 - Role of M4–Cys-loop interacting residues in nAChR function and C418W-induced potentiation.

Mutation(s)	Dose Response[a]						Potentiation (fold)[f]
	WT-nAChR[c]			C418W-nAChR[d]			
	EC_{50} (μM)	Hill Slope	*n*	EC_{50} (μM)	Hill Slope	*n*	
None	7.61 ± 1.25	1.70 ± 0.47	50	0.47 ± 0.12	1.54 ± 0.23	50	16.2
F137A (Cys-loop)	3.47 ± 0.26[b]	1.44 ± 0.24	9	0.37 ± 0.04	1.67 ± 0.12	8	9.4
D138A (Cys-loop)	**No current**[e]		8	0.46 ± 0.02	1.26 ± 0.05	3	--
E432A (M4)	8.83 ± 0.62	1.92 ± 0.13	11	0.50 ± 0.12	1.45 ± 0.23	8	17.7
N434A (M4)	8.09 ± 0.68	1.94 ± 0.12	11	0.38 ± 0.11	1.57 ± 0.12	8	21.2
Q435A (M4)	8.07 ± 0.51	2.03 ± 0.12	13	0.40 ± 0.08	1.48 ± 0.09	8	20.2
E432A+Q435A	9.51 ± 1.67[b]	1.84 ± 0.31	10	0.80 ± 0.20[b]	1.63 ± 0.13	11	11.9
N434A+Q435A	7.56 ± 1.40	1.43 ± 0.14	8	0.34 ± 0.06	1.51 ± 0.21	8	22.2
F137A+E432A+Q435A	5.45 ± 0.63[b]	1.70 ± 0.09	8	0.58 ± 0.06	1.67 ± 0.15	8	9.4

[a] Measurements were performed 2 days after injection of cRNA. Error values represent standard deviation.
[b] $p < 0.001$ relative to control via one-way ANOVA followed by Dunnett's post-hoc test.
[c] WT-nAChR contains only the mutation(s) listed under the "mutation(s)" column.
[d] C418W-nAChR contains C418W in addition to the mutation(s) listed under the "mutation(s)" column.
[e] Oocytes were tested 2-7 days after injection of 5-15 ng of mutant cRNA.
[f] EC_{50} of mutant on WT-nAChR background divided by EC_{50} of mutant on C418W-nAChR background.

suggests that the interactions between the M4 C-terminus and the Cys-loop observed in the protein structure are not critical for coupling the agonist binding sites to the channel gate.

I considered the possibility that, although M4–Cys-loop interactions are not critical to WT-nAChR function, the αM4 C418W CMS-causing mutation might enhance interactions at this location to potentiate channel function. To test whether enhanced M4–Cys-loop interactions ultimately drive C418W-induced potentiation, I examined whether the same Ala mutations impacted upon C418W-induced potentiation (Table 3.1). In my hands, the EC_{50} value for ACh decreases from 7.61 ± 1.25 μM in the WT-nAChR to 0.47 ± 0.12 μM in the C418W mutant (C418W-nAChR), which corresponds to a 16-fold potentiation of channel function (see appendix; Figure 6.1). Single, double, and triple Ala mutations of potentially interacting M4–Cys-loop residues superimposed onto the C418W-nAChR background all had EC_{50} values similar to that of the C418W-nAChR. The different mutations also had little effect on C418W-induced potentiation, with the degrees of potentiation (i.e. the EC_{50} for the Ala mutation(s) alone versus the EC_{50} for C418W + Ala mutation(s)) varying between ~10- and ~20-fold (Table 3.1). The lack of dramatic effects on potentiation with these mutations suggests that M4–Cys-loop interactions do not drive C418W-induced potentiation. This conclusion, however, is clouded by the fact that changes in potentiation can be observed when calculating the ratio between the measured EC_{50} for two mutants, even when the individual mutations yield EC_{50} values that are statistically insignificant relative to their respective controls, or vice versa.

To more conclusively assess the hypothesized role of M4–Cys-loop interactions in C418W-induced potentiation, I cast the data as mutant cycles (see Chapter 2), and then compared the energetic coupling between residues of M4 and the Cys-loop, both in the presence and absence of the C418W mutation. The mutant cycle analysis allows one to determine the extent

to which two or more residues are energetically coupled (Carter et al., 1984; Daeffler et al, 2012; Horovitz and Fersht, 1990; Lee and Sine, 2005). Specifically, the EC_{50} values for two individual point mutations, the respective double mutation, and the control are compared to calculate a value for Ω, where a Ω value of 1 indicates that the two residues are not energetically coupled and that any effects of the two individual mutations on EC_{50} values occur independently. Following the approach of Daeffler *et al*, I considered two residues to be energetically coupled only when Ω differs from 1 by a factor of at least 2 (i.e. $\Omega \geq 2$ or $\Omega \leq 1/2$). In such cases, the free energy of coupling between the residues contributes ≥ 1.72 kJ/mol or ≤ -1.72 kJ/mol toward channel gating. A negative free energy indicates that an interaction between the residues in question is beneficial to gating or potentiation, while a positive free energy indicates the opposite. It is important to note that the calculated coupling energy is a thermodynamic parameter and does not disclose whether coupling arises through a direct or propagated interaction. If two residues, however, are in direct contact in the protein structure, the energetic coupling likely occurs through a direct physical interaction.

Mutant cycle analysis suggests that neither Phe137, Glu432, Asn434, nor Gln435 are indirectly coupled with C418W (Table 3.2). In other words, the individual Ala mutations lead to changes in the measured EC_{50} values that occur independently of the effects of C418W on the measured EC_{50} values. Neither the Asn434/Gln435 nor the Glu432/Gln435 pairs were found to be energetically coupled in either the WT-nAChR or C418W-nAChR background. Most importantly, the two M4 residues Glu432 and Gln435 are not energetically coupled with Phe137 of the Cys-loop in either the presence or absence of the C418W mutation. It can thus be concluded that the noted interactions between and M4 and the Cys-loop do not contribute to either channel function or C418W-induced potentiation.

Table 3.2 - Energetic coupling between residues at the M4-C-terminus and the Cys-loop.

Mutants	Ω	ΔΔG (kJ/mol)
Phe137/Trp418	0.58	-1.35
Asp138/Trp418	--[a]	--
Glu432/Trp418	1.09	0.21
Asn434/Trp418	1.31	0.67
Gln435/Trp418	1.25	0.55
Glu432-Gln435/Trp418	0.73	-0.78
Asn434-Gln435/Trp418	1.37	0.78
Phe137-Glu432-Gln435/Trp418	0.58	-1.35

Mutants	WT-nAChR[b]		C418W-nAChR[c]	
	Ω	ΔΔG (kJ/mol)	Ω	ΔΔG (kJ/mol)
Glu432/Gln435	1.02	0.05	1.88	1.56
Asn434/Gln435	0.88	-0.32	1.05	0.12
Phe137/Glu432-Gln435	1.25	0.55	0.91	-0.23

[a] Could not calculate energetic coupling because of non-functional/non-expressing mutants.
[b] WT-nAChR contains only the mutation(s) listed under the "mutants" column.
[c] C418W-nAChR contains C418W in addition to the mutation(s) listed under the "mutation(s)" column.

Finally, I tested the possibility that other residues at the M4 C-terminus influence channel function and play a role in C418W-induced potentiation by measuring the functional effects of sequential M4 C-terminal deletions (Table 3.3; Figure 3.2). Deletion of from one to four C-terminal residues (i.e. up to one full turn at the C-terminus of the M4 α-helix), including the potential Cys-loop interacting residues Gln435 (*ΔQQG*) and Asn434 (*ΔNQQG*), had little effect on the dose response with each of the four deletion mutants yielding EC_{50} values similar to that of the WT-nAChR. Subsequent deletion of the aliphatic, lipid-facing residue, Leu433, led to a slight increase in EC_{50} from 8.49 ± 1.39 μM (*ΔNQQG)* to 11.8 ± 1.0 μM (*ΔLNQQG*), representing a slight loss of channel function, while deletion of the next three residues, including Glu432, had little additional effect. Further deletions from 9 to 12 residues led to subtle, but increasing right-shifts in the dose response curves, although even the 11-deletion mutation, *ΔAGRLIELNQQG*, exhibited only a 3-fold loss of function relative to WT-nAChR (Table 3.3). Note that the loss-of-function phenotypes with increasing M4 C-terminal deletions correlated with a progressive loss of cell-surface expression, as measured by [^{125}I]-α-bungarotoxin binding (Figure 3.3). Cell-surface expression was abolished after deletion of the final 12 C-terminal residues. The lack of a dramatic loss of folding/expression or function with the deletion of any particular residue suggests that none of the residues in the M4 C-terminus are directly involved in interactions that are essential to channel function. Instead, the progressive loss of function and expression with increasing deletions may be due to a general disruption of the M4 α-helical structure within the membrane.

The M4 C-terminal deletions also had minimal effects on C418W-induced potentiation (Table 3.3; Figure 3.2). When C418W was superimposed onto the one to four residue M4 C-terminal deletions, the resulting mutants all had EC_{50} values similar to that of C418W-nAChR.

Table 3.3 - Effect of M4 C-terminal deletions in nAChR function and C418W-induced potentiation.

Deletion(s)	Dose Response[a]						Potentiation (fold)[f]
	WT-nAChR[c]			C418W-nAChR[d]			
	EC_{50} (μM)	Hill Slope	*n*	EC_{50} (μM)	Hill Slope	*n*	
None	7.61 ± 1.25	1.70 ± 0.47	50	0.47 ± 0.12	1.54 ± 0.23	50	16.2
ΔG	6.86 ± 0.86	2.66 ± 0.67	9	0.49 ± 0.15	1.66 ± 0.14	10	14.0
ΔQG	6.37 ± 0.94	2.62 ± 0.54	9	0.50 ± 0.18	1.36 ± 0.30	8	12.7
ΔQQG	7.14 ± 1.09	2.36 ± 0.38	8	0.69 ± 0.23	1.38 ± 0.23	8	10.3
ΔNQQG	8.49 ± 1.39	2.13 ± 0.44	8	0.76 ± 0.21	1.36 ± 0.17	9	11.2
ΔLNQQG	11.8 ± 1.0[b]	1.65 ± 0.33	10	1.29 ± 0.37[b]	1.55 ± 0.21	9	9.1
ΔELNQQG	12.3 ± 1.2[b]	1.59 ± 0.25	10	1.28 ± 0.13[b]	1.62 ± 0.18	9	9.6
ΔIELNQQG	12.7 ± 1.7[b]	1.54 ± 0.15	10	1.47 ± 0.12[b]	1.71 ± 0.37	9	8.6
ΔLIELNQQG	14.7 ± 2.6[b]	1.46 ± 0.29	10	1.42 ± 0.25[b]	1.70 ± 0.08	9	10.4
ΔRLIELNQQG	14.9 ± 2.5[b]	1.77 ± 0.35	10	1.65 ± 0.34[b]	1.63 ± 0.21	9	9.0
ΔGRLIELNQQG	21.4 ± 4.2[b]	1.35 ± 0.12	10	1.87 ± 0.11[b]	1.76 ± 0.24	9	11.4
ΔAGRLIELNQQG	23.0 ± 5.0[b]	1.69 ± 0.36	10	2.88 ± 0.54[b]	1.72 ± 0.25	9	8.0
ΔFAGRLIELNQQG	**No current**[e]		10	3.92 ± 0.35[b]	1.39 ± 0.12	3	--

[a] Measurements were performed 2 days after injection of cRNA. Error values represent standard deviation.
[b] $p < 0.001$ relative to control via one-way ANOVA followed by Dunnett's post-hoc test.
[c] WT-nAChR contains only the mutation(s) listed under the "deletion(s)" column.
[d] C418W-nAChR contains C418W in addition to the mutation(s) listed under the "deletion(s)" column.
[e] Oocytes were tested 2-7 days after injection of 5-15 ng of mutant cRNA.
[f] EC_{50} of mutant on WT-nAChR background divided by EC_{50} of mutant on C418W-nAChR background.

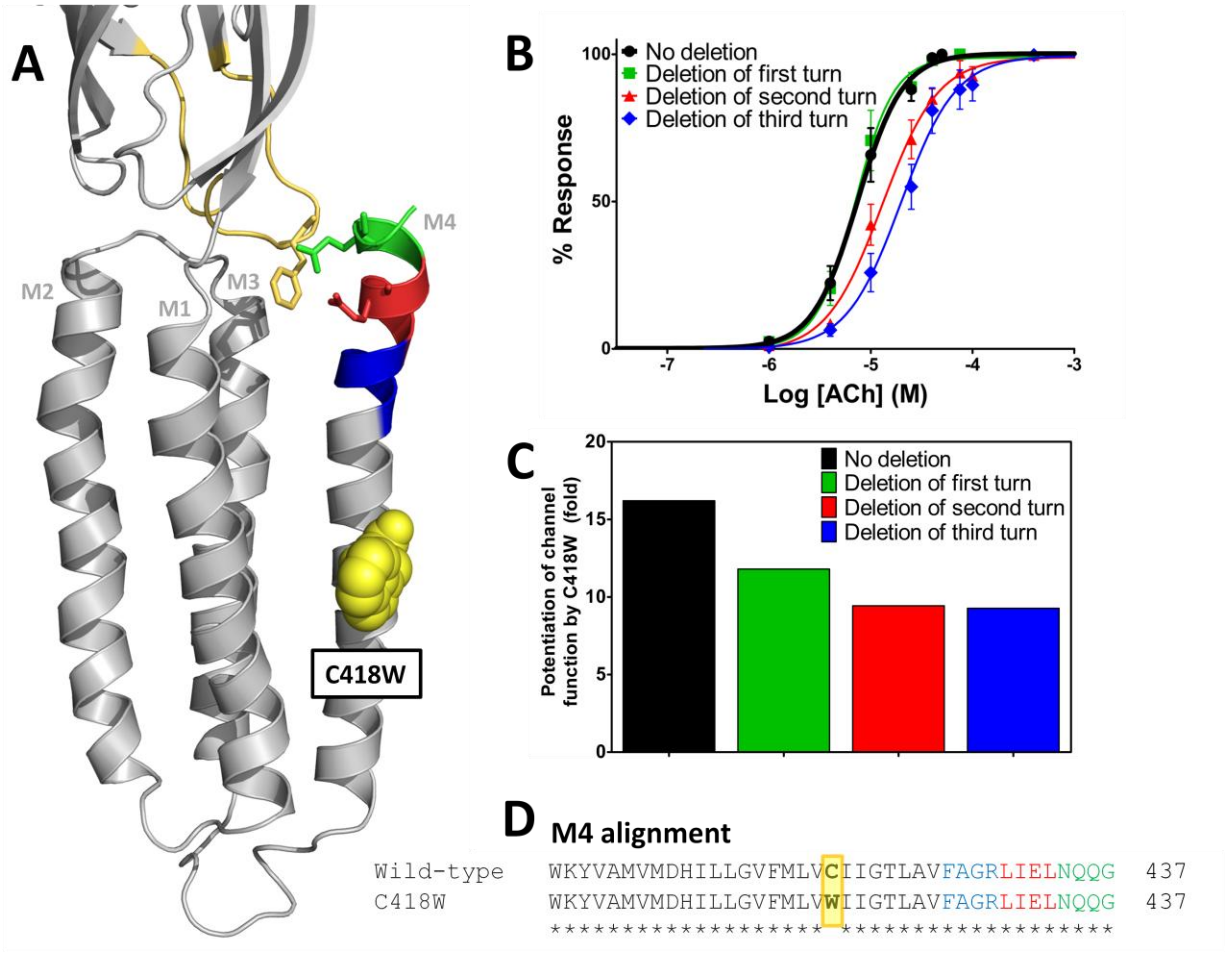

Figure 3.2 - Effect of M4 C-terminal deletions on nAChR function and C418W-induced potentiation. (A) The human muscle-type α-subunit homology model based on the cryo-electron microscopy structure of the *Torpedo* nAChR (PDB: 2BG9). The C418W mutant is shown as yellow spheres. The residues of interest involved in putative M4–Cys-loop interactions are shown as sticks and colour-coded based upon their location in the structure: the Cys-loop (Phe137) is yellow, the first α-helical turn (Gln435) is green, the second α-helical turn (Glu432) is red, and the third α-helical turn is blue. (B) Normalized dose response curves for each deletion on the WT-nAChR background were averaged together for each α-helical turn showing that the deletions have a subtle loss-of-function effect compared to WT-nAChR. Error bars represent standard deviation. (C) Graph comparing the effects of M4 C-terminal deletions on C418W-induced potentiation. (D) Sequence alignment of M4 showing residues involved in each α-helical turn as well as the location of C418W in relation.

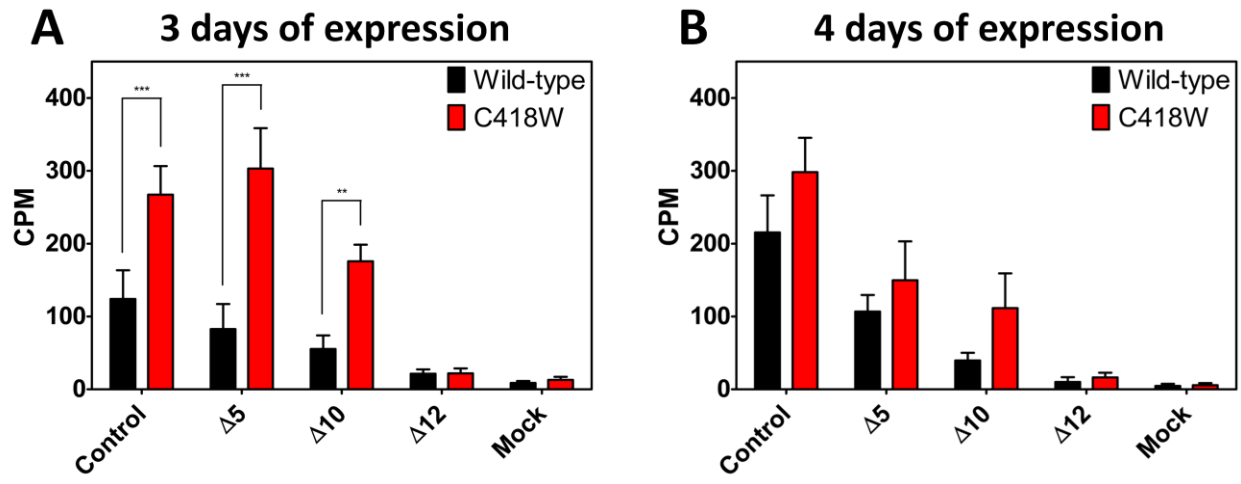

Figure 3.3 - Surface expression levels of M4 C-terminal deletions as measured by [^{125}I]-α-bungarotoxin binding. Cell surface binding of [I^{125}]-α-bungarotoxin as detected by γ counting 3 days (A) and 4 days (B) after injection of 50 ng of either wild-type or mutant cRNA. Δ5, Δ10, and Δ12 represent deletion of 5, 10, and 12 M4 C-terminal residues, respectively. Mock oocytes were injected with buffer that did not contain any cRNA.

Subsequent deletion of the lipid-facing Leu433 residue (*ΔLNQQG-C418W)* led to a slight reduction in the C418W-induced potentiation of channel function, with further losses of potentiated function not occurring until after deletion of the final two full turns of M4. In addition, mutant cycle analyses revealed that the functional effects of the M4 C-terminal deletions were independent from those of the C418W mutation (Table 3.4). Altogether, these data show conclusively that M4–Cys-loop interactions do not play a role in either human muscle-type nAChR function or the potentiation of function that occurs with the αM4 C418W CMS-causing mutation.

3.2.2 Does Trp418 promote local interactions between M4 and M1 to potentiate channel function?

I next considered the possibility that direct physical interactions between the Trp side chain at position 418 on αM4 and adjacent residues on M1 and/or M3 ultimately drive potentiation of channel function. To address this hypothesis, I first tested whether the nAChR is functionally sensitive to side-chain substitutions at this location (Table 3.5). The minor modification of the small, polar Cys418 to the small, aliphatic Ala residue led to a slight loss-of-function. In contrast, substitution of Cys418 with the relatively large aromatic Phe, positively-charged Lys, or negatively-charged Glu residues each led to a potentiation of channel function, with the values of potentiation varying from ~3- to ~5-fold relative to the WT-nAChR. Although the degree of potentiation with these mutations is not as large as that seen with the αM4 C418W mutation (16-fold), the results confirm that channel gating in the nAChR is sensitive to side-chain chemistry and/or volume at position 418 on αM4. In fact, single-channel analyses of multiple amino acid substitutions at different lipid-facing positions along M4 (Leu410, Met415, Cys418, Thr422, and Phe426) in the mouse muscle-type nAChR show that

Table 3.4 - Energetic coupling between M4 C-terminal deletions and C418W

Mutants	Ω	ΔΔG (kJ/mol)
ΔG/Trp418	0.86	-0.37
ΔQG/ Trp418	0.79	-0.58
ΔQQG/ Trp418	0.64	-1.11
ΔNQQG/ Trp418	0.69	-0.92
ΔLNQQG/ Trp418	0.56	-1.44
ΔELNQQG/ Trp418	0.59	-1.31
ΔIELNQQG/ Trp418	0.53	-1.57
ΔLIELNQQG/ Trp418	0.64	-1.11
ΔRLIELNQQG/ Trp418	0.56	-1.44
ΔGRLIELNQQG/ Trp418	0.71	-0.85
ΔAGRLIELNQQG/ Trp418	0.49	-1.77[a]
ΔFAGRLIELNQQG/ Trp418	--[b]	--

[a] The free energy is sufficient to indicate energetic coupling
[b] Could not calculate energetic coupling because of non-functional/non-expressing mutants.

Table 3.5 - Role of side-chain volume and chemistry at position αM4 418 on nAChR function.

Dose Response[a]				Potentiation (fold)[c]
Mutation	**EC_{50} (μM)**	**Hill Slope**	***n***	
None	7.61 ± 1.25	1.70 ± 0.47	50	--
C418A	10.6 ± 2.9[b]	1.82 ± 0.33	9	0.7
C418F	1.67 ± 0.66[b]	1.58 ± 0.25	8	4.6
C418K	3.06 ± 0.62[b]	1.27 ± 0.06	8	2.5
C418E	1.66 ± 0.65[b]	1.58 ± 0.25	8	4.6
C418W	0.47 ± 0.12[b]	1.54 ± 0.23	50	16.2

[a] Measurements were performed 2 days after injection of cRNA. Error values represent standard deviation.
[b] $p < 0.001$ relative to control via one-way ANOVA followed by Dunnett's post-hoc test.
[c] Wild-type EC_{50} divided by mutant EC_{50}.

gating is more sensitive to side-chain substitutions at position 418 on αM4 than at other positions along the lipid-protein interface (Mitra et al., 2004).

A change in orientation of M4, due to the C418W mutation, could position Trp418 and/or two adjacent residues on M4, the aromatic Phe414 and polar Thr422, to interact with residues on the M1 α-helix. Specifically, a reorientation of M4 could facilitate interactions between Trp418 and the adjacent M1 residues, Leu223, Ser226, and/or Phe227. Such a reorientation could also facilitate interactions between Phe414 and Thr422 on M4 and either Phe233/Tyr234 or Ser226 on M1, respectively (Figure 3.4). An Ala-scan of these potentially interacting residues suggested that Ser226, Phe227, and Thr422 may be important to C418W-induced potentiation (Table 3.6). Specifically, the F227A mutation had no effect on channel function in the WT-nAChR, but the same mutation superimposed onto the C418W-nAChR background, F227A+C418W, did not express to the cell surface (see appendix; Figure 6.2), indicating that an interaction between Trp418 and Phe227 is likely required for folding, and thus may influence function in the folded state. Similarly, the S226A mutation had little effect on the function of the WT-nAChR (less than 2-fold change in EC_{50}), but the S226A+C418W double mutation led to an ~8-fold loss-of-function relative to C418W-nAChR, reducing C418W-induced potentiation from 16-fold down to 3-fold. Mutant cycle analysis shows a direct coupling between Trp418 and Ser226 that contributes -3.87 kJ/mol to channel gating (Table 3.7). Finally, although T422A decreased channel function ~4-fold relative to WT-nAChR (see also Bouzat et al; 1998; Mitra et al., 2004), the T422A+C418W double mutation led to a 7-fold loss-of-function relative to C418W-nAChR, suggesting that Thr422 becomes more important to channel activity when C418W is present. Indeed, the T422A mutation subtly decreased C418W-induced potentiation from 16- to 9-fold.

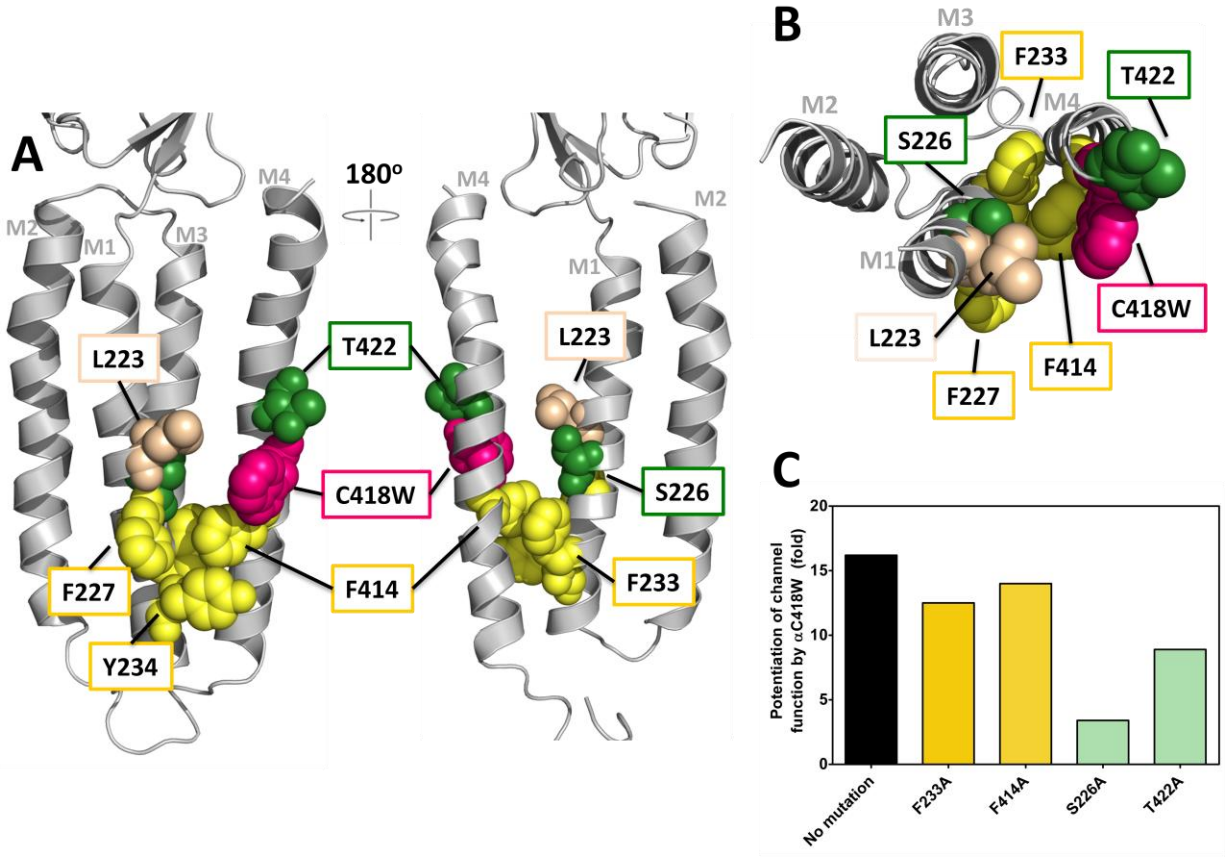

Figure 3.4 - Role of adjacent residues in C418W-induced potentiation. (A) The human muscle-type α-subunit homology model based on the cryo-electron microscopy structure of the *Torpedo* nAChR (PDB: 2BG9). Residues local to the position of C418W (shown as pink spheres), are shown as spheres where aromatic residues are yellow, polar residues are green, and aliphatic residues are tan. (B) Top-down view of the TMD where residues local to the position of C418W are shown as before. (C) Graph comparing the effects of single Ala mutations of the residues local to the position of C418W on C418W-induced potentiation. It was not possible to calculate potentiation for L223A or F227A as I could not obtain data from these mutations on both the WT-nAChR and C418W-nAChR backgrounds. Data show that polar residues are involved in C418W-induced potentiation.

Table 3.6 - Role of residues surrounding αM4 C418W in nAChR function and C418W-induced potentiation.

Mutation	Dose Response[a]						Potentiation (fold)[f]
	WT-nAChR[c]			C418W-nAChR[d]			
	EC_{50} (μM)	Hill Slope	*n*	EC_{50} (μM)	Hill Slope	*n*	
None	7.61 ± 1.25	1.70 ± 0.47	50	0.47 ± 0.12	1.54 ± 0.23	50	16.2
L223A (M1)	**No current[e]**		8	2.26 ± 0.43[b]	1.57 ± 0.11	10	--
S226A (M1)	12.3 ± 3.3[b]	1.52 ± 0.09	8	3.66 ± 0.82[b]	1.26 ± 0.12	8	3.4
F227A (M1)	6.51 ± 1.47	1.43 ± 0.16	8	**No current[e]**		8	--
F233A (M1)	2.63 ± 0.31[b]	1.63 ± 0.20	9	0.21 ± 0.04	1.63 ± 0.18	8	12.5
Y234A (M1)	**No current[e]**		8	**No current[e]**		8	--
F414A (M4)	4.47 ± 0.82	1.76 ± 0.34	10	0.32 ± 0.09	1.50 ± 0.16	8	14.0
T422A (M4)	31.2 ± 9.0[b]	1.40 ± 0.12	10	3.50 ± 1.29[b]	1.49 ± 0.14	10	8.9

[a] Measurements were performed 2 days after injection of cRNA. Error values represent standard deviation.
[b] $p < 0.001$ relative to control via one-way ANOVA followed by Dunnett's post-hoc test.
[c] WT-nAChR contains only the mutation listed under the "mutation" column.
[d] C418W-nAChR contains C418W in addition to the mutation listed under the "mutation" column.
[e] Oocytes were tested 2-7 days after injection of 5-15 ng of mutant cRNA.
[f] EC_{50} of mutant on WT-nAChR background divided by EC_{50} of mutant on C418W-nAChR background.

Table 3.7 - Energetic coupling between Trp418 and surrounding residues on M1 and M4.

Mutants	Ω	ΔΔG (kJ/mol)
Leu223/Trp418	--[b]	--
Ser226/Trp418	0.21	-3.87[a]
Phe227/Trp418	--[b]	--
Phe233/Trp418	0.77	-0.65
Tyr234/Trp418	--[b]	--
Phe414/Trp418	0.86	-0.37
Thr422/Trp418	0.55	-1.48

[a] The free energy is sufficient to indicate energetic coupling.
[b] Could not calculate energetic coupling because of non-functional/non-expressing mutants.

Note that the Ala scan suggested that Phe233, Tyr234, and F414 are likely not involved in C418W-induced potentiation (Table 3.6; Table 3.7; Figure 3.4). F233A and F414A led to subtle gains-of-function when superimposed onto both the WT-nAChR and C418W-nAChR backgrounds, with neither leading to a substantial change in C418W-induced potentiation. No energetic coupling contributing toward channel gating was observed with Phe233 or Phe414 and C418W. On the other hand, neither Y234A nor the Y234A+C418W double mutant expressed and/or functioned in frog oocytes. While these observations do not shed light on the role of this residue in potentiation, it is notable that a Tyr residue at this position is conserved in all the muscle-type nAChR subunits, where it is positioned to interact with the phospholipid head groups of surrounding lipids. Ala substitutions of the same Tyr in the β-, δ-, or ε-subunits also do not function/express (data not shown). A Tyr at this position in each subunit may play a role positioning M1 within the lipid bilayer to facilitate folding.

Finally, the L223A mutation did not express/function, suggesting that the bulky aliphatic side-chain plays a critical role in folding (Table 3.6). Interestingly, the L223A+C418W double mutant did express, but led to a 5-fold loss-of-function relative to C418W-nAChR. Although this could indicate that Leu223 directly contributes to C418W-induced potentiation, it is also possible that the C418W mutation rescues a functionally impaired L223A mutation. As the role of Leu223 in C418W-induced potentiation could not be tested directly in the absence of functional data for the L223A mutant, the role of Leu223 was not pursued further.

3.2.3 Role of Trp418 – Phe227 interactions in C418W-induced potentiation

As noted above, the F227A single mutation had no effect on WT-nAChR function, but the same mutation superimposed onto the C418W-nAChR background, F227A+C418W, did not express, suggesting that a direct interaction between Trp418 and Phe227 is involved in nAChR

folding. Given the importance of aromatic interactions at the M4-M1/M3 interface in both the folding and function of other pLGICs (Carswell et al., 2015a/b; Haeger et al., 2010; Therien and Baenziger, 2017), I next considered the possibility that canonical π-π or CH-π interactions between Trp418 and Phe227 lead to a local conformational change that contributes to C418W-induced potentiation. To test this, I substituted Phe227 with aliphatic (Val, Leu), aromatic (Tyr, Trp), and charged (Lys, Glu) residues (Table 3.8; Figure 3.5). On the WT-nAChR background, these substitutions had minimal effects on channel function, although no ACh-induced current was observed for F227L. The same substitutions superimposed on the C418W-nAChR background had modest effects on the EC_{50} for channel gating (relative to C418W-nAChR), although no current was observed for either the F227A+C418W or the F227V+C418W double mutants, suggesting that side-chain volume at this position may be important in the C418W-nAChR. Significantly, the channel potentiations observed with the Phe227"X"+C418W double mutants varied from ~10- to ~23-fold, not significantly different from the 16-fold potentiation observed with C418W-nAChR. Although the lack of a dramatic effect on C418W-induced potentiation suggests that π-π or CH-π interactions between Trp418 and Phe227 are not critical to C418W-induced potentiation, it is also possible that these interactions are replaced by either π-π or CH-π interactions between Tyr227/Trp227 and Trp418, cation-π interactions between Lys227 and Trp418, or anion-CH interactions between Glu227 and Trp418, consistent with the idea that attractive interactions between residues at these two locations drive potentiation.

To further assess whether direct interactions between Phe227 and Trp418 facilitate M1-M4 interactions to potentiate channel function, I created a series of double mutations at these positions with either like or opposite charges using the positively-charged Lys and negatively-charged Glu residues (Table 3.9; Figure 3.6). Although the F227K+C418K double mutant did

Table 3.8 - Role of side-chain volume and chemistry at position 227 in nAChR function and C418W-induced potentiation.

Mutation	Dose Response[a]						Potentiation (fold)[f]
	WT-nAChR[c]			C418W-nAChR[d]			
	EC_{50} (μM)	Hill Slope	*n*	EC_{50} (μM)	Hill Slope	*n*	
None	7.61 ± 1.25	1.70 ± 0.47	50	0.47 ± 0.12	1.54 ± 0.23	50	16.2
F227A	6.51 ± 1.47	1.43 ± 0.16	8	**No current[e]**		8	--
F227V	14.8 ± 3.8[b]	1.42 ± 0.11	8	**No current[e]**			--
F227L	**No current[e]**			0.92 ± 0.18[b]	1.46 ± 0.20	8	--
F227Y	5.21 ± 0.80[b]	1.44 ± 0.11	8	0.47 ± 0.08	1.61 ± 0.15	8	11.1
F227W	5.77 ± 0.71	1.45 ± 0.16	8	0.25 ± 0.03[b]	1.66 ± 0.08	8	23.1
F227K	8.82 ± 1.13	1.37 ± 0.13	9	0.76 ± 0.15[b]	1.58 ± 0.06	8	11.6
F227E	7.85 ± 1.97	1.54 ± 0.21	8	0.46 ± 0.10	1.56 ± 0.07	8	17.1

[a] Measurements were performed 2 days after injection of cRNA. Error values represent standard deviation.
[b] $p < 0.001$ relative to control via one-way ANOVA followed by Dunnett's post-hoc test.
[c] WT-nAChR contains only the mutation listed under the "mutation" column.
[d] C418W-nAChR receptor contains C418W in addition to the mutation listed under the "mutation" column.
[e] Oocytes were tested 2-7 days after injection of 5-15 ng of mutant cRNA.
[f] EC_{50} of mutant on WT-nAChR background divided by EC_{50} of mutant on C418W-nAChR background.

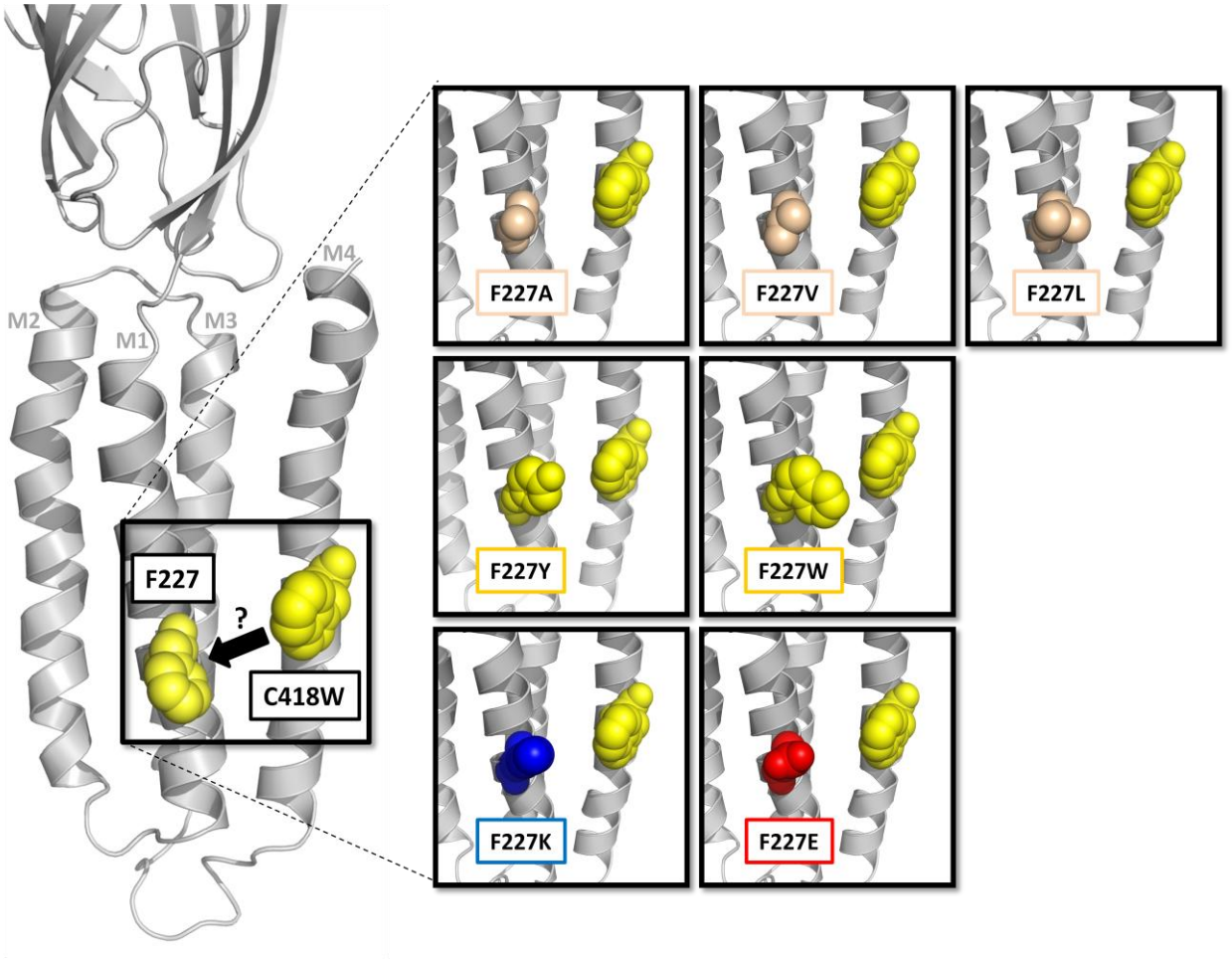

Figure 3.5 - Role of interactions between Trp418 and Phe227 on C418W-induced potentiation. The human muscle-type α-subunit homology model based on the cryo-electron microscopy structure of the *Torpedo* nAChR (PDB: 2BG9). Phe227 and C418W are shown as yellow spheres. The schematic presents the mutations at position 227 which were used to explore an interaction between Trp418 and Phe227. Residues of interest are shown as spheres where aliphatic residues are tan, aromatic residues are yellow, positively-charged residues are blue, and negatively-charged residue are red.

Table 3.9 - Effect of double mutant constructs involving substitutions at positions 227 and 418 in nAChR function.

Mutations	Dose Response[a] EC_{50} (μM)	Hill Slope	*n*	Potentiation (fold)[d]
None	7.61 ± 1.25	1.70 ± 0.47	50	--
Mutations at position 418 with F227A				
F227A+C418A	12.2 ± 1.8[b]	1.38 ± 0.12	8	1.6
F227A+ C418F	1.48 ± 0.35[b]	1.49 ± 0.11	8	5.1
F227A+ C418K	1.73 ± 0.47[b]	1.47 ± 0.05	8	4.4
F227A+ C418E	2.01 ± 0.54[b]	1.53 ± 0.19	8	3.8
F227A+C418W	**No current**[c]		8	--
Charged mutations at positions 227 and 418				
F227K+ C418K	**No current**[c]			--
F227E+ C418E	2.38 ± 0.60[b]	1.46 ± 0.11	8	3.2
F227K+ C418E	1.26 ± 0.36[b]	1.52 ± 0.27	8	6.0
F227E+ C418K	3.03 ± 1.10[b]	1.41 ± 0.19	8	2.5
Switching the aromatics at positions 227 and 418				
F227W+ C418F	1.15 ± 0.33[b]	1.59 ± 0.13	8	6.6

[a] Measurements were performed 2 days after injection of cRNA. Error values represent standard deviation.
[b] $p < 0.001$ relative to control via one-way ANOVA followed by Dunnett's post-hoc test.
[c] Oocytes were tested 2-7 days after injection of 5-15 ng of mutant cRNA.
[d] Wild-type EC_{50} divided by mutant EC_{50}.

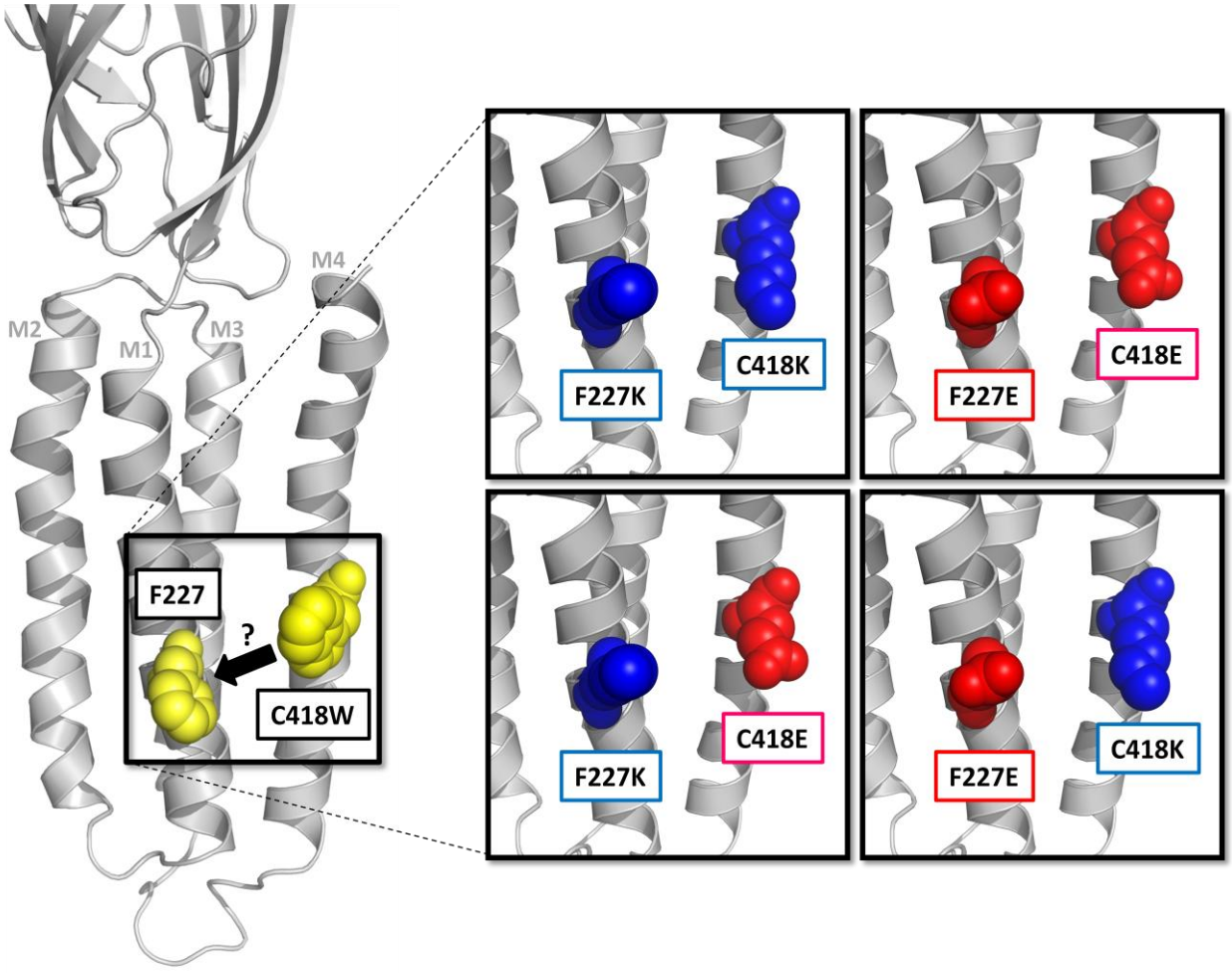

Figure 3.6 - Charged constructs at positions 227 and 418. The human muscle-type α-subunit homology model based on the cryo-electron microscopy structure of the *Torpedo* nAChR (PDB: 2BG9). Phe227 and C418W are shown as yellow spheres. The schematic presents the charged mutations at positions 227 and 418 which were used to explore an interaction between Trp418 and Phe227. Residues of interest are shown as spheres where positively-charged residues are blue and negatively-charged residue are red.

not express and/or function, the F227K+C418E, F227E+C418K, and F227E+C418E double mutants led to EC_{50} values of 1.26 ± 0.36, 3.03 ± 1.10, and 2.38 ± 0.60 μM, respectively, relative to 7.61 ± 1.25 μM for the WT-nAChR. These values correspond to potentiations in channel function of 6-, 3-, and 3-fold, respectively. Although these data further strengthen the suggestion that local structural changes in this region influence channel function, the similar degrees of potentiation, particularly with the F227E+C418K and F227E+C418E double mutants, suggests that interactions between Phe227 and Trp418 are not likely involved in driving C418W-induced potentiation. Note, however, that interpretation of the data is complicated by the fact that the charged residues substituted at these two positions may not be oriented properly for direct electrostatic interactions. In addition, the introduction of charges at both positions could lead to unexpected local rearrangements in structure.

I explored further the possibility of direct interactions between Phe227 and Trp418 by casting the mutagenesis data as mutant cycles (Table 3.10). Although I could not measure the energetic coupling directly between Phe227 and Trp418 due to the lack of expression of the F227A+C418W double mutant, mutant cycle analysis with a multitude of other double mutants at these two positions suggested that there is no energetic coupling between residues at this location that contributes significantly to potentiation (Table 3.9; Table 3.10). Specifically, this was true with Phe/Trp located at position 227 on M1 and Phe at position 418 on M4. Even the opposite charges at positions 227 and 418 (Lys227/Glu418 and Glu227/Lys418) showed minimal coupling energies that contribute to channel gating (< -2.0 kJ/mol). The fact that most of these double mutants lead to potentiated function relative to the WT-nAChR without significant coupling energies between them confirms that an interaction at this location does not

Table 3.10 - Energetic coupling between residues at positions 227 and 418.

Mutants	Ω	ΔΔG (kJ/mol)
Phe227/Cys418	1.35	0.74
Phe227/Phe418	0.97	-0.08
Phe227/Lys418	1.51	1.02
Phe227/Glu418	0.71	-0.85
Phe227/Trp418	--[b]	--
Lys227/Lys418	--[b]	--
Glu227/Glu418	0.52	-1.62
Lys227/Glu418	0.46	-1.92[a]
Glu227/Lys418	0.55	-1.48
Trp227/Phe418	0.88	-0.32

[a] The free energy is sufficient to indicate energetic coupling
[b] Could not calculate energetic coupling because of non-functional/non-expressing mutants.

drive potentiation. Thus, I concluded that, although an interaction between Phe227 and Trp418 in the C418W-nAChR is important in folding, it does not drive C418W-induced potentiation.

3.2.4 A cluster of polar residues at the interface between M1 and M4 is critical to C418W-induced potentiation

A second possibility is that a subtle reorientation of M4 leads to interactions between Trp418/Thr422 and Ser226 on M1. As noted above, both the S226A and T422A mutations reduce the degree of potentiation induced by C418W, implicating both residues in the underlying mechanism. In addition, Ser226 is energetically coupled to Trp418, contributing approximately -4 kJ/mol toward channel gating. To test further the role of both Ser226 and Thr422 in potentiation, I generated the S226A+T422A double mutant, and cast the resulting EC_{50} values as a mutant cycle (Table 3.11; Table 3.12). In the WT-nAChR, Ser226 and Thr422 are energetically coupled, contributing -3.64 kJ/mol toward channel gating. In the C418W-nAChR background, this energetic coupling increases to -4.87 kJ/mol, suggesting that interactions between these two residues are enhanced in the presence of the C418W CMS-causing mutant.

Both Trp418 and Thr422 on M4 are also close to two additional polar residues on M1 that flank Ser226 – Cys222 and Thr229 (Figure 3.7). I explored the possibility that these residues form a cluster of interacting side-chains, whose interactions are enhanced with the C418W mutation (Table 3.11). The C222A and T229A mutations alone each led to only a slight change in the EC_{50} value relative to the WT-nAChR. However, while T229A led to a relatively large reduction in the degree of C418W-induced potentiation from 16-fold down to 6-fold, suggesting a role for this residue in C418W-induced potentiation, C222A caused a more subtle loss of potentiation. From this, Thr229 couples energetically to Trp418 and contributes a modest -2.46 kJ/mol toward channel gating, while Cys222 does not (Table 3.12). The double mutants,

Table 3.11 - Role of local polar interactions between M1 and M4 in nAChR function and C418W-induced potentiation.

Mutation(s)	Dose Response[a]						Potentiation (fold)[e]
	WT-nAChR[c]			C418W-nAChR[d]			
	EC_{50} (μM)	Hill Slope	*n*	EC_{50} (μM)	Hill Slope	*n*	
None	7.61 ± 1.25	1.70 ± 0.47	50	0.47 ± 0.12	1.54 ± 0.23	50	16.2
C222A (M1)	4.75 ± 0.84	1.52 ± 0.15	8	0.51 ± 0.13	1.87 ± 0.15	9	9.3
S226A (M1)	12.3 ± 3.3[b]	1.52 ± 0.09	8	3.66 ± 0.82[b]	1.26 ± 0.12	8	3.4
T229A (M1)	7.72 ± 1.37	1.40 ± 0.07	8	1.30 ± 0.33[b]	1.53 ± 0.36	8	5.9
T422A (M4)	31.2 ± 9.0[b]	1.40 ± 0.12	10	3.50 ± 1.29[b]	1.49 ± 0.14	10	8.9
S226A+T229A	11.1 ± 1.9	1.40 ± 0.08	8	7.24 ± 1.37[b]	1.48 ± 0.16	8	1.5
S226A+T422A	11.8 ± 3.3	1.41 ± 0.22	8	4.00 ± 1.39[b]	1.45 ± 0.27	7	3.0
S226A+T229A+T422A	16.6 ± 2.1[b]	1.47 ± 0.08	8	17.3 ± 3.3[b]	1.48 ± 0.11	8	1.0

[a] Measurements were performed 2 days after injection of cRNA. Error values represent standard deviation.
[b] $p < 0.001$ relative to control via one-way ANOVA followed by Dunnett's post-hoc test.
[c] WT-nAChR contains only the mutation(s) listed under the "mutation(s)" column.
[d] C418W-nAChR contains C418W in addition to the mutation(s) listed under the "mutation(s)" column.
[e] EC_{50} of mutant on WT-nAChR background divided by EC_{50} of mutant on C418W-nAChR background.

Table 3.12 - Energetic coupling between polar residues on M1 and M4.

Mutants	Ω	ΔΔG (kJ/mol)
Cys222/Trp418	0.58	-1.35
Ser226/Trp418	0.21	-3.87[a]
Thr229/Trp418	0.37	-2.46[a]
Thr422/Trp418	0.55	-1.48
Ser226+Thr229/Trp418	0.10	-5.70[a]
Ser226+Thr422/Trp418	0.18	-4.25[a]
Ser226+Thr229+Thr422/Trp418	0.06	-6.97[a]

Mutants	WT-nAChR[b]		C418W-nAChR[c]	
	Ω	ΔΔG (kJ/mol)	Ω	ΔΔG (kJ/mol)
Ser226/Thr229	0.89	-0.29	0.72	-0.81
Ser226/Thr422	0.23	-3.64[a]	0.14	-4.87[a]
Ser226+Thr229/Thr422	0.36	-2.53[a]	0.32	-2.82[a]

[a]The free energy is sufficient to indicate energetic coupling
[b] WT-nAChR contains only the mutants listed under the "mutants" column.
[c] C418W-nAChR contains C418W in addition to the mutants listed under the "mutants" column.

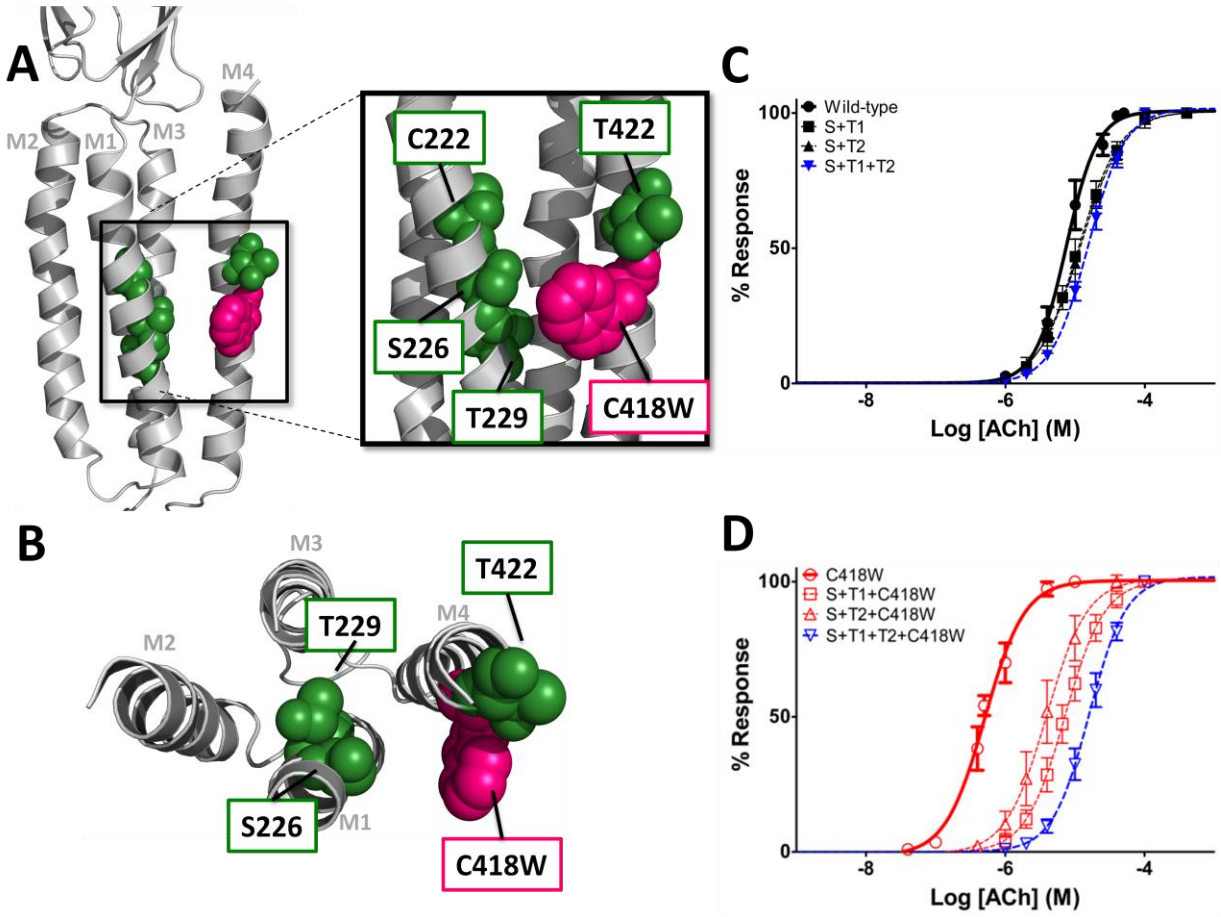

Figure 3.7 - Role of M4-M1 cluster of polar residues on C418W-induced potentiation. (A) The human muscle-type α-subunit homology model based on the cryo-electron microscopy structure of the *Torpedo* nAChR (PDB: 2BG9). C418W is shown as pink spheres and the surrounding polar residues on M1 and M4 are shown as green spheres. (B) Top-down view of the TMD showing the polar residues which are critical to the mechanism of C418W-induced potentiation as green spheres in addition to C418W. (C) and (D) Normalized dose response curves for double and triple Ala mutations of critical polar residues on the WT-nAChR (C) and C418W-nAChR (D) background showing, in blue, that the triple Ala mutant completely abrogates C418W-induced potentiation. S226A+T229A is represented as S+T1, S226A+T422A is represented as S+T2, and S226A+T229A+T422A is represented as S+T1+T2. Error bars represent standard deviation, $n \geq 8$.

S226A+T229A and S226A+T422A, both decreased C418W-induced potentiation from 16-fold down to 1.5- and 3.0-fold, respectively. Significantly, the S226A+T229A+T422A triple mutant completely eliminated C418W-induced potentiation (Table 3.11; Figure 3.7). Ser226+Thr229 couple directly with Trp418, contributing a relatively large -5.70 kJ/mol toward channel gating; whereas, the three residues, Ser226+Thr229+Thr422, collectively couple energetically with Trp418 and contribute -6.97 kJ/mol toward channel gating, accounting for the entire 16-fold potentiation (Table 3.12). The latter findings show that αM4 C418W induces potentiation of the nAChR by promoting local interactions between M4 and the adjacent M1 transmembrane α-helix, specifically interactions between Trp418/Thr422 on M4 and Ser226/Thr229 on M1.

3.3 Discussion

The αM4 C418W CMS-causing mutation is located at the protein-lipid interface at the approximate centre of the lipid bilayer where it is able to stabilize the open nAChR conformation and potentiate channel function 16-fold, likely by altering interactions between M4 and the lipids (Shen et al., 2006). This is despite the fact that this mutation is peripheral to the agonist binding sites, channel gate, and other key gating elements. αM4 C418W demonstrates that the highly lipid exposed structure of M4 and its interactions with the surrounding lipids can affect nAChR function. This is in addition to what was learned from initial studies with the *Torpedo* nAChR, homologous to the human muscle-type nAChR, where nAChRs were shown to be exquisitely sensitive to their lipid environment (Criado et al., 1984; Epstein and Racker, 1978; Fong and McNamee, 1986; Heidmann et al., 1980). However, it remains unclear how changes in the surrounding lipid environment ultimately translate into changes of nAChR function. One model proposes that M4 "senses" its lipid environment and affects nAChR function through a critical interaction between the M4 C-terminus and the highly conserved extracellular structure, the Cys-

loop. In optimal lipid environments, interactions between M4 and the Cys-loop would be promoted, leading to enhanced channel function; whereas, in non-optimal lipid environments, these same interactions would be lost, leading to stabilization of the lipid-dependent uncoupled conformation which does not undergo channel gating in response to agonist binding (daCosta & Baenziger, 2009). As the αM4 C418W mutation alters nAChR-lipid interactions via M4 to promote function, it offers an intriguing opportunity to indirectly test this model.

I initially speculated that αM4 C418W potentiates channel function by enhancing interactions between the M4 C-terminus and the Cys-loop, as per the M4 lipid sensor model, which would enhance nAChR coupling efficiency and stabilize the open state, producing the disease phenotype. Plenty of experimental evidence exists to support the idea that interactions at this location are important to pLGIC function. First, direct interaction between the M4 C-terminus and the Cys-loop is required to lock an α7 nAChR–5-HT_3 receptor chimera in an active conformation that responds to agonist (Pons et al., 2004). Second, in GLIC, aromatic-to-Ala substitutions of residues at the M4 C-terminus, some of which interact directly with adjacent aromatic residues on the β6-β7 loop (Cys-loop in eukaryotic pLGICs), result in loss of channel function (Carswell et al., 2015b). Finally, in ELIC, although such interactions between the M4 C-terminus and β6-β7 loop do not exist in the structure, the enhancement of interactions at this location potentiates channel function, presumably by enhancing the coupling efficiency between the ECD and TMD (Carswell et al., 2015b).

Specifically, in the *Torpedo* nAChR structure, two residues from the M4 C-terminus in the α-subunit, Glu432 and Gln435, are shown to interact with a highly conserved aromatic residue, Phe137, on the Cys-loop (Unwin, 2005). These residues are all conserved in the human muscle-type nAChR. The M4 lipid sensor model proposes that an interaction between these

three residues is critical to nAChR function (daCosta and Baenziger, 2009). In support of this hypothesis, the Gln435 equivalent residue from the neuronal α4-subunit is critical for mediating steroid-induced potentiation (Paradiso et al., 2001). However, my data show conclusively that neither Glu432, Gln435, nor Phe137 are important to channel function. In fact, the F137A mutant actually increases channel function, similar to what was observed in the homopentameric α7 nAChR (Aldea et al., 2007). Further, the αM4 C418W mutation does not induce potentiation by promoting interactions at this location. Two additional residues, Asn434 of M4 and Asp138 of the Cys-loop, were also shown not to be involved in a critical interaction; although the D138A mutant did reveal an important role for charged residues at the ECD-TMD interface (Xiu et al., 2005) and the Cys-loop in nAChR folding (Fu and Sine, 1996; Green and Wanamaker, 1997).

M4-C-terminal deletions in the muscle-type nAChR also revealed a similar functional phenotype to the above point mutations, where deletion of up to four C-terminal residues had no effect, and only minimal effects on both function and C418W-induced potentiation were observed with deletion of up to 12 C-terminal residues. If interactions between M4 and the Cys-loop were critical to nAChR function or C418W-induced potentiation, one would expect dramatic changes in function and potentiation with these deletions, which I did not observe. These data are in stark contrast to what is observed in GLIC, where deletion of just four residues from the M4 C-terminus abolishes channel activity, presumably due to the loss of contacts between M4 and the β6-β7 loop (Hénault et al., 2015). Similarly, in the human GABAρ1 receptor, deletion of the final four C-terminal residues causes a profound 1000-fold loss-of-function and further deletion of the fifth residue results in the loss of all channel activity (Reyes-Ruiz et al., 2010). Studies in both GLIC and GABA suggest that interactions between the M4 C-terminus and the Cys-loop are critical for proper function. Contrastingly, in ELIC, the deletion

of up to seven C-terminal residues has no detrimental effect on function, actually leading to an almost 2-fold gain-of-function relative to wild-type ELIC (Hénault et al., 2015), which is more similar to what I have observed in the muscle-type α-subunit.

Altogether, these results may highlight distinct functional roles for M4 in different pLGICs. Indeed, Therien and Baenziger (2017) have proposed two distinct pLGIC archetypes based upon the strength of contacts between M4 and M1/M3. pLGICs from the first archetypal category, such as GLIC and GABA, require strong inter-helical contacts at this interface to promote activity, while pLGICs from the second archetypal category, such as ELIC and the nAChR, do not possess such contacts, presumably to allow for greater conformational flexibility within the TMD. The importance of interactions between the M4 C-terminus and Cys-loop in promoting channel function may apply similarly to these archetypes, where GLIC requires these types of interactions for function, while ELIC and the nAChR do not. Indeed, my data do support this conclusion. Further, it is clear that αM4 C418W does not utilize M4–Cys-loop contacts to potentiate nAChR function in any capacity.

Although my M4 C-terminal deletions did not reveal a functional role for the M4 C-terminus, they did lead to a progressive loss of cell surface expression, revealing a role for the M4 C-terminus in folding and expression. Deletion of up to 12 residues from the C-terminus of αM4, F426X, resulting in the removal of three complete α-helical turns, abolished expression of the nAChR at the cell surface as measured by [^{125}I]-α-bungarotoxin binding. Phe426 is conserved amongst all muscle-type subunits and protrudes toward the lipids (Blanton & Cohen, 1994) where it interacts with the polar phospholipid head groups (Lizardi-Ortiz et al., 2008); therefore, it is possible that this residue is critical for positioning M4 within the lipid bilayer parallel to M1/M3. The elimination of Phe426 may hinder folding, leading to a loss of nAChR

expression. Additionally, deletion of Phe426 may unmask an endoplasmic reticulum (ER) retention motif on M1 resulting in loss of nAChR expression to the cell surface due to degradation within the ER (Wang et al., 2002). Numerous other studies have highlighted a role for M4 in folding, assembly, and trafficking of pLGICs. Roccamo and Barrantes (2007) found that positively-charged residues flanking αM4 in the muscle-type nAChR were important for expression, while a CMS-causing mutation, resulting in truncation of the εM4 C-terminus, abrogates cell surface expression (Ealing et al., 2002). Altogether, it is clear from my data that the C-terminus of αM4 is not important to nAChR function or C418W-induced potentiation, although a role for the M4 C-terminus in expression has been highlighted.

Many positive allosteric modulators (PAMs), which include neurosteroids, anaesthetics, alcohols, and even lipids, bind to inter- and intra-subunit cavities within the TMD of various pLGICs to modulate their activity (Collins & Millar, 2010; daCosta et al., 2011; Mihic et al., 1997; Ueno et al., 2004; Young et al., 2008). Commonly, binding sites for PAMs are located near the extracellular end of the TMD where these molecules can interact with the Cys-loop and other residues along the allosteric coupling pathway to modulate activity. However, as is demonstrated by the α7-specific potentiator, PNU-120596 (PNU), modulation of channel activity can occur when molecules interact only with residues distant from the channel gate, the coupling pathway, and the agonist binding sites (daCosta et al., 2011). I have shown that αM4 C418W does not lead to altered interactions between the M4 C-terminus and the Cys-loop; as such, this mutation may potentiate muscle-type nAChR activity in a similar manner to the way in which PNU potentiates activity of the α7 nAChR – by modifying central TMD contacts. Indeed, Young *et al* (2008) propose that the intra-subunit cavity occupied by PNU in α7 nAChRs may be a highly conserved modulatory site of the Cys-loop ion channels.

Having excluded the M4 C-terminus from the mechanism by which αM4 C418W potentiates nAChR function, and considering that some PAMs modulate activity by altering central TMD interactions, I considered that direct physical interactions between the Trp side chain at position 418 on αM4 and adjacent residues on M1 and/or M3 could ultimately drive potentiation of channel function. Previous studies have shown that position 418, and to a lesser extent, position 421 on αM4 are particularly sensitive to mutation as compared to the rest of the α-helix (Lasalde et al., 1996). Residues at both of these positions are located at the approximate centre of the TMD/lipid bilayer and are oriented toward the adjacent M1 α-helix based on the *Torpedo* nAChR structure (Unwin, 2005); however, only position 418 is lipid-exposed (Blanton and Cohen, 1992). Generally, Trp-scanning mutagenesis studies in the remaining muscle-type nAChR subunits have shown that only Trp mutations of residues at the equivalent α418 and α421 positions on M4 are able to potentiate nAChR function and that the effect of mutations at these positions in different subunits are additive (Lasalde et al., 1996; Ortiz-Acevedo et al., 2004; Tamamizu et al., 2000).

Two studies probed the effect of different side-chains at position 418 yielding similar results (Mitra et al., 2004; Tamamizu et al., 1999). Both studies found that the Cys to Trp substitution at position 418 potentiated activity the most out of all residues tested. Replacing Cys418 with small or aliphatic residues such as Ser, Ala, Val, and Leu had either no effect on nAChR function, or was actually detrimental. However, all remaining substitutions, including relatively large polar (Asn), charged (His, Glu) or aromatic (Phe, Tyr) side-chains, were able to potentiate nAChR activity to differing degrees. My data agree with these results, where C418A had no effect, and C418F, C418K, and C418E all potentiated activity ~3- to ~5-fold as compared to the WT-nAChR. Altogether, these data suggest that side-chain volume, and to a lesser extent

side-chain chemistry, are important to potentiation, and that position 418 on αM4 is especially sensitive to mutation.

As position 418 on αM4 is oriented toward M1, M4-M1 interactions may be important to potentiation. The aromatic side-chain, Phe227, on the αM1 helix protrudes toward the lipids (Blanton and Cohen, 1994) and could form canonical π-π or CH-π interactions with Trp418 in the αM4 C418W mutant to facilitate potentiation. Initial support for this hypothesis was provided from my data where the F227A mutant by itself had no effect on WT-nAChR function or expression, while the F227A+C418W double mutant did not express to the cell surface. In proteins, in addition to π-π or CH-π interactions between two aromatic residues, polar, positively-charged, and negatively-charged residues can all form stable interactions with aromatic residues (Cauët et al., 2005; Gallivan & Dougherty, 1999; Muraki et al., 1997). Thus, the driving force of potentiation by mutations at position 418 could very well be due to an interaction between X418 and Phe227; in other words, C418E, C418F, C418H, C418K, C418N, and C418W could all feasibly interact with Phe227, leading to potentiation. However, my mutant cycle analyses using multiple double mutant constructs of substitutions at positions 227 and 418 found minimal, if any, energetic coupling between residues at these two positions, suggesting that an interaction at this location is not the driving force behind C418W-induced potentiation, although it may be involved in folding and expression, specifically in the C418W-nAChR.

As polar residues are key drivers of helix-helix interactions in the hydrophobic membrane environment (Cymer et al., 2015), I looked at interactions between C418W and surrounding polar residues. In doing so, I found that interaction between C418W and a cluster of polar residues between M4 and M1 were absolutely critical to C418W-induced potentiation. Altered

M4-M1 interactions could alter the conformation of M1 in such a way as to stabilize the ECD-TMD interfacial structure, pre-M1, in its open state conformation. Arg209 and Leu210 of pre-M1 have been implicated in the principal and Cys-loop gating pathways, respectively (Lee and Sine, 2005; Lee et al., 2009), and are both important to nAChR gating. The altered conformation of pre-M1 may account entirely for C418W-induced potentiation; however, it is unlikely that altered positions/movements of M1 and M4 occur independently of both M2 and M3, which line the channel gate (M2), participate in forming the M2-M3 linker (M2 and M3), and may interact directly with the Cys-loop (M3). Thus, the mechanism of C418W-induced potentiation is likely more complicated.

3.4 Conclusions

In summary, interactions between the αM4 C-terminus and the Cys-loop are not important to channel function in the WT-nAChR, nor are they critical to the mechanism by which αM4 C418W potentiates nAChR function. Instead, C418W potentiates nAChR channel activity approximately 16-fold by altering M4-M1 interactions local to position 418 of αM4, mediated by three polar residues at the approximate centre of the TMD: Thr422 of M4, and Ser226/Thr229 of M1 in addition to Trp418. The interaction between these three polar residues is absolutely critical to C418W-induced potentiation, as the gain-of-function observed in the C418W-nAChR as compared to the WT-nAChR is completely abolished with the triple Ala mutant, S226A+T229A+T422A. In Chapter 4, I will explore further how interactions between Trp418/Thr422 and Ser226/Thr229 ultimately lead to potentiation of channel function.

Chapter 4

Effects of altered M4-M1 interactions in the αM4 C418W mutant propagate to two important gating structures to stabilize the open state

4.1 Introduction

In the previous chapter, I showed that the CMS-causing mutation, αM4 C418W, potentiates channel function 16-fold by enhancing local interactions between two transmembrane helices, M4 and M1. Specifically, the mutation leads to direct or enhanced energetic couplings between Trp418 and Thr422 on M4 and both Ser226 and Thr229 on M1. Furthermore, if all three polar residues (Thr422/Ser226/Thr229) are collectively mutated to Ala, then C418W-induced potentiation is completely lost. In this chapter, I use a similar mutant cycle approach to explore how enhanced interactions between Trp418 and Thr422 on M4 and both Ser226 and Thr229 on M1 ultimately propagate to the important structures involved in gating (i.e. the M2 α-helix and the ECD-TMD interface) to alter channel function (Figure 4.1).

4.2 Results

4.2.1 Altered M4-M1 interactions directly influence gating motions of the pore-lining M2 α-helix

I first explored the possibility that a subtle reorientation of M1 due to the C418W mutation facilitates polar interactions between Ser226/Thr229 on M1 and Ser288/Thr292 on M3 to stabilize movements of M2 in the open state (Figure 4.2). Ala mutations of Ser288 and Thr292, however, had little effect on channel activity in either the WT-nAChR or C418W-nAChR (Table 4.1), and there was no indirect energetic coupling detected between either Ser288 or Thr292 and Trp418 (Table 4.2). Although the S226A+S288A and T229A+S288A double mutants both decreased potentiation, the loss of potentiation in each case was the same as the loss of potentiation observed with the individual S226A and T229A mutations, respectively. Indeed, mutant cycle analysis confirms that neither Ser226 nor Thr229 are energetically coupled

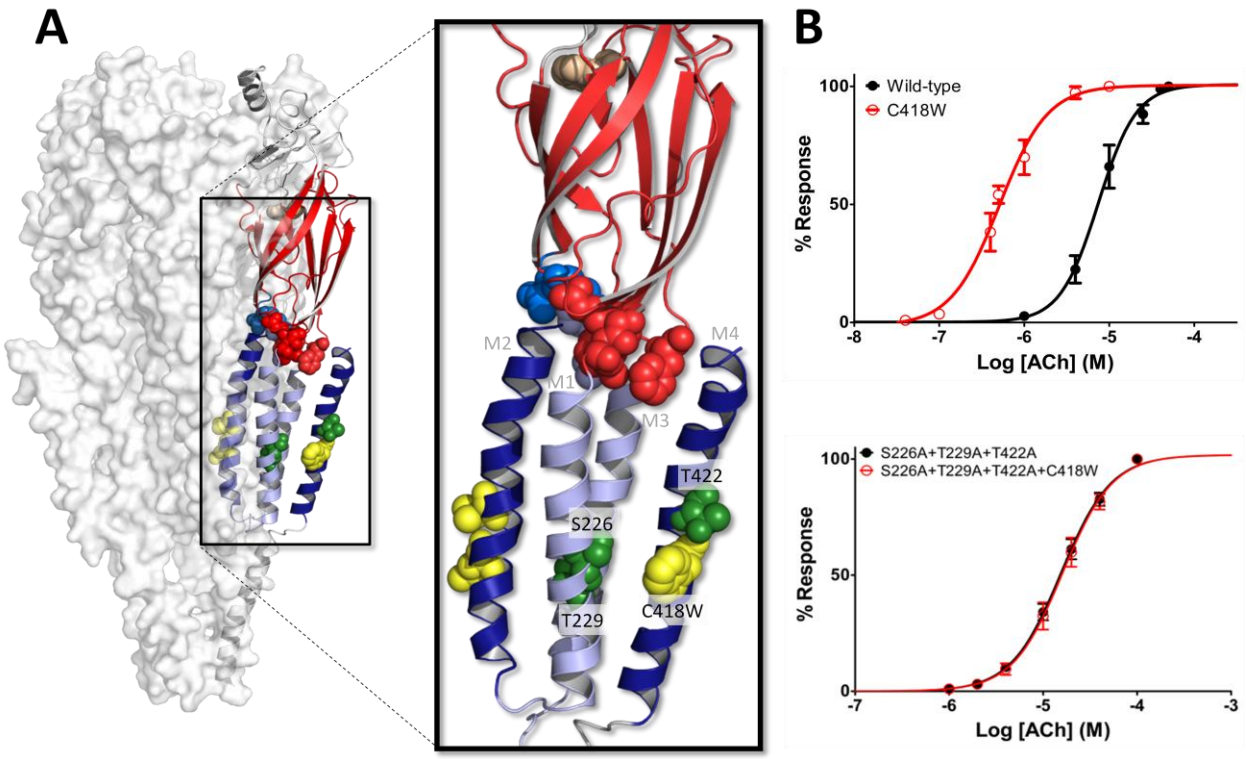

Figure 4.1 - Altered M4-M1 interactions are critical to C418W-induced potentiation. (A) Structure of the nAChR (PDB: 2BG9) where a single α-subunit is shown in cartoon. The critical Trp149 from the binding site is shown as tan spheres while the rest of the ECD is shown in red. Select residues at the ECD-TMD interface implicated in nAChR gating are shown as spheres where Glu45 and Val46 are blue, Phe135, Phe137, Arg209, and Leu210 are red, and Pro272 and Leu273 are light blue. Leu251 and Val255, which form the hydrophobic gate, are shown as yellow spheres. The channel-lining and lipid-exposed TMD α-helices, M2 and M4, respectively, are shown in dark blue, while the adjacent M1 and M3 TMD α-helices are shown in light blue. The lipid-facing C418W mutant is shown as yellow spheres. (B) Averaged dose response curves showing the potentiation of channel function in the C418W-nAChR mutant relative to the WT-nAChR (top) and that the triple Ala mutant involving three polar residues abrogates this potentiation (bottom). Error bars represent standard deviation, $n \geq 8$.

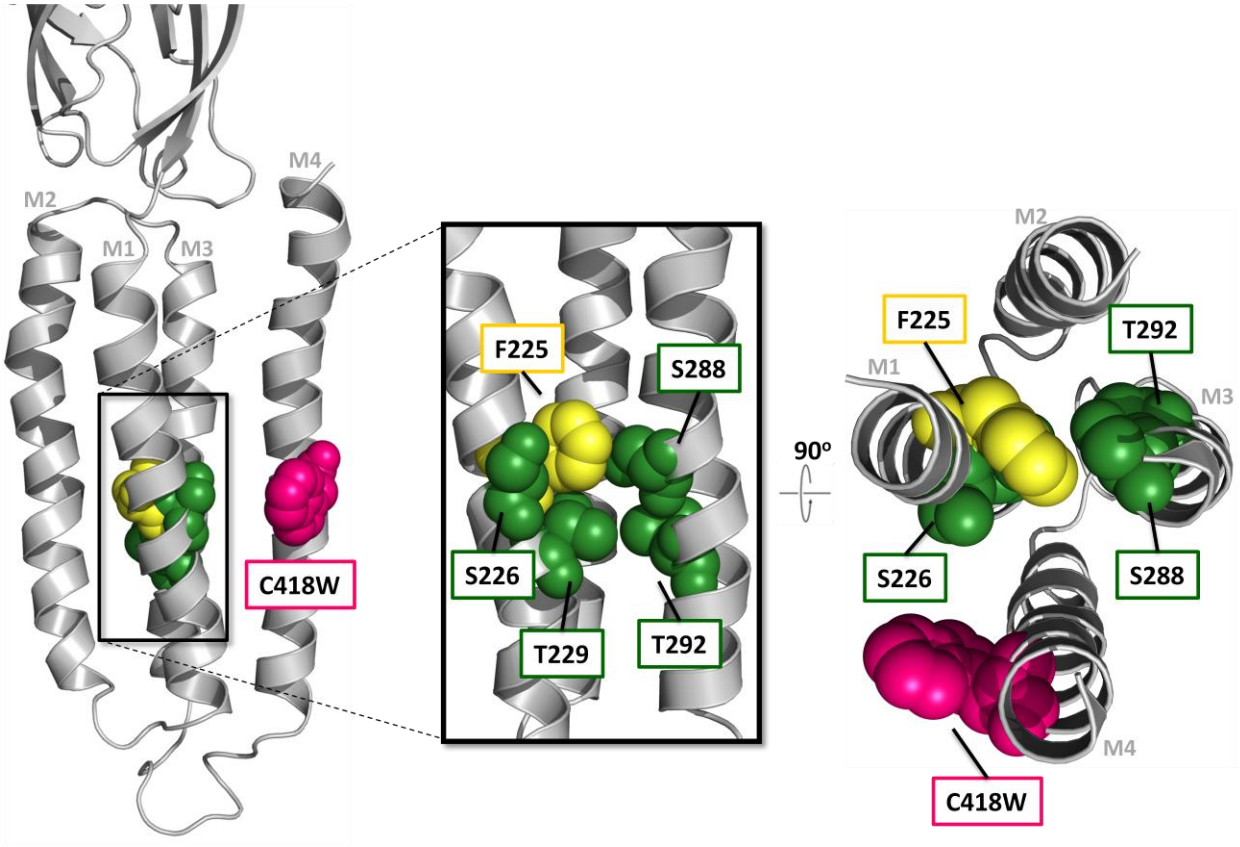

Figure 4.2 - Role of M1-M3 interactions in C418W-induced potentiation. The human muscle-type α-subunit homology model based on the cryo-electron microscopy structure of the *Torpedo* nAChR (PDB: 2BG9). The C418W mutation is shown as pink spheres. Potentially interacting residues between M1 and M3 at the centre of the TMD are shown as spheres where aromatic residues are yellow and polar residues are green. The right-most image is a top-down view of the TMD showing the residues as before. There were no energetic couplings found between residues on M1 and M3 at this location.

Table 4.1 - Role of local interactions between M1 and M3 in nAChR function and C418W-induced potentiation.

Mutation(s)	Dose Response[a]						Potentiation (fold)[f]
	WT-nAChR[c]			C418W-nAChR[d]			
	EC_{50} (μM)	Hill Slope	*n*	EC_{50} (μM)	Hill Slope	*n*	
None	7.61 ± 1.25	1.70 ± 0.47	50	0.47 ± 0.12	1.54 ± 0.23	50	16.2
F225A (M1)	0.71 ± 0.12[b]	1.57 ± 0.39	8	0.07 ± 0.02[b]	1.29 ± 0.41	9	10.1
S226A (M1)	12.3 ± 3.3[b]	1.52 ± 0.09	8	3.66 ± 0.82[b]	1.26 ± 0.12	8	3.4
T229A (M1)	7.72 ± 1.37	1.40 ± 0.07	8	1.30 ± 0.33[b]	1.53 ± 0.36	8	5.9
S288A (M3)	8.34 ± 1.67	1.53 ± 0.14	8	0.78 ± 0.07	2.60 ± 0.44	9	10.7
T292A (M3)	4.81 ± 0.79[b]	1.71 ± 0.17	8	0.53 ± 0.13	1.79 ± 0.30	8	9.1
F225A+S226A	**No current**[e]		8	0.41 ± 0.05	1.51 ± 0.20	4	--
F225A+T229A	0.68 ± 0.02[b]	1.55 ± 0.06	4	**No current**[e]		4	--
F225A+S288A	**No current**[e]		4	0.08 ± 0.01[b]	1.73 ± 0.08	4	--
S226A+S288A	14.3 ± 3.1[b]	1.53 ± 0.06	8	4.65 ± 1.00[b]	1.71 ± 0.23	8	3.1
T229A+S288A	14.0 ± 3.1[b]	1.49 ± 0.14	8	1.91 ± 0.34[b]	1.64 ± 0.13	8	7.3

[a] Measurements were performed 2 days after injection of cRNA. Error values represent standard deviation.
[b] $p < 0.001$ relative to control via one-way ANOVA followed by Dunnett's post-hoc test.
[c] WT-nAChR contains only the mutation(s) listed under the "mutation(s)" column.
[d] C418W-nAChR receptor contains C418W in addition to the mutation(s) listed under the "mutation(s)" column.
[e] Oocytes were tested 2-7 days after injection of 5-15 ng of mutant cRNA.
[f] EC_{50} of mutant on WT-nAChR background divided by EC_{50} of mutant on C418W-nAChR background.

Table 4.2 - Energetic coupling between residues on M1 and M3.

Mutants	Ω	ΔΔG (kJ/mol)
Phe225/Trp418	0.63	-1.14
Ser226/Trp418	0.21	-3.87[a]
Thr229/Trp418	0.37	-2.46[a]
Ser288/Trp418	0.66	-1.03
Thr292/Trp418	0.56	-1.44
Phe225+Ser226/Trp418	--[b]	--
Phe225+Thr229/Trp418	--[b]	--
Phe225+Ser288/Trp418	--[b]	--
Ser226+Ser288/Trp418	0.19	-4.11[a]
Thr229+Ser288/Trp418	0.45	-1.98[a]

Mutants	WT-nAChR[c]		C418W-nAChR[d]	
	Ω	ΔΔG (kJ/mol)	Ω	ΔΔG (kJ/mol)
Phe225/Ser226	--[b]	--	0.75	-0.71
Phe225/Thr229	0.94	-0.15	--[b]	--
Phe225/Ser288	--[b]	--	0.69	-0.92
Ser226/Ser288	1.06	0.14	0.77	-0.65
Thr229/Ser288	1.65	1.24	0.89	-0.29

[a] The free energy is sufficient to indicate energetic coupling.
[b] Could not calculate energetic coupling because of non-functional/non-expressing mutants.
[c] WT-nAChR contains only the mutants listed under the "mutants" column.
[d] C418W-nAChR contains C418W in addition to the mutants listed under the "mutants" column.

to Ser288 in either the WT-nAChR or C418W-nAChR background (Table 4.2). Thus, C418W on M4 does not alter local polar interactions between M1 and M3 to affect gating.

A third residue on M1, Phe225, is adjacent to both Ser226 and Thr229, and its bulky aromatic side-chain protrudes into the interface between M1, M2, and M3 (Figure 4.2). The F225A mutation led to a 10-fold enhancement in channel function showing that this residue plays a substantial, albeit detrimental role in channel gating (Table 4.1). When coupled with C418W, however, the F225A mutation led to only a subtle loss of potentiation, and does not energetically couple indirectly with Trp418 (Table 4.2). Furthermore, I created double mutants to explore whether energetic couplings between Phe225 and surrounding residues on M1/M3 change with C418W. Unfortunately, double mutants involving F225A and either Ser226/Thr229 on M1 or Ser288 on M3 did not express and/or function specifically on either the WT-nAChR or C418W-nAChR backgrounds depending on the mutant (Table 4.2). Thus, in many cases couplings could not be evaluated on either the WT-nAChR or C418W-nAChR backgrounds and I could not determine the role for any of these double mutants in potentiation. Although the bulky Phe225 along with other residues at this central location may be required to stabilize the TMD, the lack of energetic couplings between Phe225 and other residues in its vicinity suggests that interactions between Phe225 and surrounding residues on M1 and M3 do not play a critical role in C418W-induced potentiation.

A subtle reorientation of M1, independent of M3, could directly alter interactions between M1 and M2 in the open state that do not involve M3. To test this hypothesis, I next explored energetic couplings between residues on M1/M3 and M2 (Table 4.3; Table 4.4). Ser252, Leu253, and Thr254 on M2 face the adjacent M1/M3 helices (Figure 4.3). On the WT-nAChR background, S252A and T254A subtly increased channel function (3- and 2-fold,

Table 4.3 - Role of local interactions between M1/M3 and M2 in nAChR function and C418W-induced potentiation.

Mutation(s)	Dose Response[a]						Potentiation (fold)[f]
	WT-nAChR[c]			C418W-nAChR[d]			
	EC_{50} (μM)	Hill Slope	*n*	EC_{50} (μM)	Hill Slope	*n*	
None	7.61 ± 1.25	1.70 ± 0.47	50	0.47 ± 0.12	1.54 ± 0.23	50	16.2
F225A (M1)	0.71 ± 0.12[b]	1.57 ± 0.39	8	0.07 ± 0.02[b]	1.29 ± 0.41	9	10.1
T229A (M1)	7.72 ± 1.37	1.40 ± 0.07	8	1.30 ± 0.33[b]	1.53 ± 0.36	8	5.9
S252A (M2)	2.37 ± 0.75[b]	1.39 ± 0.08	8	0.49 ± 0.11	1.42 ± 0.28	8	4.8
L253A (M2)	10.2 ± 0.8	1.80 ± 0.11	8	0.31 ± 0.05	1.66 ± 0.19	10	30.9
T254A (M2)	4.48 ± 0.80[b]	1.77 ± 0.22	8	0.41 ± 0.07	1.53 ± 0.17	8	10.9
S288A (M3)	8.34 ± 1.67	1.53 ± 0.14	8	0.78 ± 0.07[b]	2.60 ± 0.44	9	10.7
T292A (M3)	4.81 ± 0.79[b]	1.71 ± 0.17	8	0.53 ± 0.13	1.79 ± 0.30	8	9.1
F225A+L253A	**No current**[e]		4	**No current**[e]		4	--
T229A+S252A	1.99 ± 0.73[b]	1.28 ± 0.20	8	0.61 ± 0.16	1.33 ± 0.15	8	3.3
T229A+L253A	32.9 ± 6.7[b]	1.51 ± 0.13	8	**No current**[e]		8	--
L253A+T292A	6.27 ± 0.44	1.90 ± 0.15	10	0.42 ± 0.06	1.58 ± 0.12	8	14.9
T254A+S288A	6.67 ± 0.92	1.81 ± 0.16	8	0.51 ± 0.08	1.50 ± 0.13	8	13.1

[a] Measurements were performed 2 days after injection of cRNA. Error values represent standard deviation.
[b] $p < 0.001$ relative to control via one-way ANOVA followed by Dunnett's post-hoc test.
[c] WT-nAChR contains only the mutation(s) listed under the "mutation(s)" column.
[d] C418W-nAChR receptor contains C418W in addition to the mutation(s) listed under the "mutation(s)" column.
[e] Oocytes were tested 2-7 days after injection of 5-15 ng of mutant cRNA.
[f] EC_{50} of mutant on WT-nAChR background divided by EC_{50} of mutant on C418W-nAChR background.

Table 4.4 - Energetic coupling between residues on M1/M3 and M2.

Mutants	Ω	ΔΔG (kJ/mol)
Phe225/Trp418	0.63	-1.14
Thr229/Trp418	0.37	-2.46[a]
Ser252/Trp418	0.30	-2.98[a]
Leu253/Trp418	2.03	1.75[a]
Thr254/Trp418	0.73	-0.78
Ser288/Trp418	0.66	-1.03
Thr292/Trp418	0.56	-1.44
Phe225+Leu253/Trp418	--[b]	--
Thr229+Ser252/Trp418	0.20	-3.99[a]
Thr229+Leu253/Trp418	--[b]	--
Leu253+Thr292/Trp418	0.92	-0.21
Thr254+Ser288/Trp418	0.81	-0.52

Mutants	WT-nAChR[c]		C418W-nAChR[d]	
	Ω	ΔΔG (kJ/mol)	Ω	ΔΔG (kJ/mol)
Phe225/Leu253	--[b]	--	--[b]	--
Thr229/Ser252	0.83	-0.46	0.46	-1.92[a]
Thr229/Leu253	3.18	2.87[a]	--[b]	--
Leu253/Thr292	0.97	-0.08	1.20	0.45
Thr254/Ser288	1.36	0.76	0.81	-0.52

[a] The free energy is sufficient to indicate energetic coupling.
[b] Could not calculate energetic coupling because of non-functional/non-expressing mutants.
[c] WT-nAChR contains only the mutants listed under the "mutants" column.
[d] C418W-nAChR contains C418W in addition to the mutants listed under the "mutants" column.

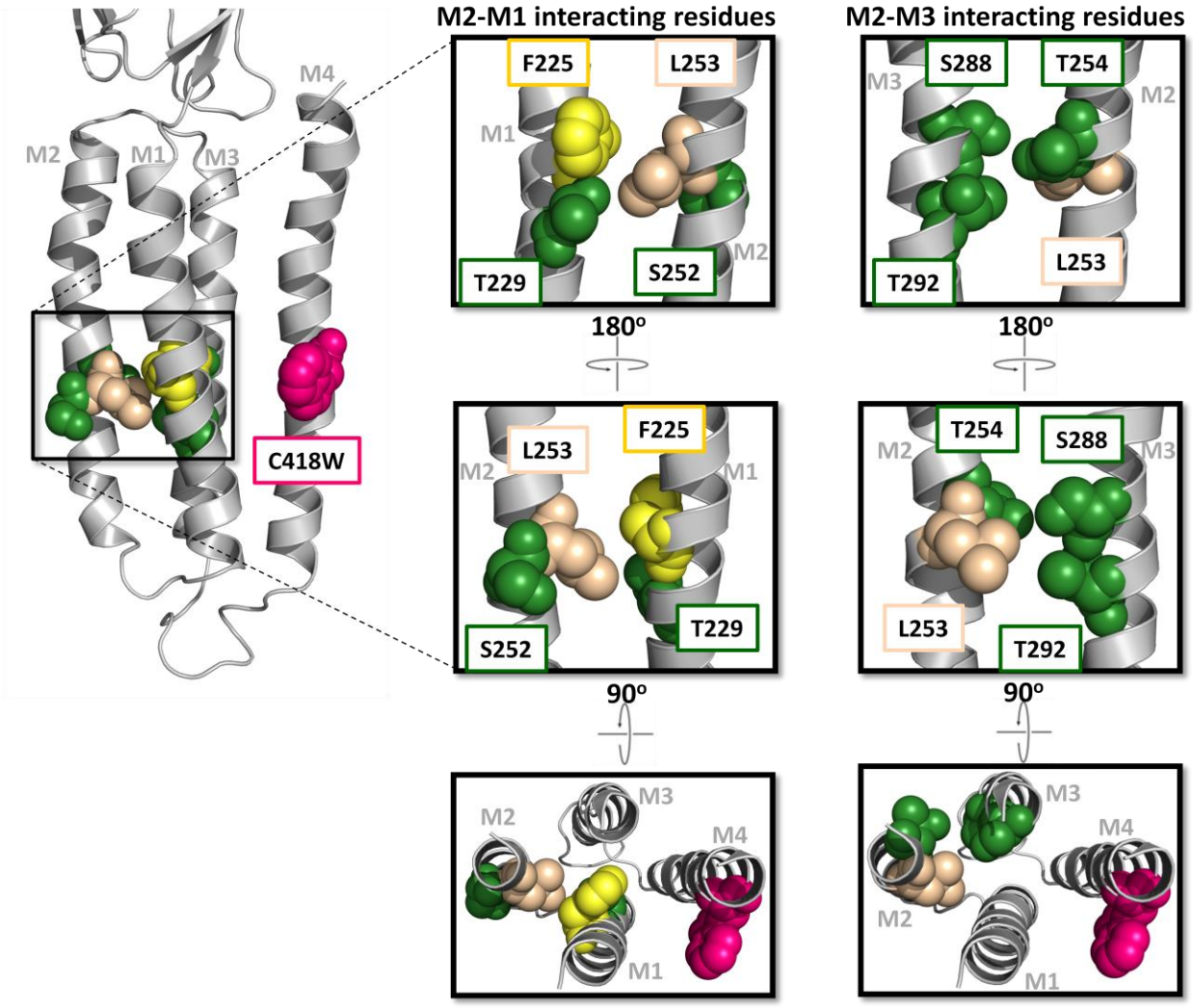

Figure 4.3 - Role of M2-M1 and M2-M3 interactions in C418W-induced potentiation. The human muscle-type α-subunit homology model based on the cryo-electron microscopy structure of the *Torpedo* nAChR (PDB: 2BG9). The C418W mutation is shown as pink spheres. Potentially interacting residues between M2 and M1 and between M2 and M3 at the centre of the TMD are shown as spheres where aromatic residues are yellow, polar residues are green, and aliphatic residues are tan. The bottom-most images display a top-down view of the TMD showing the residues as before. The only energetic coupling was found between Thr229 (M1) and Ser252 (M2). This interaction was shown to be important to C418W-induced potentiation.

respectively), while L253A had no effect. Conversely, on the C418W-nAChR background, S252A and T254A had no effect while L253A slightly increased channel function. Ser252/Thr254 and Leu253 thus influence C418W-induced potentiation in opposite ways: Ser252/Thr254 decrease potentiation from 16-fold down to 5- and 11-fold, respectively, while L253A actually increases potentiation from 16-fold up to 30-fold. Mutant cycle analysis revealed that both Ser252 and Leu253 are weakly coupled, although indirectly and oppositely, with Trp418 ($\Delta\Delta G$ = -2.98 kJ/mol and 1.75 kJ/mol, respectively; Table 4.4), while Thr254 is not ($\Delta\Delta G$ = -0.78 kJ/mol; Table 4.4).

As expected, I found there were no energetic interactions between Ser288 and Thr292 on M3 and the adjacent residues, Leu253 and Thr254, on M2 (Figure 4.3). The L253A+T292A and T254A+S288A double mutants had no effect on activity in either the WT-nAChR or the C418W-nAChR background, leading to no effect on potentiation (Table 4.4). Thus, C418W-induced potentiation is not propagated through Ser288 or Thr292 on M3 to the channel-lining M2 α-helix. Instead, the effects of αM4 C418W, propagate to the channel gate through an allosteric pathway involving only M1.

I next probed energetic couplings between M1 and M2 in both the WT-nAChR and C418W-nAChR backgrounds (Ser252 and Leu253) (Table 4.3; Table 4.4; Figure 4.3). Although Thr229 is energetically coupled to Leu253 in the WT-nAChR ($\Delta\Delta G$ = 2.87 kJ/mol), contributing negatively to nAChR gating, the T229A+L253A double mutant did not express and/or function in the presence of C418W. Thus, it is possible that an interaction between these two residues in the C418W-nAChR contributes to expression and/or function; however, it was not possible to determine the effect this interaction would have on C418W-induced potentiation. Nonetheless, it seems unlikely, given that Leu253 itself is detrimental to C418W-induced potentiation, that an

interaction involving these residues would be important to the mechanism of potentiation. Similarly, the F225A+L253A double mutant did not function/express on either background. A previous study showed an interaction between these conserved residues in the mouse muscle-type nAChR (Corradi et al., 2007), the loss of which in the human muscle-type nAChR could lead to the abrogation of nAChR function and/or expression. Regardless, it again seems unlikely that such an interaction would be important to C418W-induced potentiation as Leu253 itself is detrimental and Phe225 has no effect. Most intriguingly, Thr229 did not couple with the adjacent Ser252 in the WT-nAChR, but showed weak coupling energy in the presence of the C418W mutation ($\Delta\Delta G$ from -0.46 to -1.92 kJ/mol; Table 4.4). Additionally, this double mutant reduced C418W-induced potentiation from 16-fold down to 3-fold, contributing -3.99 kJ/mol to potentiation and highlighting the importance of these residues to the mechanism of potentiation.

In summary, although the overall mechanism underlying these data remains unclear, they do suggest that altered interactions between M4/M1 and M1/M2 in the central region of the TMD influence channel gating, while interactions between M1/M2/M4 and M3 at this same location do not exist. Although the specific interaction between Thr229 on M1 and Ser252 on M2 contributes significantly to potentiation, the energy of this interaction is not sufficient to account entirely for potentiation. Also, it is important to note that, of the residues and interactions I tested involving M1 and M2, some contributed positively to potentiation, while others contributed negatively. Thus, the entire mechanism of C418W-induced potentiation likely involves a complex network of altered interactions at this central location, some of which I may not yet have elucidated.

4.2.2 C418W alters aromatic interactions at the ECD-TMD interface

I next explored whether the C418W-induced changes in structure propagate through M1 to M3 near the coupling interface between the ECD and TMD. Given the importance of aromatic interactions at the M4-M1/M3 interface in both the folding and function of some pLGICs (Carswell et al., 2015a/b; Haeger et al., 2010; Therien and Baenziger, 2017), I first tested whether the three aromatic residues on M3, Tyr277, Phe280, and Phe284, play a role in C418W-induced potentiation (Table 4.5; Table 4.6; Figure 4.4). Ala mutations of each aromatic residue had little effect on WT-nAChR function, with Y277A leading to a slight loss-of-function, and both F280A and F284A leading to a slight gain-of-function. However, the same aromatic-to-Ala substitutions on the C418W-nAChR background each led to subtle drops in C418W-induced potentiation, decreasing from 16-fold down to 8-, 9-, and 8-fold, respectively, suggesting the involvement of these aromatic residues in the mechanism of potentiation. Mutant cycles revealed that only Phe284 is weakly, and indirectly, coupled to Trp418 ($\Delta\Delta G$ = -1.82 kJ/mol). Interestingly, the double Ala mutant involving Phe280 and Phe284 showed that these two aromatic residues are coupled on the WT-nAChR background, contributing negatively to nAChR gating ($\Delta\Delta G$ = 2.83 kJ/mol), while this interaction is lost in the presence of C418W ($\Delta\Delta G$ = -1.14 kJ/mol; Figure 4.3). These data show that C418W does indeed alter interactions involving aromatic residues on M3 at this N-terminal location.

Given my previous studies involving mutations/deletions at the M4 C-terminus (see Chapter 3), and an Ala-scan of αM4 (data not shown), it is unlikely that these aromatic residues on M3 interact with the adjacent M4 α-helix to affect function and/or C418W-induced potentiation. Thus, I explored the possibility that M3 interacts instead with aromatic residues located on two structures at the ECD-TMD interface: pre-M1 and the Cys-loop, which have both

Table 4.5 - Role of aromatic interactions between the M3 N-terminus, M1, and the Cys-loop in nAChR function and C418W-induced potentiation.

Mutation(s)	Dose Response[a]						Potentiation (fold)[f]
	WT-nAChR[c]			C418W-nAChR[d]			
	EC_{50} (μM)	Hill Slope	*n*	EC_{50} (μM)	Hill Slope	*n*	
None	7.61 ± 1.25	1.70 ± 0.47	50	0.47 ± 0.12	1.54 ± 0.23	50	16.2
F135A (Cys-loop)	**No current**[e]		8	6.24 ± 3.32[b]	1.09 ± 0.21	8	--
F137A (Cys-loop)	3.47 ± 0.26[b]	1.44 ± 0.24	9	0.37 ± 0.04	1.67 ± 0.12	8	9.4
F214A (M1)	**No current**[e]		8	0.40 ± 0.06	1.57 ± 0.25	8	--
Y277A (M3)	11.2 ± 2.0[b]	1.78 ± 0.58	8	1.33 ± 0.12[b]	1.72 ± 0.20	12	8.4
F280A (M3)	4.25 ± 1.00[b]	1.56 ± 0.29	8	0.47 ± 0.04	1.51 ± 0.10	8	9.0
F284A (M3)	4.80 ± 0.75[b]	1.33 ± 0.21	8	0.62 ± 0.06[b]	1.63 ± 0.25	9	7.7
F135A+F214A	**No current**[e]		8	6.18 ± 1.34[b]	1.66 ± 0.12	8	--
F135A+Y277A	**No current**[e]		8	**No current**[e]		8	--
F137A+F214A	**No current**[e]		8	**No current**[e]		8	--
F137A+Y277A	1.11 ± 0.28[b]	1.91 ± 0.14	9	0.54 ± 0.02	1.64 ± 0.19	4	2.1
F137A+F280A	1.32 ± 0.17[b]	1.72 ± 0.27	8	0.30 ± 0.03[b]	1.55 ± 0.19	8	4.4
F137A+F284A	2.36 ± 0.63[b]	1.80 ± 0.20	8	0.09 ± 0.02[b]	1.94 ± 0.33	9	26.2
F214A+Y277A	**No current**[e]		8	0.46 ± 0.04	2.17 ± 0.14	4	--
F280A+F284A	8.42 ± 2.98	1.45 ± 0.08	9	0.39 ± 0.07	1.65 ± 0.24	8	21.6

[a] Measurements were performed 2 days after injection of cRNA. Error values represent standard deviation.
[b] $p < 0.001$ relative to control via one-way ANOVA followed by Dunnett's post-hoc test.
[c] WT-nAChR contains only the mutation(s) listed under the "mutation(s)" column.
[d] C418W-nAChR receptor contains C418W in addition to the mutation(s) listed under the "mutation(s)" column.
[e] Oocytes were tested 2-7 days after injection of 5-15 ng of mutant cRNA.
[f] EC_{50} of mutant on WT-nAChR background divided by EC_{50} of mutant on C418W-nAChR background.

Table 4.6 - Energetic coupling between aromatic residues on the M3 N-terminus, M1, and the Cys-loop.

Mutants	Ω	ΔΔG (kJ/mol)
Phe135/Trp418	--[b]	--
Phe137/Trp418	0.58	-1.35
Phe214/Trp418	--[b]	--
Tyr277/Trp418	0.52	-1.62
Phe280/Trp418	0.56	-1.44
Phe284/Trp418	0.48	-1.82[a]
Phe135+Phe214/Trp418	--[b]	--
Phe135+Tyr277/Trp418	--[b]	--
Phe137+Phe214/Trp418	--[b]	--
Phe137+Tyr277/Trp418	0.13	-5.05[a]
Phe137+Phe280/Trp418	0.27	-3.24[a]
Phe137+Phe284/Trp418	1.62	1.20
Phe214+Tyr277/Trp418	--[b]	--
Phe280+Phe284/Trp418	1.33	0.71

Mutants	WT-nAChR[c]		C418W-nAChR[d]	
	Ω	ΔΔG (kJ/mol)	Ω	ΔΔG (kJ/mol)
Phe135/Phe214	--[b]	--	1.16	0.37
Phe135/Tyr277	--[b]	--	--[b]	--
Phe137/Phe214	--[b]	--	--[b]	--
Phe137/Tyr277	0.22	-3.75[a]	0.52	-1.62
Phe137/Phe280	0.68	-0.96	0.81	-0.52
Phe137/Phe284	1.08	0.19	0.18	-4.25[a]
Phe214/Tyr277	--[b]	--	0.41	-2.21[a]
Phe280/Phe284	3.14	2.83[a]	0.63	-1.14

[a] The free energy is sufficient to indicate energetic coupling.
[b] Could not calculate energetic coupling because of non-functional/non-expressing mutants.
[c] WT-nAChR contains only the mutants listed under the "mutants" column.
[d] C418W-nAChR contains C418W in addition to the mutants listed under the "mutants" column.

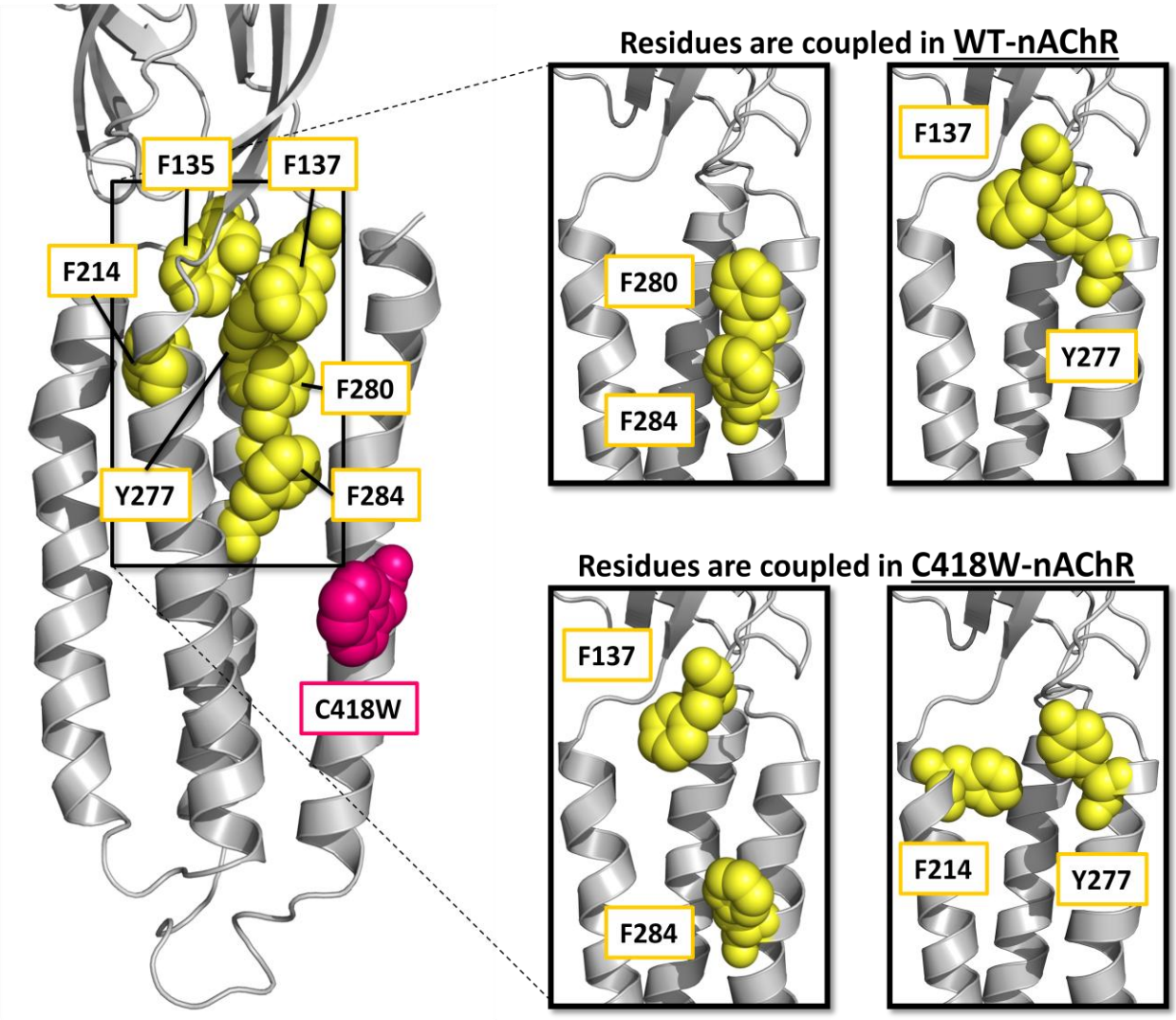

Figure 4.4 - αM4 C418W alters ECD-TMD aromatic interactions. The human muscle-type α-subunit homology model based on the cryo-electron microscopy structure of the *Torpedo* nAChR (PDB: 2BG9). The C418W mutation is shown as pink spheres. Aromatic residues on M3, M1, and the Cys-loop are shown as yellow spheres. Energetic couplings between aromatic residues is different on the WT-nAChR background as compared to the C418W-nAChR background.

been implicated in muscle-type nAChR gating (Lee and Sine, 2005; Lee et al., 2008; Lee et al., 2009). Specifically, I explored the role of Phe214 of pre-M1 and Phe135/Phe137 of the Cys-loop (Table 4.5; Table 4.6; Figure 4.4). As noted in Chapter 3, F137A resulted in a subtle gain-of-function relative to the WT-nAChR, and subtly reduced C418W-induced potentiation from 16-fold down to 9-fold. Contrastingly, both F135A and F214A did not express (see appendix; Figure 6.2). Phe135 and Phe214 face each other in the nAChR structure, suggesting that there may be an interaction between these residues that is critical for folding. Interestingly, both F135A and F214A express and function on the C418W-nAChR background (see appendix; Figure 6.2) showing that F214A has no effect on the EC_{50} of the C418W-nAChR, while the F135A+C418W double mutant exhibits a 13-fold loss-of-function relative to the C418W-nAChR. Since F135A did not express on the WT-nAChR background, it was not possible to elucidate the role of Phe135 in C418W-induced potentiation. Note, however, that mutant cycle analysis shows that F135A and F214A are not energetically coupled on the C418W-nAChR background ($\Delta\Delta G$ = 0.37 kJ/mol), indicating that, if an interaction between these two residues exists to stabilize the WT-nAChR, this interaction is lost in the presence of αM4 C418W.

I also explored energetic couplings between the above mentioned aromatic residues at the ECD-TMD interface and those located on M3 (Table 4.5; Table 4.6; Figure 4.4). All of the double Ala mutations on the WT-nAChR background that included either Phe135 or Phe214 did not express/function, which is not surprising given that F135A and F214A themselves abolish cell surface expression. Most notably, in pairing aromatic-to-Ala substitutions on M3 with F137A of the Cys-loop, the F137A+Y277A and F137A+F280A double mutants reduced C418W-induced potentiation from 16-fold down to 2- and 4-fold, respectively, contributing -5.05 and -3.24 kJ/mol to potentiation, respectively. The substantial loss of potentiation

observed with these double mutations highlights a key role for aromatic residues located at the ECD/TMD interface in potentiation.

The precise role of aromatic interactions in potentiation, however, is complex. For example, mutant cycle analysis reveals an energetic coupling ($\Delta\Delta G$ = -3.75 kJ/mol) between Tyr277 (M3) and Phe137 (Cys-loop) on the WT-nAChR background that contributes positively to channel gating (Table 4.6); however, in the presence of C418W, this positive effect is reduced ($\Delta\Delta G$ = -1.62 kJ/mol; Table 4.6; Figure 4.4). Thus, the interaction between these two residues does not contribute to stabilizing the open state on the C418W-nAChR background. However, both Phe137 and Tyr277 are critical to potentiation as the double mutant, F137A+Y277A, reduces potentiation to 2-fold, suggesting that these residues form interactions elsewhere to stabilize the open state. In fact, an energetic coupling that is important to gating was observed between Tyr277 of M3 and Phe214 of M1 on the C418W-nAChR background ($\Delta\Delta G$ = -2.21 kJ/mol; Table 4.6; Figure 4.4). Lack of expression prevented calculation of this energetic coupling in the WT-nAChR background, thus I was not able to determine the role of this interaction on C418W-induced potentiation. In addition, Phe137 of the Cys-loop and Phe284 of M3 exhibit no indirect coupling on the WT-nAChR background, but an interaction contributing positively to channel gating is observed on the C418W-nAChR background ($\Delta\Delta G$ = -4.25 kJ/mol; Table 4.6; Figure 4.4). Although it can be concluded that the C418W mutation influences channel function by altering interactions at the ECD/TMD interface, the precise mechanisms remain to be determined.

4.3 Discussion

The αM4 C418W CMS-causing mutation potentiates activity of the human muscle-type nAChR 16-fold by promoting local interactions between M4 and M1 at the approximate centre of the TMD/lipid bilayer. These interactions, mediated by three polar residues on M4 and M1, Ser226 (M1), Thr229 (M1), and Thr422 (M4), in addition to Trp418, are absolutely critical to C418W-induced potentiation; the loss of all three polar groups abrogates potentiation. Based on studies with the prokaryotic homologue, ELIC, it is perhaps unsurprising that interactions in this central TMD region would be involved in C418W-induced potentiation. Just two aliphatic-to-aromatic substitutions in combination on the M3/M4-facing side of M1 at the approximate centre of the TMD were able to potentiate channel activity ~6-fold, presumably due to enhanced interactions between M1 and M4 (Carswell et al., 2015b). Similarly, a study with the α7 nAChR-specific PAM, PNU, also implicated residues in this central region as being critical to its mechanism of potentiation (daCosta et al., 2011). Particularly, two of the five residues critical for the binding of PNU within this central region of the α7 nAChR, Ser223 (M1) and Ala226 (M1), are equivalent to the two polar residues in the muscle-type nAChR α1-subunit, Ser226 (M1) and Thr229 (M1), which I have shown are critical to potentiation by αM4 C418W. Intriguingly, both PNU and αM4 C418W prolong nAChR open times (Shen et al., 2006); although, PNU does so by slowing desensitization, while αM4 C418W stabilizes the open state. Regardless, it is possible that these two "PAMs" stabilize the TMD via a similar mechanism.

In addition to the two aforementioned residues on M1, PNU also interacts with residues on M2 (Met254) and M3 (Ile281 and Val288) to potentiate activity of the α7 nAChR (daCosta et al., 2011). These residues are all located within an intra-subunit TMD cavity that has been proposed to be a highly conserved modulatory site of pLGICs (Young et al., 2008). In line with

these studies, my experiments show that, in addition to the aforementioned residues on M1, a polar residue on M2, Ser252, is important to C418W-induced potentiation. Particularly, this residue interacts with Thr229 of M1, but only in the presence of C418W. Although these two residues do not face each other in the nAChR structure, a subtle reorientation of the M1 α-helix, resulting from altered interactions with M4, may expose Thr229 to the channel-lining M2 α-helix. Further, during gating, the αM2 helices undergo subtle rotations (Unwin and Fujiyoshi, 2012), which may allow Ser252 and Thr229 to form an interaction in the open state of the C418W-nAChR that stabilizes the αM2 helices in their open state conformation, prolonging nAChR open times. However, the removal of this interaction did not completely abrogate C418W-induced potentiation, suggesting that additional untested interactions, perhaps at this central TMD location, are involved in potentiation.

daCosta *et al* (2011) implicated two residues on M3 in the α7 nAChR as being critical to PNU-induced potentiation. Similarly, in GLIC, an interaction at this central TMD location between M2 and M3, facilitated by a protonated His residue, is critical to channel gating (Wang et al., 2012). However, my data show no inter-helical interactions with M3 at this central TMD location in the muscle-type nAChR with either M1, M2, or M4. Although my data do not implicate residues of M3 at this central location as being involved in C418W-induced potentiation, M3 has indeed been shown to be involved in muscle-type nAChR activity. Specifically, M3 is involved in activation properties of the nAChR and modifies channel open times (De Rosa et al., 2002), likely due to the ability of αM3 to adopt two different helical structures where, in the closed state, the helix is thin and elongated, and becomes thick and shrunken in the open state (Otero-Cruz et al., 2007). In particular, positions 284 and 285, nearing the M3 N-terminus, are most involved in modifying channel kinetics. αM4 Phe284 is

lipid-exposed (Blanton and Cohen, 1994) and aromatic-to-aliphatic substitutions at this position increase the mean open time (De Rosa et al., 2002). Additionally, αM4 Val285 has been implicated in a fast-channel CMS (Wang et al., 1999), revealing that both stereochemistry and volume are important for channel gating at this position. Intriguingly, effects of mutations at equivalent positions in non-α subunits often have opposite and additive effects (De Rosa et al., 2008).

Considering the importance of αM3 in muscle-type nAChR gating, I investigated further its role in C418W-induced potentiation by examining possible interactions between the M3 N-terminus and surrounding structures. My data show that three aromatic residues on M3 (Tyr277, Phe280, and Phe284) are involved in C418W-induced potentiation. Based on my previous work with the M4 C-terminus, it is unlikely that these residues interact with M4 to affect potentiation. This is in contrast to what is observed in GLIC, where aromatic interactions between M4 and M3 at this location are critical to function (Carswell et al., 2015b). However, many PAMs of pLGIC activity, including general anaesthetics such as propofol and desflurane, have been shown to bind to a cavity delineated by M1, M2, and M3 at the ECD-TMD interface (Nury et al., 2011; Olsen et al., 2014); thus, I explored whether αM4 C418W could alter interactions between M3 and structures at the ECD-TMD interface to potentiate nAChR function. My data showed that αM4 C418W did indeed influence interactions at this location; specifically, the aforementioned residue, Phe284, becomes coupled with the conserved aromatic residue, Phe137, of the Cys-loop on the C418W-nAChR background, while no such interaction exists in the WT-nAChR. Further, although Tyr277 of M3 interacts with Phe137 of the Cys-loop in the WT-nAChR, this interaction is lost on the C418W-nAChR background, and possibly replaced by an interaction between Y277 and Phe214 at the M1 N-terminus. As before, these interactions do not account entirely for

C418W-induced potentiation, suggesting that all the interactions I have previously identified may work in tandem to propagate the potentiating effects of the peripheral αM4 C418W mutation to the important gating structures (i.e. M2 α-helices and ECD-TMD interface). It is also likely that there remain additional interactions that I have not yet elucidated at either of these locations.

In the context of gating, my data do coincide with the literature. Although different pLGICs have subtly different gating mechanisms, the one thing they all have in common is that interactions between ECD and TMD structures are critical for translating the effects of agonist binding in the ECD to opening of the channel gate in the TMD formed by the channel-lining M2 helices. Specifically, in the muscle-type nAChR "principal pathway" of gating, hydrophobic "pin-in-socket" interactions link the extracellular β1-β2 loop and Cys-loop, with the M2-M3 linker of the TMD (Lee and Sine, 2005; Lee et al., 2008), while charged interactions at this same location are critical in the anionic $GABA_A$ receptor (Kash et al., 2004). The Cys-loop was also separately shown to interact with both pre-M1 and the M2-M3 linker in the "Cys-loop" gating pathway. My data further implicate the Cys-loop in gating and show that αM4 C418W affects nAChR function, at least partly, by modifying Cys-loop interactions with residues of the TMD. As interactions at the ECD-TMD interface accord each pLGIC its unique gating characteristics, such as open channel lifetime and rate of desensitization (as reviewed by Bouzat, 2012; Bouzat et al., 2008), it is unsurprising that αM4 C418W would ultimately affect these important interfacial structures to prolong channel openings. Although I did not test specific residues on pre-M1 or the M2-M3 linker, it is entirely possible that altered TMD movements due to αM4 C418W, such as enhanced interactions between M4 and M1, in addition to altered interactions between M2 and M1, also affect these additional interfacial structures to stabilize the open state.

4.4 Conclusions

In summary, αM4 C418W potentiates nAChR channel activity approximately 16-fold by altering M4-M1 interactions, which are mediated by three polar residues at the approximate centre of the TMD: Thr422 of M4, and Ser226/Thr229 of M1. The interaction between these three polar residues is absolutely critical to C418W-induced potentiation, as the gain-of-function observed in the C418W-nAChR as compared to the WT-nAChR is completely abolished with the triple mutant, S226A+T229A+T422A. Altered M4-M1 interactions, in turn, alter interactions between M1 and M2 at the approximate centre of the TMD, mediated by Thr229 on M1 and Ser252 on M2, where the Thr229/Ser252 interaction is important to C418W-induced potentiation. Further, although M3 does not form any interactions with M1, M2, or M4 at this central location, it is involved in interactions at the ECD-TMD interface, which are altered by C418W, highlighting an important role for Phe137 of the Cys-loop and Tyr277 of M3 in C418W-induced potentiation. Overall, my data suggest that C418W induces structural rearrangements of M4, which affect the position of M1, M2, and M3 within the TMD. The re-orientation of M1 may affect the conformation of pre-M1, interactions between M1 and M2 may stabilize the open conformation of the M2 α-helix, and altered interactions involving M3 at the ECD-TMD interface may stabilize these structures in their open conformation. I propose that all of these TMD structural rearrangements contribute, in tandem, to enhance channel gating and potentiate nAChR activity, none of which could be possible without the initial alteration of M4-M1 interactions by the lipid-facing αM4 C418W mutation.

Chapter 5

General Discussion

The research presented in this thesis has been focused specifically on understanding how a lipid-facing mutation at the periphery of the muscle-type nAChR, αM4 C418W, is able to stabilize the open state to potentiate nAChR function 16-fold (Shen et al., 2006), leading to a slow-channel CMS, when it does not interact directly with any of the important gating structures (Lee and Sine, 2005; Lee et al., 2008; Lee et al., 2009). Understanding how αM4 C418W modulates nAChR function not only sheds light on how protein-lipid interactions are involved in modulating nAChR function, but may also provide a basis for the development of targeted allosteric modulators for the treatment of, not only CMS, but also a multitude of pLGIC-related diseases.

Chapter 3 of this thesis focused primarily on testing the M4 lipid sensor model, in the context of the αM4 C418W mutation, to shed light onto how altered protein-lipid interactions are translated into altered nAChR function. Contrary to the M4 lipid sensor model hypothesis, which was developed using the *Torpedo* nAChR α-subunit, I find that interactions between M4 and the Cys-loop in the human muscle-type α-subunit are not required for nAChR function, nor are they involved in C418W-induced potentiation. These results are perhaps unsurprising given the recent work by Therien and Baenziger (2017) showing that pLGIC TMDs fall into one of two archetypal categories based on their chemistry at the M4-M1/M3 interface. The nAChR falls into the second category where strong interactions at this interface are not required for function, and as an extension of this, strong interactions between M4 and the Cys-loop are also not required for function. Although the αM4 C418W mutant did not potentiate activity by enhancing interactions at this location, it would be interesting to test whether it would be possible, in the muscle-type α-subunit, to potentiate nAChR function by enhancing such interactions. Indeed, in ELIC (which also falls into the second archetypal category along with the nAChR), channel

activity can be potentiated by enhancing interactions between M4 and the Cys-loop; similarly, the activity of the neuronal α4β2 nAChR can be potentiated by the binding of neurosteroids to this location (Paradiso et al., 2001). A similar study in the muscle-type nAChR could strengthen the idea that M4–Cys-loop interactions, although not ultimately required in all pLGICs, could be an important vehicle through which pLGIC function as a whole can be modified.

Chapter 4 partially elucidates an allosteric pathway from the αM4 C418W mutant to two important gating structures: the channel-lining M2 α-helices, and the ECD-TMD interface. In the presence of αM4 C418W, enhanced interactions between M4 and M1, involving three critical polar residues local to the position of C418W, account entirely for the 16-fold potentiation in the C418W-nAChR. These M4-M1 interactions lead to altered interactions between M1 and M2 in the open state, which partially account for the energy of potentiation. It is important to note that some interactions at this location are important to potentiation, while others are detrimental, suggesting that C418W may alter many interactions at this location to produce the net potentiating effect. It is likely, based on the interaction energies I have calculated, that additional interactions at this location are involved in potentiation, but have yet to be elucidated. Indeed, this cavity has been proposed to be a highly conserved modulatory site of pLGICs (Young et al., 2008) and a PAM of α7 nAChRs, PNU, binds within this cavity to potentiate function (daCosta et al., 2011). As such, if we could map out all of the intra-subunit energies at this location, this could serve as the basis for the design of allosteric modulators that would disrupt these energies in the C418W-nAChR, reverting the slow-channel channel kinetics back to the wild-type phenotype.

I also showed that αM4 C418W alters aromatic interactions at the ECD-TMD interface to affect nAChR function. Many PAMs, including general anaesthetics such as propofol and

desflurane, have also been shown to bind to this location to modify channel activity (Nury et al., 2011; Olsen et al., 2014). Many residues at this location contribute positively to potentiation; however, my data suggest that I have not elucidated all potential interactions contributing to potentiation and that interactions at this location are complex. Again, if we could map out all of the energies involving ECD-TMD interface residues and elucidate their roles in potentiation, this would serve as a starting point for the design of molecules that disrupt such interactions, abrogating the disease phenotype.

In conclusion, these studies highlight the role of the highly lipid-exposed and peripheral αM4 α-helix in the modulation of the human muscle-type nAChR and how subtle changes in the structure of this helix can ultimately propagate to affect overall function. This not only adds to our understanding of the nAChR gating mechanism, but also sheds light onto how changes to the lipid environment can modulate nAChR function. As most nAChRs, and pLGICs in general, are heteropentameric, it will be important moving forward to understand whether or not different subunits (i.e. α versus non-α) affect function via similar mechanisms, giving us a more global picture of how nAChRs function.

References

Aldea, M., Mulet, J., Sala, S., Sala, F., and Criado, M. (2007). Non-charged amino acids from three different domains contribute to link agonist binding to channel gating in alpha7 nicotinic acetylcholine receptors. J. Neurochem. *103*, 725-735.

Almarza, G., Sánchez, F., and Barrantes, F.J. (2014). Transient cholesterol effects on nicotinic acetylcholine receptor cell-surface mobility. PLoS One. *9*, e100346.

Barrantes, F.J. (2004). Structural basis for lipid modulation of nicotinic acetylcholine receptor function. Brain Res. Brain Res. Rev. *47*, 71-95.

Beckstein, O. and Sansom, M.S. (2006). A hydrophobic gate in an ion channel: the closed state of the nicotinic acetylcholine receptor.

Beeson, D. (2012). Synaptic dysfunction in congenital myasthenic syndromes. Ann. N. Y. Acad. Sci. *1275*, 63-69.

Belaya, K., Finlayson, S., Slater, C.R., Cossins, J., Liu, W.W., Maxwell, S., McGowan, S.J., Maslau, S., Twigg, S.R., Walls, T.J., et al. (2012). Mutations in DPAGT1 cause a limb-girdle congenital myasthenic syndrome with tubular aggregates. Am. J. Hum. Genet. *91*, 193-201.

Blanton, M.P. and Cohen, J.B. (1992). Mapping the lipid-exposed regions in the Torpedo californica nicotinic acetylcholine receptor. Biochemistry. *31*, 3738-3750.

Blanton, M.P. and Cohen, J.B. (1994). Identifying the lipid-protein interface of the Torpedo nicotinic acetylcholine receptor: secondary structure implications. Biochemistry. *33*, 2859-2872.

Bocquet, N., Nury, H., Baaden, M., Le Poupon, C., Changeux, J.P., Delarue, M., and Corringer, P.J. (2009). X-ray structure of a pentameric ligand-gated ion channel in an apparently open conformation. Nature. *457*, 111-114.

Boileau, A.J., Evers, A.R., Davis, A.F., and Czajkowski, C. (1999). Mapping the agonist binding site of the GABAA receptor: evidence for a beta-strand. J. Neurosci. *19*, 4847-4854.

Bouzat, C. (2012). New insights into the structural bases of activation of Cys-loop receptors. J. Physiol. Paris. *106*, 23-33.

Bouzat, C., Bartos, M., Corradi, J., and Sine, S.M. (2008). The interface between extracellular and transmembrane domains of homomeric Cys-loop receptors governs open-channel lifetime and rate of desensitization. J. Neurosci. *28*, 7808-7819.

Bouzat, C., Gumilar, F., Spitzmaul, G., Wang, H.L., Rayes, D., Hansen, S.B., Taylor, P., and Sine, S.M. (2004). Coupling of agonist binding to channel gating in an ACh-binding protein linked to an ion channel. Nature. *430*, 896-900.

Bouzat, C., Roccamo, A.M., Garbus, I., and Barrantes, F.J. (1998). Mutations at lipid-exposed residues of the acetylcholine receptor affect its gating kinetics. Mol. Pharmacol. *54*, 146-153.

Boyd, N.D. and Cohen, J.B. (1980). Kinetics of binding of [3H]acetylcholine to Torpedo postsynaptic membranes: association and dissociation rate constants by rapid mixing and ultrafiltration. Biochemistry. *19*, 5353-5358.

Brannigan, G., Henin, J., Law, R., Eckenhoff, R., and Klein, M.L. (2008). Embedded cholesterol in the nicotinic acetylcholine receptor. Proc. Natl. Acad. Sci. U.S.A. *105*, 14418-14423.

Brejc, K., van Dijk, W.F., Klaassen, R.V., Schuurmans, M., van Der Oost, J., Smit, A.B., and Sixma, T.K. (2001). Crystal structure of an ACh-binding protein reveals the ligand-binding domain of nicotinic receptors. Nature. *411*, 269-276.

Brownlow, S., Webster, R., Croxen, R., Brydson, M., Neville, B., Lin, J.P., Vincent, A., Newsom-Davis, J., and Beeson, D. (2001). Acetylcholine receptor delta subunit mutations underlie a fast-channel myasthenic syndrome and arthrogryposis multiplex congenita. J. Clin. Invest. *108*, 125-130.

Calimet, N., Simoes, M., Changeux, J.P., Karplus, M., Taly, A., and Cecchini, M. (2013). A gating mechanism of pentameric ligand-gated ion channels. Proc. Natl. Acad. Sci. U.S.A. *110*, 3987-3996.

Campos-Caro, A., Sala, S., Ballesta, J.J., Vicente-Agulló, F., Criado, M., and Sala, F. (1996). A single residue in the M2-M3 loop is a major determinant of coupling between binding and gating in neuronal nicotinic receptors. Proc. Natl. Acad. Sci. U.S.A. *93*, 6118-6123.

Carswell, C.L., Sun, J., and Baenziger, J.E. (2015a). Intramembrane aromatic interactions influence the lipid sensitivities of pentameric ligand-gated ion channels. J. Biol. Chem. *290*, 2496-2507.

Carswell, C.L., Hénault, C.M., Murlidaran, S., Therien, J.P., Juranka, P.F., Surujballi, J.A., Brannigan, G., and Baenziger, J.E. (2015b). Role of the fourth transmembrane a helix in the allosteric modulation of pentameric ligand-gated ion channels. Structure *23*, 1655-1664.

Cartaud, J., Benedetti, E.L., Cohen, J.B., Meunier, J.C., and Changeux, J.P. (1973). Presence of a lattice structure in membrane fragments rich in nicotinic receptor protein from the electric organ of Torpedo marmorata. FEBS Lett. *33*, 109-113.

Carter, P.J., Winter, G., Wilkinson, A.J., and Fersht, A.R. (1984). The use of double mutants to detect structural changes in the active site of the tyrosyl-tRNA synthetase (Bacillus stearothermophilus). Cell. *38*, 835-840.

Castillo, M., Mulet, J., Gutiérrez, L.M., Ortiz, J.A., Castelán, F., Gerber, S., Sala, S., Sala, F., and Criado, M. (2006). Role of the RIC-3 protein in trafficking of serotonin and nicotinic acetylcholine receptors. J. Mol. Neurosci. *30*, 153-156.

Cauët, E., Rooman, M., Wintjens, R., Liévin, J., and Biot, C. (2005). Histidine-aromatic interactions in proteins and protein-ligand complexes: quantum chemical study of X-ray and model structures. J. Chem. Theory Comput. *1*, 472-483.

Celie, P.H., van Rossum-Fikkert, S.E., van Dijk, W.J., Brejc, K., Smit, A.B., and Sixma, T.K. (2004). Nicotine and carbamylcholine binding to nicotinic acetylcholine receptors as studied in AChBP crystal structures. Neuron. *41*, 907-914.

Chakrapani, S. and Auerbach, A. (2005). A speed limit for conformational change of an allosteric membrane protein. Proc. Natl. Acad. Sci. U.S.A. *102*, 87-92.

Chakrapani, S., Bailey, T.D., and Auerbach, A. (2004). Gating dynamics of the acetylcholine receptor extracellular domain. J. Gen. Physiol. *123*, 341-356.

Changeux, J.P. and Edelstein, S.J. (2001). Allosteric mechanisms in normal and pathological nicotinic acetylcholine receptors. Curr. Opin. Neurobiol. *11*, 369-377.

Changeux, J.P. and Edelstein, S.J. (2005). Allosteric mechanisms of signal transduction. Science. *308*, 1424-1428.

Changeux, J.P., Kasai, M., Huchet, M., and Meunier, J.C. (1970). [Extraction from electric tissue of gymnotus of a protein presenting several typical properties characteristic of the physiological receptor of acetylcholine]. C. R. Acad. Sci. Hebd. Seances Acad. Sci. D. *270*, 2864-2867.

Changeux, J.P. and Taly, A. (2008). Nicotinic receptors, allosteric proteins and medicine. Trends Mol. Med. *14*, 93-102.

Chavez-Noriega, L.E., Crona, J.H., Washburn, M.S., Urrutia, A., Elliott, K.J., and Johnson, E.C. (1997). Pharmacological characterization of recombinant human neuronal nicotinic acetylcholine receptors h alpha 2 beta 2, h alpha 2 beta 4, h alpha 3 beta 2, h alpha 3 beta 4, h alpha 4 beta 2, h alpha 4 beta 4 and h alpha 7 expressed in Xenopus oocytes. J. Pharmacol. Exp. Ther. *280*, 346-356.

Cheng, X., Lu, B., Grant, B., Law, R.J., and McCammon, J.A. (2006). Channel opening motion of alpha7 nicotinic acetylcholine receptor as suggested by normal mode analysis. J. Mol. Biol. *355*, 310-324.

Collins, T. and Millar, N.S. (2010). Nicotinic acetylcholine receptor transmembrane mutations convert ivermectin from a positive to a negative allosteric modulator. Mol. Pharmacol. *78*, 198-204.

Corradi, J., Spitzmaul, G., De Rosa, M.J., Costabel, M., and Bouzat, C. (2007). Role of pairwise interactions between M1 and M2 domains of the nicotinic receptor in channel gating. Biophys. J. *92*, 76-87.

Cossins, J., Belaya, K., Hicks, D., Salih, M.A., Finlayson, S., Carboni, N., Liu, W.W., Maxwell, S., Zoltowska, K., Farsani, G.T., et al. (2013). Congenital myasthenic syndromes due to mutations in ALG2 and ALG14. Brain. *136*, 944-956.

Criado, M., Eibl, H., and Barrantes, F.J. (1984). Functional properties of the acetylcholine receptor incorporated in model lipid membranes. Differential effects of chain length and head group of phospholipids on receptor affinity states and receptor-mediated ion translocation. J. Biol. Chem. *259*, 9188-9198.

Croxen, R., Hatton, C., Shelley, C., Brydson, M., Chauplannaz, G., Oosterhuis, H., Vincent, A., Newsom-Davis, J., Colquhoun, D., and Beeson, D. (2002). Recessive inheritance and variable penetrance of slow-channel congenital myasthenic syndromes. Neurology. *59*, 162-168.

Croxen, R., Newland, C., Beeson, D., Oosterhuis, H., Chauplannaz, G., Vincent, A., and Newsom-Davis, J. (1997). Mutations in different functional domains of the human muscle

acetylcholine receptor alpha subunit in patients with the slow-channel congenital myasthenic syndrome. Hum. Mol. Genet. *6*, 767-774.

Cruz-Martín, A., Mercado, J.L., Rojas, L.V., McNamee, M.G., and Lasalde-Dominicci, J.A. (2001). Tryptophan substitutions at lipid-exposed positions of the gamma M3 transmembrane domain increase the macroscopic ionic current response of the Torpedo californica nicotinic acetylcholine receptor. J. Membr. Biol. *183*, 61-70.

Cui, Q. and Karplus, M. (2008). Allostery and cooperativity revisited. Protein Sci. *17*, 1295-1307.

Cymer, F., von Hejine, G., and White, S.H. (2015). Mechanisms of integral membrane protein insertion and folding. J. Mol. Biol. *427*, 999-1022.

daCosta, C.J. and Baenziger, J.E. (2009). A lipid-dependent uncoupled conformation of the acetylcholine receptor. J. Biol. Chem. *284*, 17819-17825.

daCosta, C.J. and Baenziger, J.E. (2013). Gating of pentameric ligand-gated ion channels: structural insights and ambiguities. Structure. *21*, 1271-1283.

daCosta, C.J., Free, C.R., Corradi, J., Bouzat, C., and Sine, S.M. (2011). Single-channel and structural foundations of neuronal α7 acetylcholine receptor potentiation. J. Neurosci. *31*, 13870-13879.

daCosta, C.J., Medaglia, S.A., Lavigne, N., Wang, S., Carswell, C.L., and Baenziger, J.E. (2009). Anionic lipids allosterically modulate multiple nicotinic acetylcholine receptor conformational equilibria. J. Biol. Chem. *284*, 33841-33849.

Daeffler, K.N., Lester, H.A., and Dougherty, D.A. (2012). Functionally important aromatic-aromatic and sulfur-π interactions in the D2 dopamine receptor. J. Am. Chem. Soc. *134*, 14890-14896.

De Rosa, M.J., Rayes, D., Spitzmaul, G., and Bouzat, C. (2002). Nicotinic receptor M3 transmembrane domain: position 8' contributes to channel gating. Mol. Pharmacol. *62*, 406-414.

De Rosa, M.J., Corradi, J., and Bouzat, C. (2008). Subunit-selective role of the M3 transmembrane domain of the nicotinic acetylcholine receptor in channel gating. Biochim. Biophys. Acta. *1778*, 521-529.

Duclert, A. and Changeux, J.P. (1995). Acetylcholine receptor gene expression at the developing neuromuscular junction. Physiol. Rev. *75*, 339-368.

Ealing, J., Webster, R., Brownlow, S., Abdelgany, A., Oosterhuis, H., Muntoni, F., Vaux, D.J., Vincent, A., Beeson, D. (2002). Mutations in congenital myasthenic syndromes reveal an epsilon subunit C-terminal cysteine, C470, crucial for maturation and surface expression of adult AChR. Hum. Mol. Genet. *11*, 3087-3096.

Engel, A.G. (2007). The therapy of congenital myasthenic syndromes. Neurotherapeutics. *4*, 252-257.

Engel, A.G., Lambert, E.H., Mulder, D.M., Torres, C.F., Sahashi, K., Bertorini, T.E., and Whitaker, J.N. (1982). A newly recognized congenital myasthenic syndrome attributed to a prolonged open time of the acetylcholine-induced ion channel. Ann. Neurol. *11*, 553-569.

Engel, A.G., Ohno, K., Milone, M., Wang, H.L., Nakano, S., Bouzat, C., Pruitt, J.N., Hutchinson, D.O., Brengman, J.M., Bren, N., et al. (1996a). New mutations in acetylcholine receptor subunit genes reveal heterogeneity in the slow-channel congenital myasthenic syndrome. Hum. Mol. Genet. *5*, 1217-1227.

Engel, A.G., Ohno, K., Bouzat, C., Sine, S.M., and Griggs, R.C. (1996b). End-plate acetylcholine receptor deficiency due to nonsense mutations in the epsilon subunit. Ann. Neurol. *40*, 810-817.

Engel, A.G., Ohno, K., Shen, X.M., and Sine, S.M. (2003a). Congenital myasthenic syndromes: multiple molecular targets at the neuromuscular junction. Ann. N.Y. Acad. Sci. *998*, 138-160.

Engel, A.G., Ohno, K., and Sine, S.M. (2003b). Sleuthing molecular targets for neurological diseases at the neuromuscular junction. Nat. Rev. Neurosci. *4*, 339-352.

Engel, A.G., Shen, X.M., Selcen, D., and Sine, S.M. (2015). Congenital myasthenic syndromes: pathogenesis, diagnosis, and treatment. Lancet Neurol. *14*, 420-434.

Epstein, M. and Racker, E. (1978). Reconstitution of carbamylcholine-dependent sodium ion flux and desensitization of the acetylcholine receptor from Torpedo californica. J. Biol. Chem. *253*, 6660-6662.

Fong, T.M. and McNamee, M.G. (1986). Correlation between acetylcholine receptor function and structural properties of membranes. Biochemistry. *25*, 830-840.

Fu, D.X. and Sine, S.M. (1996). Asymmetric contribution of the conserved disulfide loop to subunit oligomerization and assembly of the nicotinic acetylcholine receptor. J. Biol. Chem. *271*, 31479-31484.

Gallivan, J.P. and Dougherty, D.A. (1999). Cation-pi interactions in structural biology. Proc. Natl. Acad. Sci. U.S.A. *96*, 9459-9464.

Gao, F., Bren, N., Burghardt, T.P., Hansen, S., Henchman, R.H., Taylor, P., McCammon, J.A., and Sine, S.M. (2005). Agonist-mediated conformational changes in acetylcholine-binding protein revealed by simulation and intrinsic tryptophan fluorescence. J. Biol. Chem. *280*, 8443-8451.

Gao, F., Mer, G., Tonelli, M., Hansen, S.B., Burghardt, T.P., Taylor, P., and Sine, S.M. (2006). Solution NMR of acetylcholine binding protein reveals agonist-mediated conformational change of the C-loop. Mol. Pharmacol. *70*, 1230-1235.

Gomez, C.M., Maselli, R., Gammack, J., Lasalde, J., Tamamizu, S., Cornblath, D.R., Lehar, M., McNamee, M., Kuncl, R.W. (1996). A beta-subunit mutation in the acetylcholine recepor channel gate causes severe slow-channel syndrome. Ann. Neurol. *39*, 712-723.

Gomez, C.M., Maselli, R., Gundeck, J.E., Chao, M., Day, J.W., Tamamizu, S., Lasalde, J.A., McNamee, M., and Wollmann, R.L. (1997). Slow-channel transgenic mice: a model of postsynaptic organellar degeneration at the neuromuscular junction. J. Neurosci. *17*, 4170-4179.

Gonzalez-Ros, J.M., Llanillo, M., Paraschos, A., and Martinez-Carrion, M. (1982). Lipid environment of acetylcholine receptor from Torpedo californica. Biochemistry. *21*, 3467-3474.

Govind, A.P., Walsh, H., and Green, W.N. (2012). Nicotine-induced upregulation of native neuronal nicotinic receptors is caused by multiple mechanisms. J. Neurosci. *32*, 2227-2238.

Green, W.N. and Wanamaker, C.P. (1997). The role of the cystine loop in acetylcholine receptor assembly. J. Biol. Chem. *272*, 20945-20953.

Grosman, C., Zhou, M., and Auerbach, A. (2000a). Mapping the conformational wave of acetylcholine receptor channel gating. Nature. *403*, 773-776.

Grosman, C., Salamone, F.N., Sine, S.M., and Auerbach, A. (2000b). The extracellular linker of muscle acetylcholine receptor channels is a gating control element. J. Gen. Physiol. *116*, 327-340.

Grutter, T., de Carvalho, L.P., Dufresne, V., Taly, A., Edelstein, S.J., and Changeux, J.P. (2005). Molecular tuning of fast gating in pentameric ligand-gated ion channels. Proc. Natl. Acad. Sci. U.S.A. *102*, 18207-18212.

Haeger, S., Kuzmin, D., Detro-Dassen, S., Lang, N., Kilb, M., Tsetlin, V., Betz, H., Laube, B., and Schmalzing, G. (2010). An intramembrane aromatic network determines pentameric assembly of Cys-loop receptors. Nat. Struct. Mol. Biol. *17*, 90-98.

Hamouda, A.K., Chiara, D.C., Sauls, D., Cohen, J.B., and Blanton, M.P. (2006). Cholesterol interactions with transmembrane alpha-helices M1, M3, and M4 of the Torpedo nicotinic acetylcholine receptor: photolabeling studies using [3H]Azicholesterol. Biochemistry. *45*, 976-986.

Hansen, S.B., Sulzenbacher, G., Huxford, T., Marchot, P., Taylor, P., and Bourne, Y. (2005). Structures of Aplysia AChBP complexes with nicotinic agonists and antagonists reveal distinctive binding interfaces and conformations. EMBO J. *24*, 3635-3646.

Hansen, S.B., Tao, X., and MacKinnon, R. (2011). Structural basis of PIP2 activation of the classical inward rectifier K+ channel Kir2.2. Nature. *477*, 495-498.

Heidmann, T., Sobel, A., Popot, J.L., and Changeux, J.P. (1980). Reconstitution of a functional acetylcholine receptor. Conservation of the conformational and allosteric transitions and recovery of the permeability response; role of lipids. Eur. J. Biochem. *110*, 35-55.

Hénault, C.M., Juranka, P.F., and Baenziger, J.E. (2015). The M4 transmembrane a-helix contributes differently to both the maturation and function of two prokaryotic pentameric ligand-gated ion channels. J Biol. Chem. *290*, 25118-25128.

Hibbs, R.E., Radic, Z., Taylor, P., and Johnson, D.A. (2006). Influence of agonists and antagonists on the segmental motion of residues near the agonist binding pocket of the acetylcholine-binding protein. J. Biol. Chem. *281*, 39708-39718.

Horovitz, A. and Fersht, A.R. (1990). Strategy for analysing the co-operativity of intramolecular interactions in peptides and proteins. J. Mol. Biol. *214*, 613-617.

Huang, L.Y., Catterall, W.A., and Ehrenstein, G. (1978). Selectivity of cations and nonelectrolytes for acetylcholine-activated channels in cultured muscle cells. J Gen. Physiol. *71*, 397-410.

Hughes, B.W., Kusner, L.L., and Kaminski, H.J. (2006). Molecular architecture of the neuromuscular junction. Muscle Nerve. *33*, 445-461.

Ivanov, I., Chenx, X., Sine, S.M., and McCammon, J.A. (2007). Barriers to ion translocation in cationic and anionic receptors from the Cys-loop family. J. Am. Chem. Soc. *129*, 8217-8224.

Jackson, M.B. (1989). Perfection of a synaptic receptor: kinetics and energetics of the acetylcholine receptor. Proc. Natl. Acad. Sci. U.S.A. *86*, 2199-2203.

Jha, A., Cadugan, D.J., Purohit, P., and Auerbach, A. (2007). Acetylcholine receptor gating at extracellular transmembrane domain interface: the cys-loop and M2-M3 linker. J. Gen. Physiol. *130*, 547-558.

Jin, X. and Steinbach, J.H. (2011). A portable site: a binding element for 17β-estradiol can be placed on any subunit of a nicotinic α4β2 receptor. J. Neurosci. *31*, 5045-5054.

Jones, M.V. and Westbrook, G.L. (1996). The impact of receptor desensitization on fast synaptic transmission. Trends Neurosci. *19*, 96-101.

Kash, T.L., Kim, T., Trudell, J.R., and Harrison, N.L. (2004). Evaluation of a proposed mechanism of ligand-gated ion channel activation in the GABAA and glycine receptors. Neurosci. Lett. *371*, 230-234.

Katz, B. and Thesleff, S. (1957). A study of the desensitization produced by acetylcholine at the motor end-plate. J. Physiol. *138*, 63-80.

Kelley, S.P., Dunlop, J.I., Kirkness, E.F., Lambert, J.J., and Peters, J.A. (2003). A cytoplasmic region determines single-channel conductance in 5-HT3 receptors. Nature. *424*, 321-324.

Labarca, C., Nowak, M.W., Zhang, H., Tang, L., Deshpande, P., and Lester, H.A. (1995). Channel gating governed symmetrically by conserved leucine residues in the M2 domain of nicotinic receptors. Nature. *376*, 514-516.

Labriola, J.M., Pandhare, A., Jansen, M., Blanton, M.P., Corringer, P.J., and Baenziger, J.E. (2013). Structural sensitivity of a prokaryotic pentameric ligand-gated ion channel to its membrane environment. J. Biol. Chem. *288*, 11294-11303.

Laitko, U., Juranka, P.F., and Morris, C.E. (2006). Membrane stretch slows the concerted step prior to opening in a Kv channel. J. Gen. Physiol. *127*, 687-701.

Langley, J.N. (1905). On the reaction of cells and of nerve-endings to certain poisons, chiefly as regards the reaction of striated muscle to nicotine and to curari. J. Physiol. *33*, 374-413.

Lape, R., Colquhoun, D., and Sivilotti, L.G. (2008). On the nature of partial agonism in the nicotinic receptor superfamily. Nature. *454*, 722-727.

Lape, R., Plested, A.J., Moroni, M., Colquhoun, D., and Sivilotti, L.G. (2012). The α1K276E startle disease mutation reveals multiple intermediate states in the gating of glycine receptors. J. Neurosci. *32*, 1336-1352.

Lasalde, J.A., Tamamizu, S., Butler, D.H., Vibat, C.R., Hung, B., and McNamee, M.G. (1996). Tryptophan substitutions at the lipid-exposed transmembrane segment M4 of Torpedo californica acetylcholine receptor govern channel gating. Biochemistry. *35*, 14139-14148.

Law, R.J., Henchman, R.H., and McCammon, J.A. (2005). A gating mechanisms proposed from a simulation of a human alpha7 nicotinic acetylcholine receptor. Proc. Natl. Acad. Sci. U.S.A. *102*, 6813-6818.

Le Novère, N., Corringer, P.J., and Changeux, J.P. (2002). The diversity of subunit composition in nAChRs: evolutionary origins, physiologic and pharmacologic consequences. J. Neurobiol. *53*, 447-456.

Lee, A.G. (2004). How lipids affect the activities of integral membrane proteins. Biochim. Biophys. Acta. *1666*, 62-87

Lee, W.Y. and Sine, S.M. (2005). Principal pathway coupling agonist binding to channel gating in nicotinic receptors. Nature. *438*, 243-247.

Lee, W.Y., Free, C.R., and Sine, S.M. (2008). Nicotinic receptor interloop proline anchors beta1-beta2 and Cys loops in coupling agonist binding to channel gating. J. Gen. Physiol. *132*, 265-278.

Lee, W.Y., Free, C.R., and Sine, S.M. (2009). Binding to gating transduction in nicotinic receptors: Cys-loop energetically couples to pre-M1 and M2-M3 regions. J. Neurosci. *29*, 3189-3199.

Lee, Y.H., Li, L., Lasalde, J., Rojas, L., McNamee, M., Ortiz-Miranda, S.I., and Pappone, P. (1994). Mutations in the M4 domain of Torpedo californica acetylcholine receptor dramatically alter ion channel function. Biophys. J. *66*, 646-653.

Li, L., Lee, Y.H., Pappone, P., Palma, A., and McNamee, M.G. (1992). Site-specific mutations of nicotinic acetylcholine receptor at the lipid-protein interface dramatically alter ion channel gating. Biophys. J. *62*, 1-3.

Liu, X., Xu, Y., Li, H., Wang, X., Jiang, H., and Barrantes, F.J. (2008). Mechanics of channel gating of the nicotinic acetylcholine receptor. PLoS Comput. Biol. *4*, 19.

Lizardi-Ortiz, J.E., Hyzinski-García, M.C., Fernández-Genera, J.L., Osorio-Martínez, K.M., Velázquez-Rivera, E., Valle-Avilés, F.L., and Lasalde-Dominicci, J.A. (2008). Aromaticity at

the water-hydrocarbon core interface of the membrane: consequences on the nicotinic acetylcholine receptor. Channels (Austin). *2*, 191-201.

Lummis, S.C., Beene, D.L., Lee, L.W., Lester, H.A., Broadhurst, R.W., and Dougherty, D.A. (2005). Cis-trans isomerization at a proline opens the pore of a neurotransmitter-gated ion channel. Nature. *438*, 248-252.

Lyford, L.K., Sproul, A.D., Eddins, D., McLaughlin, J.T., and Rosenberg, R.L. (2003). Agonist-induced conformational changes in the extracellular domain of alpha 7 nicotinic acetylcholine receptors. Mol. Pharmacol. *64*, 650-658.

Méthot, N., Demers, C.N., and Baenziger, J.E. (1995). Structure of both the ligand- and lipid-dependent channel-inactive states of the nicotinic acetylcholine receptor probed by FTIR spectroscopy and hydrogen exchange. Biochemsitry. *34*, 15142-15149.

Mihic, S.J., Ye, Q., Wick, M.J., Koltchine, V.V., Krasowski, M.D., Finn, S.E., Mascia, M.P., Valenzuela, C.F., Hanson, K.K., Greenblatt, E.P., et al. (1997). Sites of alcohol and volatile anaesthetic action on GABA(A) and glycine receptors. Nature. *389*, 385-389.

Milone, M., Wang, H.L., Ohno, K., Fukudome, T., Pruitt, J.N., Bren, N., Sine, S.M., and Engel, A.G. (1997). Slow-channel myasthenic syndrome caused by enhanced activation, desensitization, and agonist binding affinity attributable to mutation in the M2 domain of the acetylcholine receptor alpha subunit. J. Neurosci. *17*, 5651-5665.

Milone, M., Wang, H.L., Ohno, K., Prince, R., Fukudome, T., Shen, X.M., Brengman, J.M., Griggs, R.C., Sine, S.M., and Engel, A.G. (1998). Mode switching kinetics produced by a naturally occurring mutation in the cytoplasmic loop of the human acetylcholine receptor epsilon subunit. Neuron. *20*, 575-588.

Mishina, M., Takai, T., Imoto, K., Noda, M., Takahashi, T., Numa, S., Methfessel, C., and Sakmann, B. (1986). Molecular distinction between fetal and adult forms of muscle acetylcholine receptor. Nature. *321*, 406-411.

Mitra, A., Bailey, T.D., and Auerbach, A.L. (2004). Structural dynamics of the M4 transmembrane segment during acetylcholine receptor gating. Structure. *12*, 1909-1918.

Miyazawa, A., Fujiyoshi, Y., and Unwin, N. (2003). Structure and gating mechanism of the acetylcholine receptor pore. Nature. *423*, 949-955.

Monod, J., Wyman, J., and Changeux, J.P. (1965). On the nature of allosteric transitions: a plausible model. J. Mol. Biol. *12*, 88-118.

Muraki, M., Goda, S., Nagahora, H., and Harata, K. (1997). Importance of van der Waals contact between Glu 35 and Trp 109 to the catalytic action of human lysozyme. Protein Sci. *6*, 473-476.

Nemecz, Á., Prevost, M.S., Menny, A., and Corringer, P.J. (2016). Emerging molecular mechanisms of signal transduction in pentameric ligand-gated ion channels. Neuron. *90*, 452-470.

Nury, H., Van Renterghem, C., Weng, Y., Tran, A., Baaden, M., Dufresne, V., Changeux, J.P., Sonner, J.M., Delarue, M., and Corringer, P.J. (2011). X-ray structures of general anaesthetics bound to a pentameric ligand-gated ion channel. Nature. *469*, 428-431.

Ohno, K., Engel, A.G., Shen, X.M., Selcen, D., Brengman, J., Harper, C.M., Tsujino, A., and Milone, M. (2002). Rapsyn mutations in humans cause endplate acetylcholine-receptor deficiency and myasthenic syndrome. Am. J. Hum. Genet. *70*, 875-885.

Ohno, K., Hutchinson, D.O., Milone, M., Brengman, J.M., Bouzat, C., Sine, S.M., and Engel, A.G. (1995). Congenital myasthenic syndrome caused by prolonged acetylcholine receptor channel openings due to a mutation in the M2 domain of the epsilon subunit. Proc. Natl. Acad. Sci. U.S.A. *92*, 758-762.

Ohno, K., Quiram, P.A., Milone, M., Wang, H.L., Harper, M.C., Pruitt, J.N., Brengman, J.M., Pao, L., Fischbeck, K.H., Crawford, T.O., et al. (1997). Congenital myasthenic syndromes due to heteroallelic nonsense/missense mutations in the acetylcholine receptor epsilon subunit gene: identification and functional characterization of six new mutations. Hum. Mol. Genet. *6*, 753-766.

Ohno, K., Wang, H.L., Milone, M., Bren, N., Brengman, J.M., Nakano, S., Quiram, P., Pruitt, J.N., Sine, S.M., and Engel, A.G. (1996). Congenital myasthenic syndrome caused by decreased agonist binding affinity due to a mutation in the acetylcholine receptor epsilon subunit. Neuron. *17*, 157-170.

Olsen, R.W., Li, G.D., Wallner, M., Trudell, J.R., Bertaccini, E.J., Lindahl, E., Miller, K.W., Alkana, R.L., and Davies, D.L. (2014). Structural models of ligand-gated ion channels: sites of action for anesthetics and ethanol. Alcohol Clin. Exp. Res. *38*, 595-603.

Ortiz-Acevedo, A., Melendez, M., Asseo, A.M., Biaggi, N., Rojas, L.V., and Lasalde-Dominicci, J.A. (2004). Tryptophan scanning mutagenesis of the gammaM4 transmembrane domain of the acetylcholine receptor from Torpedo californica. J. Biol. Chem. *279*, 42250-42257.

Otero-Cruz, J.D., Báez-Pagán, C.A., Caraballo-González, I.M., and Lasalde-Dominicci, J.A. (2007). Tryptophan-scanning mutagenesis in the alphaM3 transmembrane domain of the muscle-type acetylcholine receptor. A spring model revealed. J. Biol. Chem. *282*, 9162-9171.

Papke, D., Gonzalez-Gutierrez, G., and Grosman, C. (2011). Desensitization of neurotransmitter-gated ion channels during high-frequency stimulation: a comparative study of Cys-loop, AMPA and purinergic receptors. J. Physiol. *589*, 1571-1585.

Paradiso, K., Zhang, J., and Steinbach, J.H. (2001). The C terminus of the human nicotinic alpha4beta2 receptor forms a binding site required for potentiation by an estrogenic steroid. J. Neurosci. *21*, 6561-6568.

Paulsen, I.M., Martin, I.L., and Dunn, S.M. (2009). Isomerization of the proline in the M2-M3 linker is not required for activation of the human 5-HT3A receptor. J. Neurochem. *110*, 870-878.

Pons, S., Sallette, J., Bourgeois, J.P., Taly, A., Changeux, J.P., and Devillers-Thiéry, A. (2004). Critical role of the C-terminal segment in the maturation and export to the cell surface of the homopentameric alpha 7-5HT3A receptor. Eur. J. Neurosci. *20*, 2022-2030.

Price, K.L., Millen, K.S., and Lummis, S.C. (2007). Transducing agonist binding to channel gating involves different interactions in 5-HT3 and GABAC receptors. J. Biol. Chem. *282*, 25623-25630.

Purohit, P. and Auerbach, A. (2007). Acetylcholine receptor gating at extracellular transmembrane domain interface: the "pre-M1" linker. J. Gen. Physiol. *130*, 559-568.

Purohit, P., Gupta, S., Jadey, S., and Auerbach, A. (2013). Functional anatomy of an allosteric protein. Nat. Commun. *4*, 2984.

Purohit, P., Mitra, A., and Auerbach, A. (2007). A stepwise mechanism for acetylcholine receptor channel gating. Nature. *446*, 930-933.

Ramarao, M.K. and Cohen, J.B. (1998). Mechanism of nicotinic acetylcholine receptor cluster formation by rapsyn. Proc. Natl. Acad. Sci. U.S.A. *95*, 4007-4012.

Reyes-Ruiz, J.M., Ochoa-de la Paz, L.D., Martínez-Torres, A., and Miledi, R. (2010). Functional impact of serial deletions at the C-terminus of the human GABArho1 receptor. Biochim. Biophys. Acta. *1798*, 1002-1007.

Roccamo, A.M. and Barrantes, F.J. (2007). Charged amino acid motifs flanking each extreme of the alphaM4 transmembrane domain are involved in assembly and cells-surface targeting of the muscle nicotinic acetylcholine receptor. J. Neurosci. Res. *85*, 285-293.

Sakmann, B., Patlak, J., and Neher, E. (1980). Single acetylcholine-activated channels show burst-kinetics in presence of desensitizing concentrations of agonist. Nature. *286*, 71-73.

Sanes, J.R. and Lichtman, J.W. (2001). Induction, assembly, maturation and maintenance of a postsynaptic apparatus. Nat. Rev. Neurosci. *2*, 791-805.

Santiago, J., Guzmàn, G.R., Rojas, L.V., Marti, R., Asmar-Rovira, G.A., Santana, L.F., McNamee, M., Lasalde-Dominicci, J.A. (2001). Probing the effects of membrane cholesterol in the Torpedo californica acetylcholine receptor and the novel lipid-exposed mutation alpha C418W in Xenopus oocytes. J. Biol. Chem. *276*, 46523-46532.

Sauguet, L., Shahsavar, A., Poitevin, F., Huon, C., Menny, A., Nemecz, À., Haouz, A., Changeux, J.P., Corringer, P.J., and Delarue, M. (2014). Crystal structures of a pentameric ligand-gated ion channel provide a mechanism for activation. Proc. Natl. Acad. Sci. U.S.A. *111*, 966-971.

Schiebler, W. and Hucho, F. (1978). Membranes rich in acetylcholine receptor: characterization and reconstitution to excitable membranes from exogenous lipids. Eur. J. Biochem. *85*, 55-63.

Schwede, T., Kopp, J., Guex, N., and Peitsch, M.C. (2003). SWISS-MODEL: An automated protein homology-modeling server. Nucleic Acids Res. *31*, 3381-3385.

Selcen, D., Shen, X.M., Milone, M., Brengman, J., Ohno, K., Deymeer, F., Finkel, R., Rowin, J., and Engel, A.G. (2013). GFPT1-myasthenia: clinical, structural, and electrophysiologic heterogeneity. Neurology. *81*, 370-378.

Selcen, D., Shen, X.M., Brengman, J., Li, Y., Stans, A.A., Wieben, E., and Engel, A.G. (2014) DPAGT1 myasthenia and myopathy: genetic, phenotypic, and expression studies. Neurology. *82*, 1822-1830.

Senderek, J., Müller, J.S., Dusl, M., Strom, T.M., Guergueltcheva, V., Diepolder, I., Laval, S.H., Maxwell, S., Cossins, J., Krause, S., et al. (2011). Hexosamine biosynthetic pathway mutations cause neuromuscular transmission defect. Am. J. Hum. Genet. *88*, 162-172.

Shen, X.M., Brengman, J.M., Edvardson, S., Sine, S.M., and Engel, A.G. (2012a). Highly fatal fast-channel syndrome caused by AChR ε subunit mutation at the agonist binding site. Neurology. *79*, 449-454.

Shen, X.M., Brengman, J.M., Sine, S.M., and Engel, A.G. (2012b). Myasthenic syndrome AChRα C-loop mutant disrupts initiation of channel gating. J. Clin. Invest. *122*, 2613-2621.

Shen, X.M., Deymeer, F., Sine, S.M., and Engel, A.G. (2006). Slow-channel mutation in acetylcholine receptor alphaM4 domain and its efficient knockdown. Ann. Neurol. *60*, 128-136.

Shen, X.M., Fukuda, T., Ohno, K., Sine, S.M., and Engel, A.G. (2008). Congenital myasthenia-related AChR delta subunit mutation interferes with intersubunit communication essential for channel gating. J. Clin. Invest. *118*, 1867-1876.

Shen, X.M., Ohno, K., Tsujino, A., Brengman, J.M., Gingold, M., Sine, S.M., and Engel, A.G. (2003). Mutation causing severe myasthenia reveals functional asymmetry of AChR signature cystine loops in agonist binding and gating. J. Clin. Invest. *111*, 497-505.

Shen X.M., Ohno, K., Sine, S.M., and Engel, A.G. (2005). Subunit-specific contribution to agonist binding and channel gating revealed by inherited mutation in muscle acetylcholine receptor M3-M4 linker. Brain. *128*, 345-355.

Sine, S.M. (2002). The nicotinic receptor ligand binding domain. J. Neurobiol. *53*, 431-446.

Sine, S.M. and Engel, A.G. (2006). Recent advances in Cys-loop receptor structure and function. Nature. *440*, 448-455.

Sine, S.M., Ohno, K., Bouzat, C., Auerbach, A., Milone, M., Pruitt, J.N., Engel, A.G. (1995). Mutation of the acetylcholine receptor alpha subunit causes a slow-channel myasthenic syndrome by enhancing agonist binding affinity. Neuron. *15*, 229-239.

Sine, S.M., Shen, X.M., Wang, H.L., Ohno, K., Lee, W.Y., Tsujino, A., Brengman, J., Bren, N., Vajsar, J., and Engel, A.G. (2002). Naturally occurring mutations at the acetylcholine receptor binding site independently alter ACh binding and channel gating. J. Gen. Physiol. *120*, 483-496.

Taly, A., Delarue, M., Grutter, T., Nilges, M., Le Novère, N., Corringer, P.J., and Changeux, J.P. (2005). Normal mode analysis suggests a quaternary twist model for the nicotinic receptor gating mechanism. Biophys. J. *88*, 3954-3965.

Tamamizu, S., Guzmán, G.R., Santiago, J., Rojas, L.V., McNamee, M.G., Lasalde-Dominicci, J.A. (2000). Functional effects of periodic tryptophan substitutions in the alpha M4 transmembrane domain of the Torpedo californica nicotinic acetylcholine receptor. Biochemistry. *39*, 4666-4673.

Tamamizu, S., Lee, Y., Hung, B., McNamee, M.G., Lasalde-Dominicci, J.A. (1999). Alteration in ion channel function of mouse nicotinic acetylcholine receptor by mutations in the M4 transmembrane domain. J. Membr. Biol. *170*, 157-164.

Tasneem, A., Iyer, L.M., Jakobsson E., and Aravind, L. (2005). Identification of the prokaryotic ligand-gated ion channels and their implications for the mechanisms and origins of animal Cys-loop ion channels. Genome Biol. *6*, R4.

Therien, J.P.D. and Baenziger, J.E. (2017). Pentameric ligand-gated ion channels exhibit distinct transmembrane domain archetypes for folding/expression and function. Sci. Rep. *7*, 450.

Tobimatsu, T., Fujita, Y., Fukuda, K., Tanaka, K., Mori, Y., Konno, T., Mishina, M., and Numa, S. (1987). Effects of substitution of putative transmembrane segments on nicotinic acetylcholine receptor function. FEBS Lett. *222*, 56-62.

Ueno, S., Tsutsui, M., Toyohira, Y., Minami, K., and Yanagihara, N. (2004). Sites of positive allosteric modulation by neurosteroids on ionotropic gamma-aminobutyric acid receptor subunits. FEBS Lett. *566*, 213-217.

Unwin, N. (2005). Refined structure of the nicotinic acetylcholine receptor at 4A resolution. J. Mol. Biol. *346*, 967-989.

Unwin, N. and Fujiyoshi, Y. (2012). Gating movement of acetylcholine receptor caught by plunge-freezing. J. Mol. Biol. *422*, 617-634.

Unwin, N., Miyazawa, A., Li, J., and Fujiyoshi, Y. (2002). Activation of the nicotinic acetylcholine receptor involves a switch in conformation of the alpha subunits. J. Mol. Biol. *319*, 1165-1176.

Vallejo, Y.F., Buisson, B., Bertrand, D., and Green, W.N. (2005). Chronic nicotine exposure upregulates nicotinic receptors by a novel mechanism. J. Neurosci. *25*, 5563-5572.

Wang, H.L., Auerbach, A., Bren, N., Ohno, K., Engel, A.G., and Sine, S.M. (1997). Mutation in the M1 domain of the acetylcholine receptor alpha subunit decreases the rate of agonist dissociation. J. Gen. Physiol. *109*, 757-766.

Wang, H.L., Cheng, X., and Sine, S.M. (2012). Intramembrane proton binding site linked to activation of bacterial pentameric ion channel. J. Biol Chem. *287*, 6482-6489.

Wang, H.L., Milone, M., Ohno, K., Shen, X.M., Tsujino, A., Batocchi, A.P., Tonali, P., Brengman, J., Engel, A.G., and Sine, S.M. (1999). Acetylcholine receptor M3 domain: stereochemical and volume contributions to channel gating. Nat. Neurosci. *2*, 226-233.

Wang, H.L., Ohno, K., Milone, M., Brengman, J.M., Evoli, A., Batocchi, A.P., Middleton, L.T., Christodoulou, K., Engel, A.G., and Sine, S.M. (2000). Fundamental gating mechanism of

nicotinic receptor channel revealed by mutation causing a congenital myasthenic syndrome. J. Gen. Physiol. *116*, 449-462.

Wang, J., Lester, H.A., and Dougherty, D.A. (2007). Establishing an ion pair interaction in the homomeric rho1 gamma-aminobutyric acid type A receptor that contributes to the gating pathway. J. Biol. Chem. *282*, 26210-26216.

Wang, J.M., Zhang, L., Yao, Y., Viroonchatapan, N., Rothe, E., Wang, Z.Z. (2002). A transmembrane motif governs the surface trafficking of nicotinic acetylcholine receptors. Nat. Neurosci. *5*, 963-970.

Webster, R., Maxwell, S., Spearman, H., Tai, K., Beckstein, O., Sansom, M., and Beeson, D. (2012). A novel congenital myasthenic syndrome due to decreased acetylcholine receptor ion-channel conductance. Brain. *135*, 1070-1080.

Xiu, X., Hanek, A.P., Wang, J., Lester, H.A., and Dougherty, D.A. (2005). A unified view of the role of electrostatic interactions in modulating the gating of Cys loop receptors. J. Biol. Chem. *280*, 41655-41666.

Xu, Y., Barrantes, F.J., Luo, X., Chen, K., Shen, J., and Jiang, H. (2005). Conformational dynamics of the nicotinic acetylcholine receptor channel: a 35-ns molecular dynamics simulation study. J. Am. Chem. Soc. *127*, 1291-1299.

Xu, W., Orr-Urteger, A., Nigro, F., Gelber, S., Sutcliffe, C.B., Armstrong, D., Patrick, J.W., Role, L.W., Beaudet, A.L., and De Biasi, M. (1999). Multiorgan autonomic dysfunction in mice lacking the beta2 and the beta4 subunits of neuronal nicotinic acetylcholine receptors. J. Neurosci. *19*, 9298-9305.

Young, G.T., Zwart, R., Walker, A.S., Sher, E., and Millar, N.S. (2008). Potentiation of alpha7 nicotinic acetylcholine receptors via an allosteric transmembrane site. Proc. Natl. Acad. Sci. U.S.A. *105*, 14686-14691.

Yuan, S., Filipek, S., and Vogel, H. (2016). A gating mechanism of the serotonin 5-HT3 receptor. Structure. *24*, 816-825.

Zhou, M., Engel, A.G., and Auerbach, A. (1999). Serum choline activates mutant acetylcholine receptors that cause slow channel congenital myasthenic syndromes. Proc. Natl. Acad. Sci. U.S.A. *96*, 10466-10471.

Zuber, B. and Unwin, N. (2013). Structure and superorganization of acetylcholine receptor-rapsyn complexes. Proc. Natl. Acad. Sci. U.S.A. *110*, 10622-10627.

Appendix

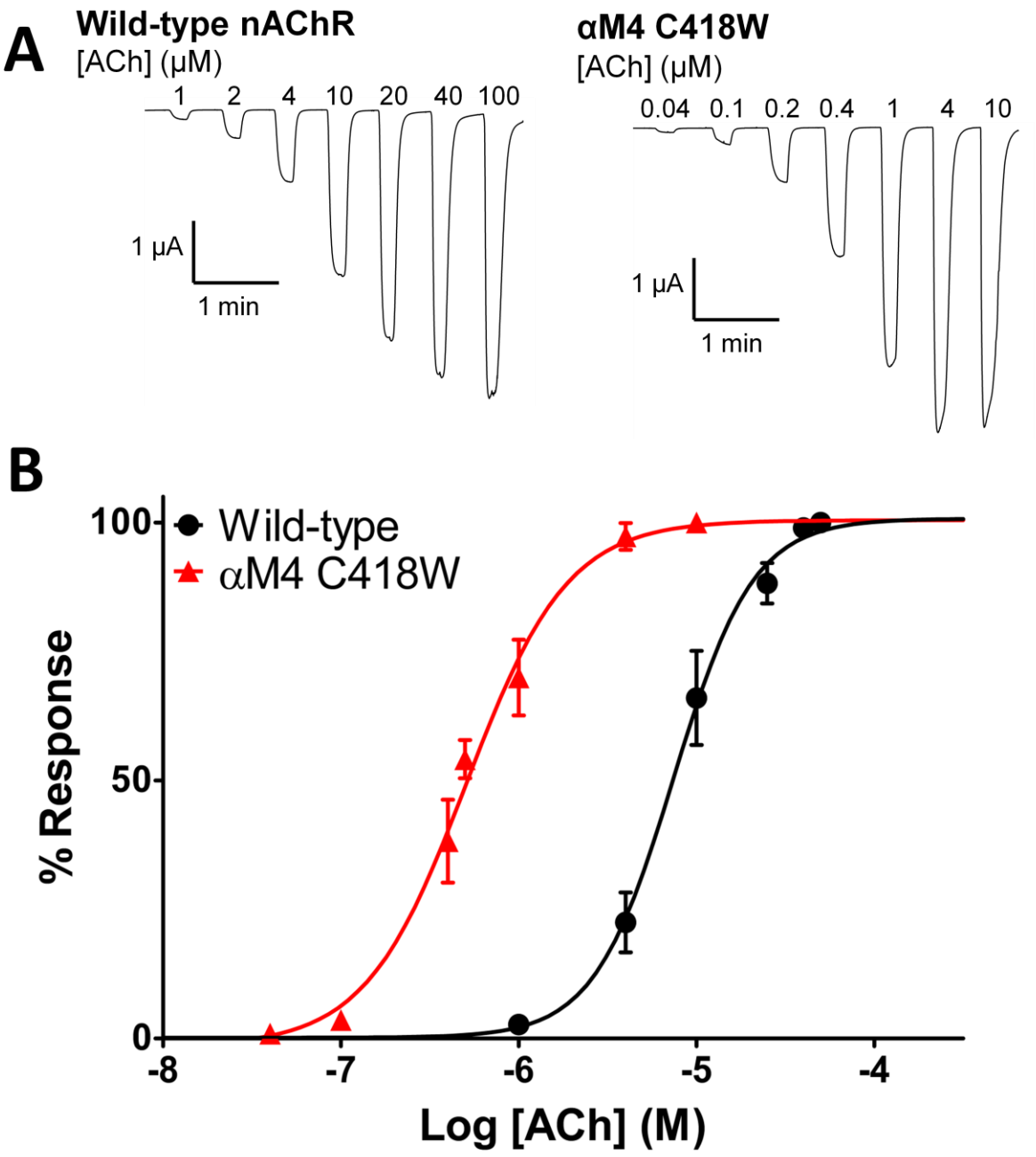

Figure 6.1 - WT-nAChR versus C418W-nAChR. (A) Whole cell electrophysiological traces recorded using TEVC. Currents were recorded from *Xenopus laevis* oocytes expressing either WT-nAChR or C418W-nAChR in response to increasing concentrations of ACh. (B) Averaged dose response curves for WT-nAChR (EC_{50} = 7.61 ± 1.25 μM) and C418W-nAChR (EC_{50} = 0.47 ± 0.12 μM). Error bars represent standard deviation.

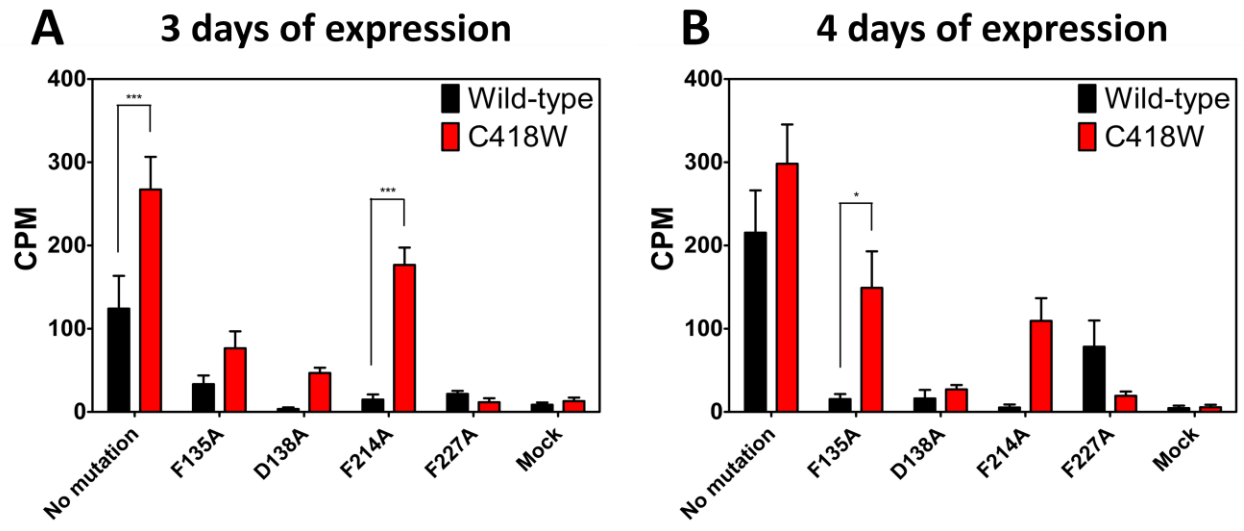

Figure 6.2 - Surface expression levels of select mutants as measured by [^{125}I]-α-bungarotoxin binding. Cell surface binding of [^{125}I]-α-bungarotoxin as detected by γ counting 3 days (A) and 4 days (B) after injection of 50 ng of either wild-type or mutant cRNA. Mock oocytes were injected with buffer that did not contain any cRNA.

Curriculum Vitae

Education	
Fall 2015 - Fall 2017	Master of Science, Biochemistry University of Ottawa - Ottawa, Ontario, Canada
Fall 2012 - Winter 2015	Honour's Bachelor of Science, with Specialization in Biochemistry, option in Microbiology Immunology Degree obtained - *Magna Cum Laude* University of Ottawa - Ottawa, Ontario, Canada
Fall 2010 - Winter 2012	Diploma of Collegial Studies - Science Degree obtained - *with distinction* CÉGEP Heritage College - Gatineau, Québec, Canada
Research Experience	
Fall 2015 - Fall 2017	Master of Science, Biochemistry Thesis Topic: Mechanism underlying potentiation of the nicotinic acetylcholine receptor by a lipid-facing mutation implicated in a congenital myasthenic syndrome
Summer 2015	Summer Research Student Continuation of Honour's Research Project
Fall 2014 - Winter 2015	Undergraduate Honour's Research Project Honour's Thesis Topic: The role of αM4 as an allosteric modulator of nicotinic acetylcholine receptor function
Summer 2014	Summer Research Student Research Project: The role of αM4 in the gating and allosteric modulation of the human muscle-type nicotinic acetylcholine receptor
Scholarships and Awards	
Winter 2017	3rd Place in BMI Graduate Seminar Day (Biochemistry, Master's Student)
Fall 2015	University of Ottawa Graduate Admission Scholarship
Summer 2014	CIHR Summer Research Student Award in Neurodegenerative Lipidomics Scholarship
Fall 2012	University of Ottawa Undergraduate Admission Scholarship

Publications

Papers published in refereed journals:

- Baenziger, J.E., **Domville, J.A.**, and Therien, J.P.D. (2017). The role of cholesterol in the activation of nicotinic acetylcholine receptors. Curr. Top. Membr. *80*, 95-137.

Papers in preparation:

- **Domville, J.A.** and Baenziger, J.E. (2018). An allosteric link connecting the lipid-protein interface of the nicotinic acetylcholine receptor to channel gating. *Submitted.*
- **Domville, J.A.** and Baenziger, J.E. (2018). Mapping the allosteric pathway leading from a mutation in the nicotinic acetylcholine receptor to a Congenital Myasthenic Syndrome. *In preparation.*

- **Domville, J.A.** Edrington, C., Wagner-Searle, C., Balasubramaniam, S., and Baenziger, J.E. (2017). The differential role of M4 in the muscle-type nicotinic acetylcholine receptor subunits. *In preparation.*

Non-refereed Contributions

- **Jaimee A. Domville** and John E. Baenziger. Mechanism underlying potentiation of the nicotinic acetylcholine receptor by a lipid-facing mutation implicated in a congenital myasthenic syndrome. University of Ottawa BMI Graduate Seminar Day. Ottawa, Ontario, Canada. March 8th, 2017 - Seminar
- **Jaimee A. Domville** and John E. Baenziger. Potentiation of nicotinic acetylcholine receptor function by a lipid-facing mutation implicated in a congenital myasthenic syndrome. University of Ottawa BMI Graduate Poster Day. Ottawa, Ontario, Canada. May 12th, 2016 - Poster
- **Jaimee A. Domville** and John E. Baenziger. The role of αM4 in the gating and allosteric modulation of the human muscle-type nicotinic acetylcholine receptor. University of Ottawa Undergraduate Research Poster Day. Ottawa, Ontario, Canada. April 14th, 2015 - Poster

Graduate Coursework

Winter 2016	BCH8107: Advanced Topics in Structure and Function of Plasma Lipoproteins
Fall 2015	NSC8106: Mechanisms of Neurological Disease

Skills

Computer Programs

- Microsoft Office (Word/Excel/PowerPoint) - Advanced
- PyMOL - Advanced
- GraphPad Prism - Advanced
- BLAST/ExPASy (Intermediate)

Lab Techniques

- PCR/Mutagenesis/Ligation
- DNA and cRNA preparation
- Molecular cloning
- Electrophysiology
- Agarose gel electrophoresis